Check for updates

# Hydrogen-bonded π-conjugated supramolecular polymers

Pedro Ximenis, [ID] Daniel Martínez, [ID] Llorenç Rubert [ID] and Bartolome Soberats [ID] *

The self-assembly of π-conjugated molecules offers a promising route for designing advanced functional materials with tailored optical and electronic properties. Owing to their nature, organic π-conjugated scaffolds spontaneously assemble by π–π stacking, while the introduction of hydrogen-bonding (H-bonding) interactions in these systems has emerged as a key strategy to gain control over self-assembly processes and the resulting supramolecular assemblies. H-bonding provides both specificity and directionality in non-covalent interactions, facilitating the formation of well-ordered and stable structures, such as supramolecular polymers. This review examines recent advances in design strategies that leverage H-bonding chromophores to fine-tune self-assembly behavior in solution, discussing the impact of monomer design and the experimental conditions on molecular packing and the morphologies of the resulting assemblies. Along with the thermodynamic advantages of H-bonding, its impact on self-assembly kinetics is also discussed, highlighting phenomena such as pathway complexity and related concepts like living supramolecular polymerization, secondary nucleation and supramolecular polymorphism. By providing a comprehensive overview of the current state of the field, this work aims to guide future research efforts toward the rational design of hierarchically ordered π-conjugated supramolecular materials.

Department of Chemistry, Universitat de les Illes Balears, 07122 Palma de Mallorca, Spain. E-mail: b.soberats@uib.es

## 1. Introduction

### 1.1. Prologue

The field of supramolecular chemistry has, over the past few decades, evolved from the early studies of host–guest interactions, to embrace more complex systems capable of dynamic,

*Pedro Ximenis obtained his BSc Chemistry from the University of the Balearic Islands (UIB) and then his MSc Molecular Nanoscience and Nanotechnology from the Universitat de Valencia (UV), where he began his research in supramolecular assemblies under the supervision of Dr. Soberats. Now, he is currently a PhD student in the same group at the UIB. His main research topic is the design and study of non-conventional supramolecular assemblies based on dyes driven by Hydrogen Bonding. He is working on liquid crystalline systems and supramolecular polymers and copolymers*

**Pedro Ximenis**

*Daniel Martínez received his BSc Chemistry and MSc Chemical Science and Technology from the University of the Balearic Islands (UIB) in which both bachelor's and master's theses were supervised by Dr Ángel García Raso. In 2022, he joined the Supramolecular Chemistry research group, at the same institution, as a support researcher, and in 2024 he started his PhD studies under the supervision of Dr Bartolomé Soberats. His research focuses on the study of supramolecular polymers and liquid crystals based on unconventionally assembled organic chromophores.*

**Daniel Martínez**

This journal is © The Royal Society of Chemistry 2025

*Chem. Soc. Rev.*, 2025, **54**, 11659–11698 | 11659

adaptive behaviour and hierarchical self-organization.[1–6] In this context, the concept of supramolecular polymerization has gained increasing attention, not only as a model to study biological processes but also as a tool to develop innovative materials.[7–10] Supramolecular polymers are large, dynamic assemblies formed through reversible non-covalent interactions (such as hydrogen bonding (H-bonding), π–π stacking, metal coordination, or hydrophobic effects) between monomeric units. These monomeric units can vary in structure and nature but typically consist of organic or organometallic components with suitable solubility in either aqueous or organic solvents. Unlike traditional covalent polymers,[11] these materials exhibit adaptive properties, self-healing behaviour, and stimuli-responsiveness, making them ideal candidates for a wide range of applications.[12–16]

Among the diverse molecular systems explored for supramolecular polymerization, extended π-conjugated organic scaffolds or dyes have emerged as versatile monomeric building blocks, not only for their intrinsic optoelectronic properties but also for their ability to promote directional π–π stacking between the aromatic surfaces.[17–21] Furthermore, by tailoring the molecules and adding peripheral groups, it is possible to introduce additional interactions like H-bonding, electrostatic forces, or solvophobic effects, enhancing the self-assembly tendency. The combination of different non-covalent interactions has been shown to be an effective strategy for constructing π-conjugated supramolecular polymers with well-defined morphologies, tuneable photophysical properties, and dynamic behaviour. In this context, a key advantage of self-assembled π-conjugated materials lies in the fact that their properties emerge from the entire supramolecular architecture rather than solely from the molecular structures of the monomers, leading to emergent features such as exciton delocalization, aggregation-induced emission or quenching and enhanced charge mobility.[22,23] Through rational design of the monomeric b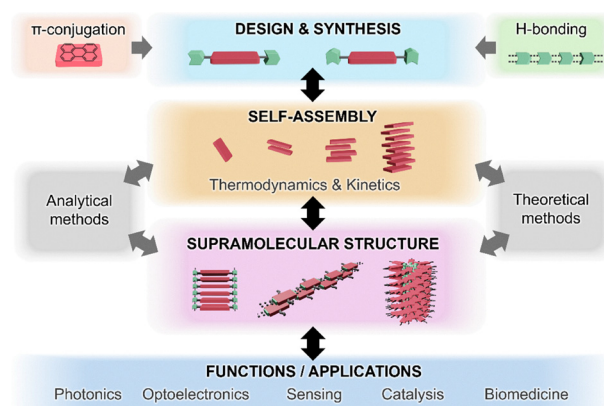uilding blocks, the structure and properties of the polymers can be finely tuned, making such systems highly attractive for applications in organic electronics, photovoltaics, sensing, and bioimaging.[24,25]

The incorporation of H-bonding motifs into a chromophore scaffold offers several advantages for the construction of supramolecular polymers.[26–28] The directionality in hydrogen bonds (H-bonds) guides hierarchical self-assembly, typically into one-dimensional polymers or more complex architectures, and provides additional stability to the resulting architecture. This strategy has been successfully applied to a variety of dye-systems, including perylene bisimides (PBIs),[29] naphthalene diimides (NDIs),[30] BODIPY,[31] and diketopyrrolopyrroles (DPPs),[32] among others. For instance, PBIs readily form stable, columnar stacks solely by π–π interactions,[33] while the introduction of H-bonding amide units in the monomer design results in highly ordered supramolecular structures with excellent thermal and photostability.[34] The introduction of H-bonds in supramolecular polymerization affects the thermodynamics of the process but it can also interfere in the kinetics, altering the energy landscape.[35]



Fig. 1 Outlook of the scope of this review covering different aspects of H-bonded supramolecular polymers based on π-conjugated systems.

*Llorenç Rubert is a PhD candidate under the supervision of Dr Bartolomé Soberats in the University of the Balearic Islands, Spain. His research focuses on design, study and control of supramolecular polymers and liquid crystals. He has worked on 2D-supramolecular polymers, pathway complexity and co-assembled luminescent liquid crystals.*

**Llorenç Rubert**

*Dr Bartolomé Soberats is an Associate Professor at the University of the Balearic Islands (UIB). He obtained his PhD from UIB and subsequently held postdoctoral positions at the University of Tokyo and the University of Würzburg. His research focuses on the design and development of supramolecular polymers and functional liquid crystals. He has contributed to the advancement of unconventional assemblies of liquid-crystalline dyes, dynamic covalent liquid crystals, and the exploration of pathway complexity and two-dimensional supramolecular polymers.*

**Bartolome Soberats**

This review aims to provide a focused overview of recent progress in the development of H-bonded π-conjugated polymers (Fig. 1). A special emphasis will be placed on how H-bonding is strategically implemented in the monomer structure to gain control over the self-assembly processes, molecular packing, and polymer morphology, as well as the photophysical properties. In this context, we aim to highlight not only the fundamental insights but also new avenues for the rational design of next-generation supramolecular materials.

### 1.2. Supramolecular polymers and H-bonding

The concept of supramolecular polymers began to crystallize in the early 1990s, fuelled by the idea that non-covalent interactions could drive the formation of polymer-like structures with dynamic and reversible properties. A pivotal early example was published in 1988, when T. Aida and S. Inoue reported the formation of fibrous aggregates from the porphyrin derivative **1** (Fig. 2a).[36] Their study revealed significant changes in the UV/vis absorption spectra by increasing concentration, which was related to an aggregation process, highlighting the effects of supramolecular polymerization on the chromophore

properties. Interestingly, in this case, the assembly was stabilized by π–π interactions, with no participation of H-bonding.

Around the same time, Jean-Marie Lehn introduced the concept of dynamic polymers capable of adapting and reorganizing in response to external stimuli due to the reversible nature of non-covalent interactions. Notably, they reported polymeric assemblies formed through triple H-bonds using bifunctional diamidopyridines and uracil derivatives (**2a** and **2b**), highlighting the potential of H-bonding as a key driving force (Fig. 2b).[37] H-bonds are directional and relatively strong non-covalent interactions with binding energies ranging from 5 to 40 kJ mol$^{-1}$, depending on the chemical environment and the strength of the donor and acceptor.[2] Compared to other non-covalent forces, H-bonds are stronger and more directional than van der Waals interactions (*e.g.*, London dispersion forces), which are generally weak and non-directional. Unlike π–π stacking or hydrophobic interactions, which rely on electronic polarizability or solvent exclusion, respectively, H-bonds are highly specific and contribute significantly to conformational control and molecular alignment in supramolecular assemblies.

Accordingly, H-bonding emerged as a key motif in the design of supramolecular polymers. In this context, the works on H-bonded supramolecular polymers of Meijer and co-workers using ureidopyrimidinones (UPy)[38] (Fig. 2c) and later benzene-1,3,5-tricarboxamides (BTAs)[39] (Fig. 2d) proved to be especially influential. These systems have since served as model platforms for in-depth thermodynamic and mechanistic studies of supramolecular polymerization.[7–16] In recent years, advances in molecular design, supported by synthetic chemistry, have been pivotal in expanding the scope and robustness of H-bonded supramolecular polymers. The incorporation of well-defined and highly directional motifs such as diaminotriazines-uracyl,[40] bis(acylamino)triazines, barbiturates,[41] ureas,[42] and squaramides,[43–45] (Fig. 2e) among others, has led to a versatile toolkit of H-bonding units capable of establishing predictable and tuneable interaction patterns. These motifs not only provide strong and reversible interactions but also enable fine control over the polymer architecture, stability, and responsiveness. Notably, many of these units, along with simpler functional groups like amides or amino acid sequences, can be seamlessly integrated into various organic scaffolds, including π-conjugated systems.[17–25] This strategy allows for the creation of supramolecular polymers that combine superior structural order with electronic or optical functionality.

### 1.3. Self-assembly of dyes and electronic considerations

Historically, the interest in organic π-conjugated molecules can be traced back to their use in textile coloration in the 19th century, when synthetic dyes such as mauveine and indigo marked the beginning of industrial organic chemistry. These early dyes were valued for their chromatic properties, but only much later their potential in photonics, electronics, and sensing become fully recognized.[46] The transition from simple colorants to functional molecular materials has paralleled developments in synthetic chemistry, which enabled to gain control to prepare complex molecules with the desired
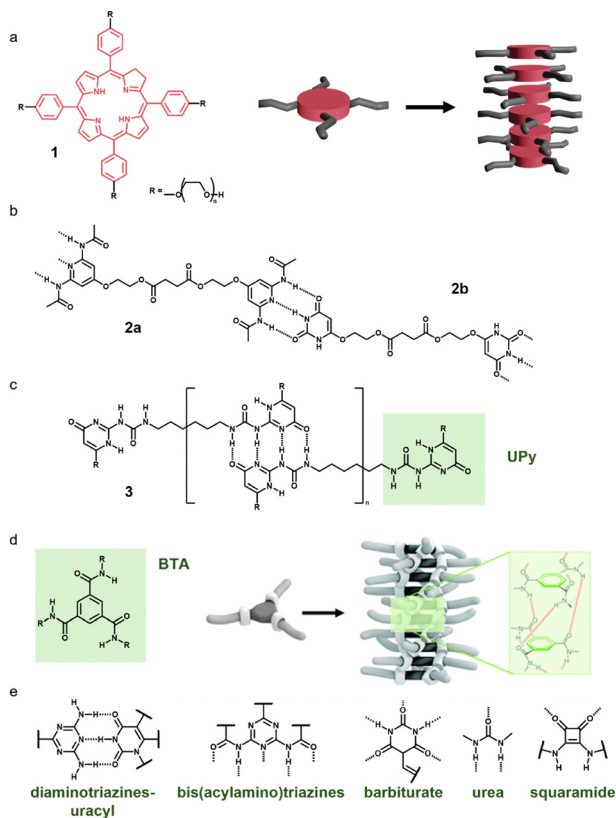


**Fig. 2** (a) Molecular structure of porphyrin **1** and the proposed assembly pattern. Molecular structure and H-bonding patterns of compounds (b) **2a,b** and (c) **3**. (d) General molecular structure of a BTA monomer and the representation of its self-assembly pattern *via* triple H-bonds (reproduced from ref. 39, with permission from the Royal Society of Chemistry, copyright 2012). (e) Different H-bonding motifs relevant for the development of supramolecular polymers.

This journal is © The Royal Society of Chemistry 2025

*Chem. Soc. Rev.*, 2025, **54**, 11659–11698 | **11661**

structure, planarity, and substitution patterns. This control has enabled the design of dyes not merely as isolated chromophores, but as building blocks capable of spontaneously assembling into higher-order architectures.[47]

The delocalization of π-electrons across the π-conjugated organic systems imparts unique electronic properties to these molecules. This configuration defines the energy gap between the highest occupied molecular orbital (HOMO) and the lowest unoccupied molecular orbital (LUMO), dictating the absorption and emission properties.[48] The electronic characteristics of π-conjugated systems can be precisely tuned through molecular engineering strategies such as extending the conjugation length, introducing electron-donating or -withdrawing substituents, and incorporating heteroatoms into the π-framework. These structural modifications directly influence key parameters like energy levels and absorption/emission profiles.

Importantly, the photophysical behavior of dye molecules changes upon self-assembly due to the interaction between individual monomeric units. These monomer–monomer interactions are crucial in dictating the optical absorption, emission properties, and excited-state dynamics of the resulting assemblies. The first approximation to this phenomenon was studied in the molecular exciton theory,[48–50] which was then extended to include vibronic coupling,[51–55] and finally address short-range charge transfer interactions.[52] Collectively, these methods offer a comprehensive description of how supramolecular packing modulates the electronic features of chromophore-based polymers.

Molecular exciton theory, originally formulated by Kasha and grounded in earlier work by Davydov on excitonic splitting, conceptualizes chromophores as point oscillators, so-called molecular oscillators, that interact via their transition dipole moments, described as the sum of position vectors of all particles with charge, characterized by their direction and probability.[48–50] In this context, the simplest model involves a dimer of two interacting molecules, where each monomer is treated as an independent oscillator. When two molecules are brought close enough, their transition dipoles ($\mu$) interact through coulombic dipole–dipole coupling. This interaction leads to a splitting of the excited-state energy levels into two excitonic states, one higher and one lower in energy than the monomeric excited state. Note that the splitting is not centered on the $s_1$ level, because this is slightly displaced due to van der Waals interactions ($\Delta E_{vdW}$) (Fig. 3a).

The relative orientation of the dipoles determines the permitted and forbidden states, leading to what are commonly known as H-type interactions (hypsochromic, blue-shifted), where the permitted excitonic state is the one with higher energy, and J-type interactions (bathochromic, red-shifted), where the permitted excitonic state is the one with lower energy (Fig. 3a–c).[56,57] A critical angle of $\theta = 54.7°$ indicates the transition point between the H-type and J-type coupling regimes (Fig. 3b). Other geometries may present non-aligned dipoles leading to mixed exciton states or partially allowed transitions as for example by relative rotation with the respect of the angle $\alpha$ (Fig. 3c).[58,59] However, these approximations consist of idealized geometries (e.g. spherical dipoles or

perfectly parallel arrangements) and may differ from real supramolecular structures.

The exciton model can be extended to higher-order aggregates (trimers, tetramers, etc.), treating each additional chromophore as a new dipolar oscillator in the assembly. This progression leads to band formation, exciton delocalization, and spectral changes including band narrowing and loss of vibronic fine structure. However, these extensions rely on high structural order and limited environmental perturbation, limiting their applicability to ideal systems. Accordingly, the classical exciton theory can be applied to systems with large transition dipole moments and negligible vibronic coupling, but fails for most organic chromophores, which exhibit significant vibrational coupling and/or charge transfer character.[60]

To overcome these limitations, vibronic coupling was incorporated into exciton theory, most notably by Spano and co-workers. The updated model considers both electronic coupling and coupling to molecular vibrations, characterized by the Franck–Condon principle and the Huang–Rhys factor, which correlates the electronic and molecular vibrations.[51–55] In the weak coupling regime, the vibronic structure of aggregates can be described quantitatively using intensity ratios between successive vibronic peaks. The relative intensities depend on the interplay between the exciton coupling, vibrational energy, and the vibronic overlap functions. As shown in Fig. 3d, in H-aggregates, increasing exciton coupling shifts intensity from $A_1$ to $A_2$ levels and beyond, while in J-aggregates, intensity accumulates in the $A_1$ level with minimal contribution from higher vibronic levels. This refined theory enables a more accurate interpretation of experimental spectra, particularly in systems where the vibrational fine structure is evident and traditional exciton theory fails to account for spectral intensities.[61]

A second major correction to exciton coupling theory involves the inclusion of short-range charge transfer interactions.[52] These interactions arise from direct wavefunction overlap between adjacent chromophores, typically occurring at intermolecular distances below ~4 Å, well within the range of typical supramolecular contacts. Charge transfer interactions are highly sensitive to geometry and molecular electronic structure as shown in Fig. 3e for perylene. Two principal contributions define charge transfer coupling: (i) hole transfer ($t_h$) integral (HOMO–HOMO overlap) and (ii) electron transfer ($t_e$) integral (LUMO–LUMO overlap). Their combined effect ($-t_e \cdot t_h$) contributes to total coupling energy, which modifies the coulombic term (Fig. 3e) and must be considered jointly with vibrational coupling for accurate spectral predictions. Depending on the relative signs and magnitudes, coulomb and charge transfer contributions may reinforce or cancel each other, leading to cases where aggregate formation occurs without noticeable spectral shifts, known as null exciton coupling.[62] This behavior has been observed in carefully designed systems, such as foldamers, where geometrical precision can control the electronic coupling geometry.[63,64] More recently, the formation of aggregates with null exciton coupling interactions has been reported in a Z-shape PBI (see Section 4.1).[65]

11662 | Chem. Soc. Rev., 2025, 54, 11659–11698

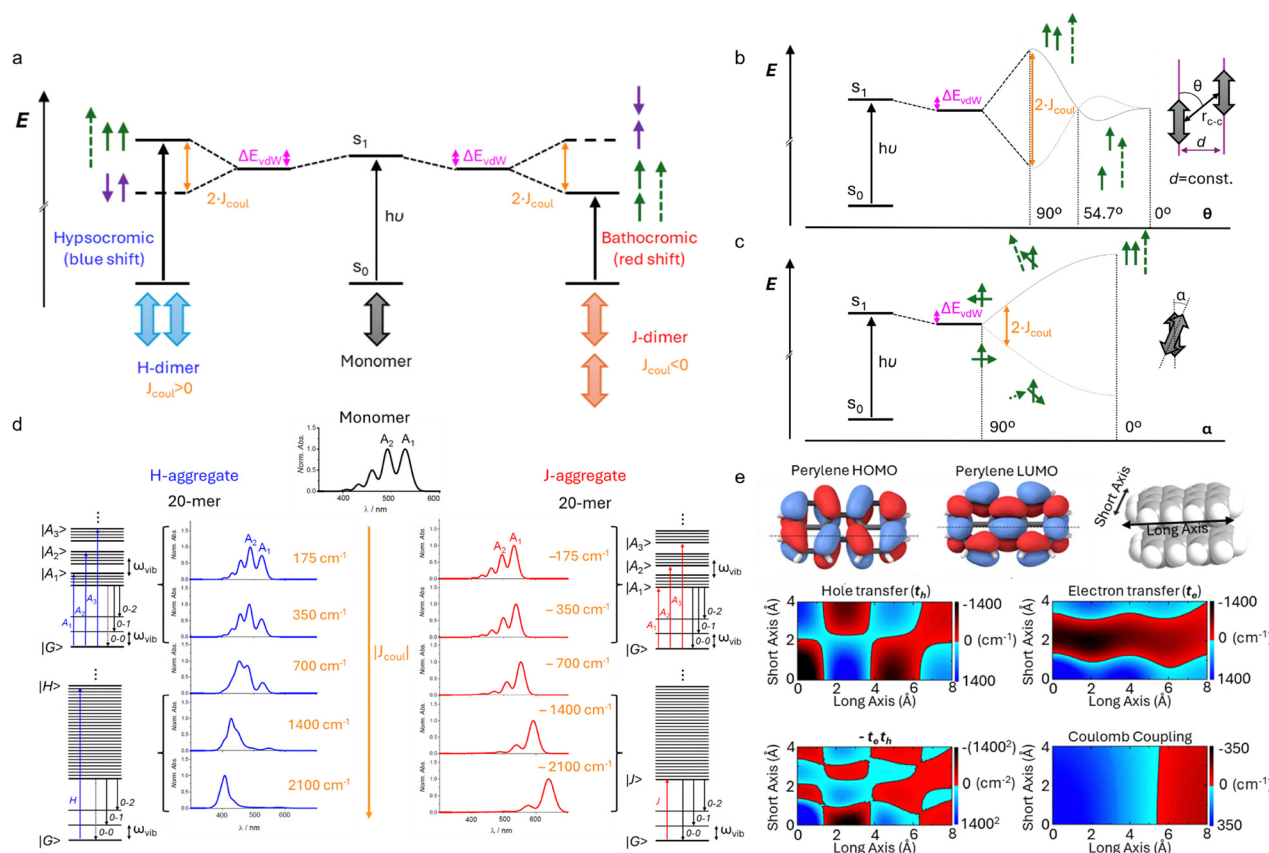This journal is © The Royal Society of Chemistry 2025

Fig. 3 (a) Representation of the energetic levels for a monomer, an H-dimer and a J-dimer. (b) and (c) Representation of the energetic levels for dimers in different geometries: changing $\theta$ maintaining $d$ constant (b) and changing $\alpha$ (c). (a)–(c) Green solid arrows represent the relative orientation of the molecular transition dipole moments of the allowed transitions; the global transition dipole moment of the dimer is represented with dashed green arrows; and purple solid arrows indicate the relative orientation of the molecular transition dipole moments of the forbidden transitions. (d) Representation of the vibrational energetic levels and absorption bands for a monomer and H or J-type aggregates with different levels of coulomb coupling and strong vibrational coupling. (e) The HOMO and LUMO of perylene. Hole transfer ($t_h$) and electron transfer ($t_e$) contributions within a π-stacked perylene dimer (3.5 Å stacking distance) as a function of short- and long-axis displacements. The product $-t_e\,t_h(\propto$ JCT) and coulomb coupling as a function of short- and long-axis displacements. Red regions indicate a negative coupling (J-aggregation), and blue regions indicate a positive coupling (H-aggregation) (reproduced from ref. 52 with permission from the American Chemical Society, copyright 2018).

In terms of emission properties, H-type dimers typically suppress fluorescence due to forbidden transitions from the lowest excitonic state, whereas J-type dimers enhance emission due to allowed transitions with increased oscillator strength. These differences underlie many observed trends in supramolecular chromophore assemblies, such as the pronounced fluorescence quenching in H-aggregates and enhanced brightness in J-aggregates.[60,66,67]

Understanding the interactions between chromophores is essential for designing supramolecular materials with tailored functions. These interactions directly influence key optical properties, making molecular-level control a powerful tool in material design.

## 2. Supramolecular polymerization and thermodynamics

The study of supramolecular polymers is predominantly conducted in solution, as they are dynamic species existing as supramolecular entities in solvated states in equilibrium with the monomers. In this review, we primarily focus on systems that assemble in organic solvents, as aqueous environments are considerably more complex and often weaken H-bonding due to competition with water molecules.[10] Supramolecular polymerization processes in organic solvents are typically favoured by increasing the monomer concentration and decreasing the temperature. Moreover, the nature of solvent has a strong influence on the polymerization behaviour. For a given system, a good solvent is one that dissolves the monomer and prevents aggregation, while a bad solvent promotes self-assembly.[68–74] Thus, in solvent mixtures, the ratio of good to poor solvent governs the polymerization tendency of the system.

In this section, we will explore various aspects of the study of π-conjugated supramolecular polymers, considering mechanistic aspects of supramolecular polymerization, as well as the different methods applied to the characterization of supramolecular species.

### 2.1. Supramolecular polymerization mechanisms

A monomeric species can self-assemble into supramolecular polymers *via* different mechanisms depending, for example, on

This journal is © The Royal Society of Chemistry 2025

*Chem. Soc. Rev.*, 2025, **54**, 11659–11698 | **11663**

its molecular structure, the solvent and the intermolecular interactions involved in the self-assembly process.[75] These mechanisms are typically classified into two main types: isodesmic and nucleation–elongation, and are studied considering the assembly into one-dimensional (1D) assemblies (Fig. 4). In studies of supramolecular polymerization mechanisms, the systems are typically treated as equilibria involving only two species: the monomer and the polymer. To evaluate the supramolecular polymerization mechanism of a given system, the parameter "degree of aggregation ($\alpha_{agg}$)" is used, which varies depending on the conditions (concentration, temperature and solvent composition) (see Section 2.2). The degree of aggregation is a numerical representation of the aggregated species in solution, where $\alpha_{agg} = 1$ indicates full aggregation and $\alpha_{agg} = 0$ corresponds to the monomeric state.[76] This parameter can be experimentally calculated using eqn (1):

$$\alpha_{agg} = \frac{X_c - X_m}{X_a - X_m} \qquad (1)$$

where $X$ is the value of a physical property of the system obtained from the experimental technique (see Section 2.3). In particular, $X_c$ is the value at the specific experimental conditions, $X_m$ is the value for the pure monomeric species, and $X_a$ is the value for the totally aggregated species. Accordingly, $\alpha_{agg}$ can be determined when the monomer ($X_m$) and the polymer ($X_a$) present a markedly distinct physical property

measurable by an experimental technique, such as the absorption spectrum in π-conjugated systems.

**2.1.1. Isodesmic mechanism.** In a supramolecular polymerization event where the monomers associate forming stacked assemblies, the process is denominated as isodesmic when the addition of each monomer to the growing polymer chain occurs with the same free energy change (Fig. 4a–c). In other words, the interaction strength between a newly added monomer to the polymer chain is independent of the polymer's length. Consequently, the entire process can be described with a single association constant ($K_e$) (Fig. 4a).[77] An isodesmic mechanism can be identified when the degree of aggregation ($\alpha_{agg}$) is plotted against a suitable variable (depending on the method, see Section 2.2), resulting in all the cases in a characteristic sigmoidal curve.

It is noteworthy that while the isodesmic mechanism is common in simple π-conjugated supramolecular polymers formed solely by π–π stacking, it is rarely observed when H-bonding groups are introduced into the monomeric scaffold. One of the scarce examples of a H-bonded π-conjugated supramolecular polymers formed by an isodesmic mechanism was reported by Xiaoming He and coworkers.[78] They found that an anthanthrene derivative (**4**) with amide-amide or amide-ester motifs at the molecular spacers forms H- or J-aggregates (Fig. 5a). In particular, the amide-ester motif promotes the formation of J-aggregates *via* an isodesmic mechanism, as it
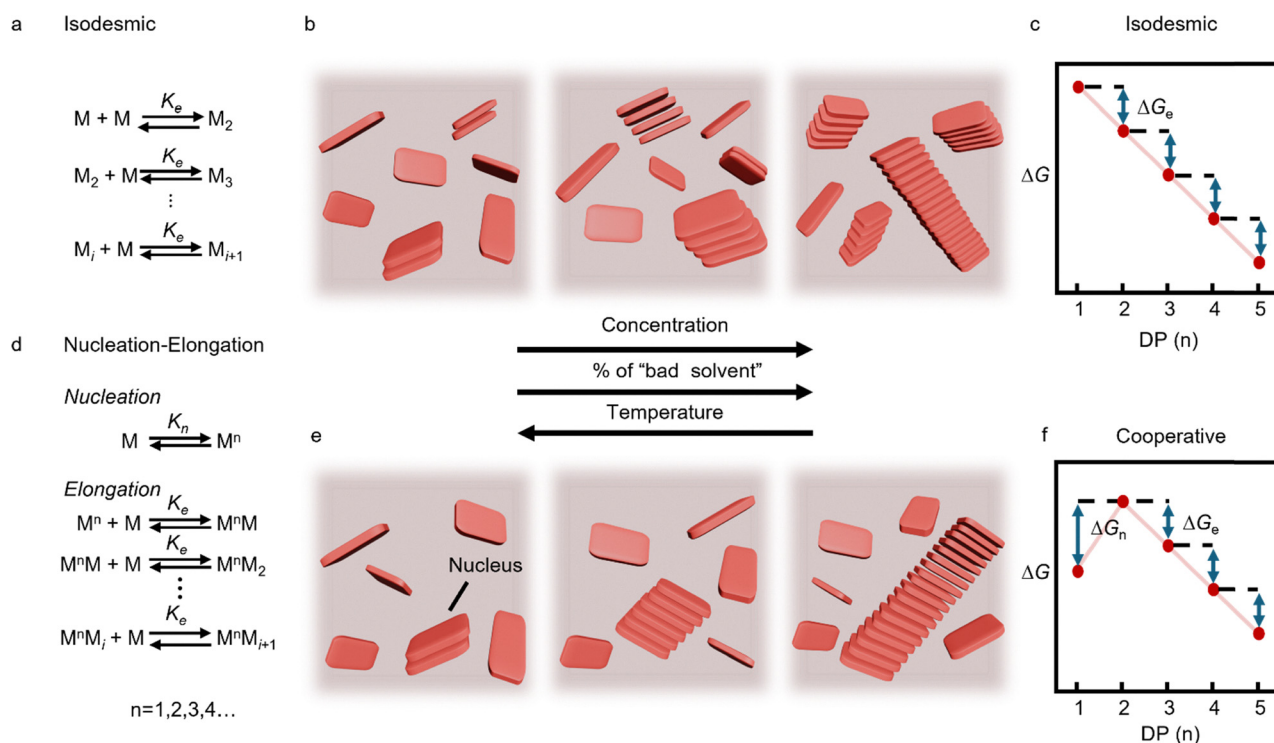


**Fig. 4** Schematic equilibria for the (a) and (b) isodesmic and the (d) and (e) nucleation-elongation aggregation mechanisms, where M is the monomer and M$^n$ the nucleus. Schematic illustration of an (b) isodesmic and (e) nucleation–elongation processes represented as a function of concentration, rate of "bad solvent" and temperature. Evolution in Gibbs free energy ($\Delta G$) for (c) isodesmic and (f) cooperative mechanisms along the polymerization process. The $\Delta G$ of the processes is represented as a function of the degree of polymerization (DP). $\Delta G_e$ = Gibbs free energy for the elongation step; $\Delta G_n$ = Gibbs free energy for the nucleation step (reproduced from ref. 76 and 96).
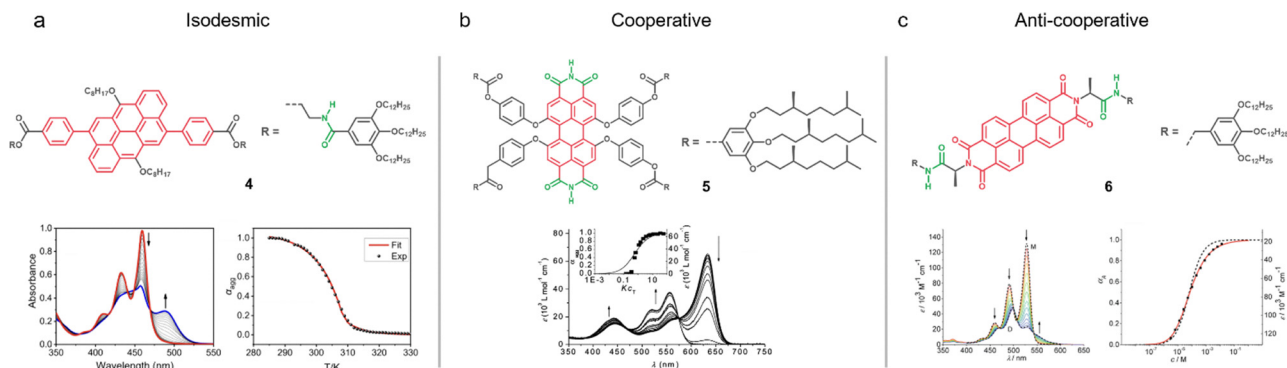
**Fig. 5** (a) Molecular structure of compound **4**, and the corresponding temperature dependent UV/vis absorption study and the aggregation curve fitted to an isodesmic mechanism. (reproduced from ref. 78, with permission of Wiley-VCH GmbH, copyright 2025) (a) Molecular structure of compound **5**, and the corresponding concentration dependent UV/vis absorption study and the experimental aggregation curve (inset, black dots) (reproduced from ref. 84, with permission of the American Chemical Society, copyright 2009). The solid line shows the theoretical curve for an isodesmic mechanism, while the non-sigmoidal experimental data indicate the operation of a cooperative mechanism. (c) Molecular structure of compound **6**, and the corresponding concentration dependent UV/vis absorption study and the experimental aggregation curve fitted to an anti-cooperative mechanism (reproduced from ref. 82 with permission of the Royal Society of Chemistry, copyright 2015).

can be deduced from the sigmoidal trend of the variable temperature aggregation curve (Fig. 5a). The authors do not provide an explanation for the isodesmic nature of this system; however, we assume that the molecular structure is not fully planar, which partially disrupts the concomitant H-bonding and $\pi$–$\pi$ interactions, thereby preventing cooperativity in the self-assembly process. Other relevant examples of isodesmic H-bonded supramolecular polymers can be found in the literature, although they remain scarce.[79–81]

**2.1.2. Nucleation-elongation mechanism.** The nucleation–elongation mechanism involves two distinct stages, the nucleation and the elongation steps, which take place consecutively. Initially, during the nucleation stage, a nucleus, that can be a dimer, a trimer, a tetramer… is formed.[82] Once this critical threshold is surpassed, elongation proceeds, and the nucleus starts to grow to form bigger aggregates (Fig. 4d and e). Each stage is governed by different association constants: $K_n$ for the nucleation step and $K_e$ for the elongation step, implying that the amount of free energy required for the formation of the nucleus is different from the amount needed for the elongation of the polymer (Fig. 4f).[76]

The elongation-nucleation mechanism encompasses two sub-types: cooperative and anti-cooperative. To distinguish the cooperative and anti-cooperative mechanisms is useful to calculate the cooperativity factor ($\sigma$), defined as $\sigma = K_n/K_e$. For the cooperative mechanism $\sigma$ value must be $\sigma < 1$, implying that the nucleation step is less favourable than the elongation one. On the other hand, if $\sigma > 1$, the nucleation step is more favourable, and the self-assembly mechanism can be stablished as anti-cooperative.[83] In the case that $\sigma = 1$, an isodesmic mechanism operates.

In H-bonded $\pi$-conjugated supramolecular polymers, the most common mechanism is the cooperative one, characterized by a more favourable elongation step compared to the nucleation one. This mechanism often results in the formation of long supramolecular fibres. In a reference study, Würthner and coworkers presented a chiral PBI twisted scaffold (**5**) that

self-assembles forming J-aggregates *via* H-bonding interactions between diimide groups following a cooperative mechanism (Fig. 5b). This fact could be demonstrated through concentration-dependent experiments.[84] The corresponding aggregation curve, obtained by plotting $\alpha_{agg}$ *vs.* $KC_T$, describes a non-sigmoidal behaviour characterized by a sharp increase of $\alpha_{agg}$ once reaching a critical concentration (Fig. 5b).

When the nucleation constant ($K_n$) is larger than the elongation constant ($K_e$), the mechanism becomes anti-cooperative. This results in the formation of short oligomers with narrow size distributions due to the less favourable elongation step.[8,85] This mechanism was observed for the PBI **6** functionalized with two chiral amino acids with benzylamine groups and solubilizing pendants (Fig. 5c).[82] For the first time an anti-cooperative supramolecular polymerization mechanism could be elucidated in detail from the theoretical point of view using a new $K_2$–$K$ model (Fig. 5c) derived from the previous model reported by R. F. Goldstein and L. Stryer.[86] Following this work other examples of H-bonding chromophores were found to assemble *via* the anti-cooperative mechanism.[83,87] This polymerization mechanism is relatively uncommon, but the resulting materials are of interest due to their short length, and inefficient packing, which in some cases has been found to be advantageous for preserving the emission properties of the monomer.[87]

As previously mentioned, the presence of H-bonding units in the monomer scaffold plays a critical role in the polymerization mechanism. Importantly, the interplay of two non-covalent interactions (H-bonding and $\pi$–$\pi$ stacking) during the polymerization process seems to promote the cooperative mechanism. Indeed, various studies compared similar scaffolds with amide *versus* ester groups, consistently supporting this statement.[78,88]

## 2.2. Methodologies to determine supramolecular polymerization mechanisms

Under thermodynamic equilibrium, the monomer and aggregated species coexist in a constant ratio. Importantly, this ratio is highly sensitive to experimental conditions, and therefore the

This journal is © The Royal Society of Chemistry 2025

*Chem. Soc. Rev.*, 2025, **54**, 11659–11698 | **11665**

polymerization mechanism is studied by systematically varying the experimental conditions.[8] Several methods are available to monitor these processes, which can be followed using various experimental techniques. The three most widely used approaches to experimentally determine the supramolecular polymerization mechanism are the concentration-dependent, solvent-dependent, and temperature-dependent methods.

The experimental curves obtained from these experiments can be fitted by applying the corresponding mathematical model, which permits extracting the association constants and thermodynamic parameters for the system. In the last few years, several authors have laid the theoretical foundation for understanding the behaviour of supramolecular systems. The $K_2$–$K$ model described by Goldstein and Stryer[86] and its extension to anti-cooperative mechanism by F. Würthner and coworkers,[82] the nucleation-elongation model by Zhao and Moore[89] or the van der Schoot model[90] are just a few examples of the vast work performed in this field.[91–93] Also it is worth remarking the work from ten Eikelder and coworkers in the study of more complex systems and coassemblies.[94,95] Details about these mathematical models are out of the scope of this review.

In concentration dependent experiments the $\alpha_{agg}$ is plotted *versus* the concentration normalized with the elongation constant $K_e$,[82] according to the appropriate mathematical model. Variable concentration experiments are technically demanding, due to the several solutions that must be prepared, which sometimes implies the lack of data points and poor fitting to the mathematical models.[96] The concentration dependent experiments are essential to apply the Goldstein-Stryer $K_2$–$K$ mathematical model to describe anti-cooperative systems.[86,97]

In variable-temperature experiments, changes in the degree of polymerization ($\alpha_{agg}$) are monitored as a function of temperature. This is the most widely used procedure to assess the polymerization mechanisms due to its simplicity and the high numbers of data points that can be automatically obtained, leading to more reliable experimental curves.[96] However, this methodology is sensible to kinetic effects. To mitigate these kinetic effects, the experiments can be carried out at relatively slow heating/cooling rates. The comparison of the heating and cooling curves is usually utilized to evaluate the magnitude of the kinetic effects in the system.[8]

Finally, solvent-dependent experiments are carried out at constant concentration and temperature in mixtures of two solvents, a "good solvent" and a "bad solvent". Good solvents are those that solvate the monomer effectively, while bad solvents promote aggregation. In this context, in solvent dependent or "denaturation" experiments the degree of aggregation ($\alpha_{agg}$) is monitored as a function of the ratio of good/bad solvent and fitted to the appropriate model.[68] The use of this technique has spread in the last few years due to its simplicity compared to the concentration dependent methodology and the higher reliability compared to the temperature dependent one which is sensible to kinetic effects and the sample decomposition at higher temperatures.[98]

## 2.3. Common techniques to study supramolecular polymers

A combination of complementary techniques is typically employed not only to characterize the polymerization processes itself, but also to elucidate the structural features and morphology of the resulting supramolecular polymers.[3,99,100]

Nuclear magnetic resonance (NMR) spectroscopy provides detailed insights into binding interactions and the dynamics of reversible association.[101] NMR enables the monitoring of polymerization processes as a function of temperature or concentration, typically at relatively high concentrations ($>10^{-4}$ M). Moreover, by more complex NOESY/ROESY or DOSY experiments it is possible to extract information about the supramolecular interactions in the system and the size of the supramolecular polymers. Other spectroscopic methods, such as UV/vis absorption and fluorescence spectroscopy, have proven particularly powerful for tracking the aggregation behaviour at lower concentrations. Remarkably, these techniques are especially well suited for studying π-conjugated polymers due to their absorption/emission profiles in the UV, visible or near infrared (NIR) regions. Related spectroscopic techniques like circular dichroism (CD) and circularly polarized luminescence (CPL)[102] can be used to study chiral systems. In addition to the techniques mentioned above, Fourier-transform infrared (FT-IR) spectroscopy is frequently used to monitor the formation and strength of H-bonds within the assemblies.[103]

Supramolecular polymerization processes can also be investigated using calorimetric techniques, including differential scanning calorimetry (DSC) and isothermal titration calorimetry (ITC), which provide quantitative data on the thermodynamics of the self-assembly processes.[104]

Light scattering,[105] along with X-ray and neutron scattering,[106] are widely used to determine the morphology and size of supramolecular assemblies in the solution state. However, the morphologies of the aggregates are often studied in the solid state by microscopic techniques after deposition of liquid samples on substrates and evaporation of the solvent. Atomic force microscopy (AFM)[107] and transmission electron microscopy (TEM)[108] provide direct visualization of nanoscale morphology and hierarchical organization at nanometre resolution.

The integration of theoretical calculations into the study of supramolecular polymers has proven increasingly valuable, offering a complementary perspective to experimental approaches and deepening our understanding of the underlying molecular processes.[109] Computational methods such as density functional theory (DFT) allow for the precise modelling of non-covalent interactions at the atomic level, helping to elucidate the structural features and energetics of monomer association.[110] More recently, Grimme's GFN2-xTB method,[111] a semiempirical tight-binding approach optimized for large systems, has been increasingly used to model supramolecular assemblies. This method efficiently models non-covalent interactions, including dispersion forces, through advanced treatments of atomic multipole moments and self-consistent incorporation of the D4 dispersion model. It provides reliable

**11666** | *Chem. Soc. Rev.*, 2025, **54**, 11659–11698

This journal is © The Royal Society of Chemistry 2025

geometries and interaction energies, making it well-suited for studying the structure and stability of supramolecular polymers. On the other hand, molecular dynamics (MD) simulations allow the exploration of the dynamic behaviour and structural evolution of supramolecular polymers over time, providing insight into assembly pathways, stability, and responsiveness to external stimuli at the molecular level.[112–114]

# 3. Monomer design in π-conjugated supramolecular polymers

Given the electronic factors that are involved in the self-assembly of π-conjugated molecules, precise control over aggregation processes is essential to obtain supramolecular polymers with the desired morphology, molecular packing, and functional properties. One of the most effective strategies for guiding self-assembly is rational monomer design. By carefully selecting the structural configuration and combining different functional groups within the monomer structure, it is possible to program its spontaneous assembly into well-defined supramolecular architectures. Importantly, rational monomer design does not only enable to gain control over the self-assembly under thermodynamic conditions but can also affect the kinetics of the process, generating in some cases pathway complexity (see Section 7).

In the design of π-conjugated supramolecular polymers, the key structural element is the chromophore or π-conjugated scaffold, which provides the optical properties and promotes assembly through π–π stacking interactions. The nature of the π-conjugated core, its planarity, the presence of heteroatoms, and the extent of conjugation determine the electronic properties of the system, including its absorption and emission characteristics. Simple π-conjugated scaffolds typically exhibit poor solubility in water and in many organic solvents, which limits the study of their self-assembly behaviour in solution. To address this, π-conjugated monomers are commonly functionalized with solubilizing groups (Fig. 6), which vary depending on the solvent used. For example, alkyl chains are often introduced to improve solubility in low-polarity organic solvents such as methylcyclohexane (MCH), while oligoethylene glycol (OEG) chains provide solubility in polar media. In this context, the 3,4,5-tris(alkyloxy)benzene unit is a widely used solubilizing motif, known not only for enhancing solubility in organic solvents but also for imparting liquid-crystalline behaviour.[29] To gain further control over self-assembly, H-bonding units are frequently incorporated. These are typically positioned either in the linker between the conjugated core and the solubilizing groups (Fig. 6) or, in some cases, are directly integrated into the core itself. Amides are the most employed H-bonding functionalities in the development of H-bonded π-conjugated polymers, although other groups such as ureas, imides, and related motifs have also been successfully utilized (Fig. 2e).

Monomer design influences the self-assembly process and consequently the molecular packing and morphology of the outcome supramolecular structure. As discussed before the
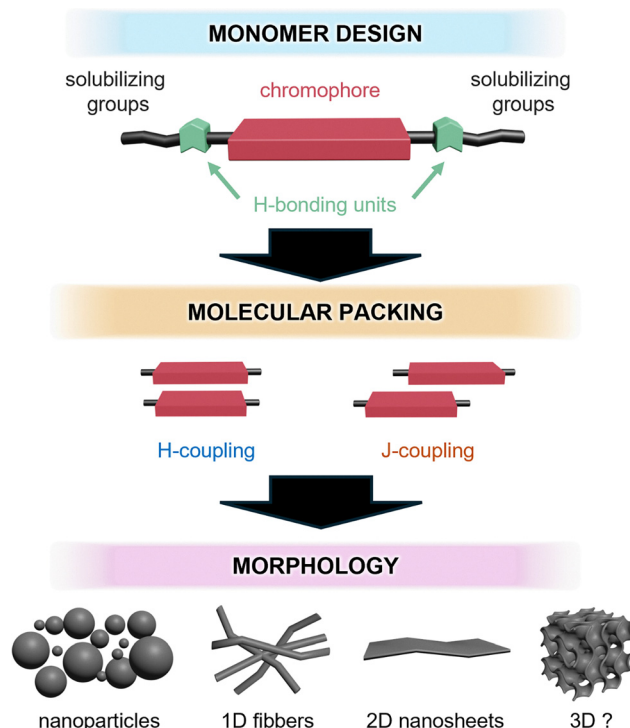


Fig. 6 Outlook on the general monomer design structure for developing H-bonded π-conjugated supramolecular polymers, and the possible molecular packing modes and morphologies of the resulting assembled structures.

molecular packing is critical for the material properties as for example in the formation of H- or J-aggregates (Fig. 6). However, the morphology of the aggregates is also relevant for their anisotropic features and their potential applicability. Most π-conjugated supramolecular polymers consist of 1D assemblies (Section 4), which are among the most accessible to characterize. Notably, regardless of monomer design, many systems also form particle-like aggregates ranging in size from nanometres to microns (Fig. 6). These aggregates are often ill-defined and are typically not classified strictly as supramolecular polymers due to their discrete nature, although they are frequently observed as kinetically trapped species (Section 7) and remain relevant to the self-assembly landscape. As a variation of 1D supramolecular polymers, helical structures have proven highly relevant for fundamental studies of chirality and for advanced functional applications (Section 5).[8,102] In recent years, two-dimensional (2D) supramolecular polymers have also attracted increasing attention (Section 6), although their modes of assembly remain under active investigation.[115] In contrast, far less is known about ordered three-dimensional (3D) supramolecular structures (Fig. 6).[116] While these assemblies are relevant in liquid-crystalline states,[117] their formation and stabilization in the solution state is probably hindered by challenges such as precise 3D assembly control and uncontrolled precipitation/crystallization of the final species.

Increasing attention has recently been directed not only toward single-component systems but also towards more complex, multicomponent assemblies, as copolymers, which

This journal is © The Royal Society of Chemistry 2025

Chem. Soc. Rev., 2025, 54, 11659–11698 | 11667

offer new opportunities for understanding hierarchical organization and emergent functionalities.[118] Multicomponent systems share a symbiotic relationship with other areas of supramolecular polymerization. For instance, they have proven to be essential in the discovery and development of the chirality amplification phenomenon (Section 5). Moreover, kinetic control and pathway complexity (Section 7) have enabled the formation of a wide variety of copolymers, particularly block copolymers,[119–121] which were largely inaccessible through thermodynamic control, with only a few notable exceptions.[122,123] Despite some specific examples, the design and development of supramolecular co-polymers will not be largely discussed in this review. For a more comprehensive overview of supramolecular copolymerization, readers are referred to several excellent and exhaustive reviews already available in the literature.[124–128]

# 4. 1D supramolecular polymers

In this section, we provide an overview of the various types of H-bonded π-conjugated 1D supramolecular polymers, highlighting key monomer design features that govern their formation and properties. In particular, we will discuss four distinct types of 1D assemblies: simple stacked, complex/tubular, main-chain, and stranded architectures.

## 4.1. Simple stacked assemblies

Organic π-conjugated molecules spontaneously assemble into 1D polymers through π–π stacking interactions along the polymer axis. This type of assembly facilitates the overlap of the molecular orbitals and the corresponding excitonic coupling, providing in turn electron/hole transport. An early example of such 1D assemblies was reported by Aida for the amphiphilic porphyrin 1 (Fig. 2a) that forms H-type aggregates according to the UV/vis experiments.[36] However, such π-stacked polymers are often weakly bonded and can exhibit highly dynamic behaviour, particularly in terms of rotational and translational order. The introduction of H-bonding units into the monomeric structure significantly strengthens the non-covalent interactions. In the common monomer design, the chromophore central core is surrounded by H-bonding units, and the corresponding supramolecular polymers are fibrillar structures where the aromatic cores align at the centre, stabilized by peripheral H-bonds along the fibre axis (Fig. 7, centre). The enhanced stability of these assemblies arises from the cooperative interplay between π–π stacking and H-bonding, both operating along the stacking direction, leading to reinforced 1D supramolecular polymers. As a result, these polymers typically exhibit cooperative self-assembly mechanisms, giving rise to long, stable fibrillar structures, which, depending on the conditions, can entangle and form gels.[129]

Many examples of π-extended supramolecular polymers incorporating H-bonding units were inspired by BTA systems, which are well known for engaging in directional triple H-bonding and π–π stacking, leading to the formation of fibre-like assemblies (Fig. 7).[130,131] For example, a $C_3$-symmetric oligo phenylene ethynylene(OPE)-based tricarboxamide 7 was reported to self-assemble through multiple hydrogen bonds
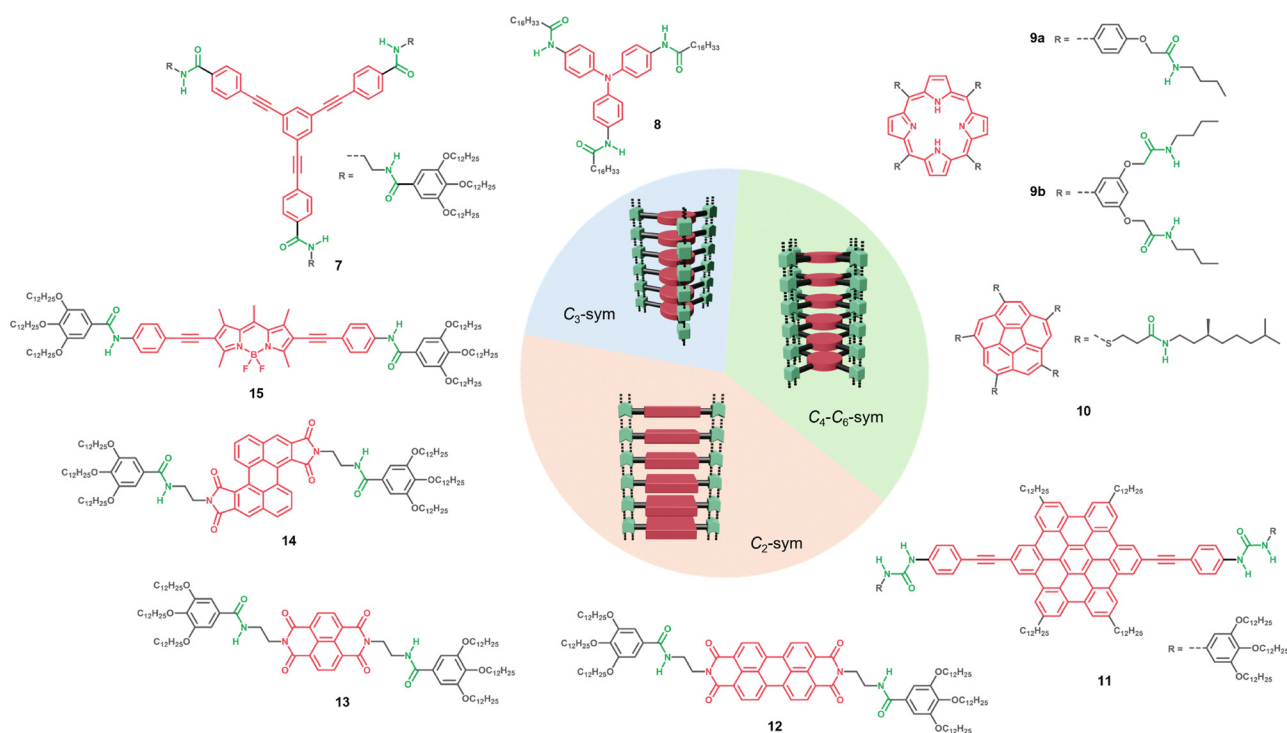


**Fig. 7** Schematic representation of simple-stacked 1D assembly structures depending on their symmetry (sym) and the molecular structures of monomers **7–15**. $C_3$-sym (**7** and **8**), $C_4$–$C_6$-sym (**9a**, **9b**, **10** and **11**) and $C_2$-sym (**11–15**).

**11668** | *Chem. Soc. Rev.*, 2025, **54**, 11659–11698

This journal is © The Royal Society of Chemistry 2025

and π–π stacking interactions, forming 1D assemblies that further entangle to create gels.[132] Importantly, in this example each of the three arms of the central core was functionalized with two amide groups reinforcing the interaction strength and cooperativity in the system. A similar behaviour was observed for the tris-amide triarylamine **8**, which also forms 1D H-bonded assemblies.[133] Remarkably, the triarylamine core provides the resulting polymer distinctive electronic, magnetic, and optical properties, indicating potential applications in organic electronics and spintronics.[134]

Other examples rely on disk-like π-conjugated monomers that typically exhibit a higher degree of symmetry, where the chromophore unit offers two to six functionalization sites for the incorporation of H-bonding motifs and solubilizing groups. A notable example of a supramolecular polymer formed from a monomer with $C_4$ symmetry was reported by the Shinkai group.[135] The porphyrin derivative **9a** is functionalized with four amide groups and four lateral alkyl chains and forms organogels in different solvents based on fibrillar H-aggregates. Interestingly, when the number of amide groups is increased (**9b**), the new configuration leads to the formation of J-aggregates, maintaining the one-dimensional fibrillar structure. This represents a remarkable example of how closely related compounds, forming polymers with similar morphologies, can exhibit distinct molecular packing and optical properties. In another example, Aida reported a $C_5$-symmetric corannulene **10**, functionalized with five alkyl chains via amide linkages.[136,137] This bowl-shape molecule presents different monomeric conformations (discussed in Section 7.2), but under the appropriate conditions self-assemble by multiple H-bonds forming a 1D stacked supramolecular polymer. Klaus Müllen and co-workers[138] reported a hexabenzocoronene **11** functionalized with urea moieties at two of the six peripheral positions. This design leads to the self-assembly of the monomers via complementary H-bonding and π-stacking. The other four peripheral positions are functionalised with alkyl chains which provides solubility in organic solvents.

In many cases, the substitution pattern of the π-conjugated monomers is dictated by the shape of the chromophore as well as synthetic limitations. In this context, the design of linear π-conjugated monomers with $C_2$ symmetry has been widely utilized in the field. Representative examples of $C_2$-monomer designs leading to stacked 1D assemblies were reported using the rylene diimide derivatives, known for their highly conjugated aromatic cores and for their electron deficient nature.[29,139] For example, Würthner[34] and Shinkai[140] reported PBI **12** and NDI **13**, forming supramolecular polymers with excellent gelation properties in apolar solvents. More recently, Sánchez and coworkers reported the Z-shaped PBI **14**.[65] Remarkably, this unconventional molecular design leads to the formation of distinct aggregates, including a thermodynamically stable species that exhibits null exciton coupling. This so-called "null aggregate" is characterized by an absorption spectrum nearly identical to that of the monomer, but slightly red-shifted.

In another example based on a rod-like molecule, Fernández and coworkers reported the planar BODIPY dye **15** bearing two amide groups on both sides.[88] In this case the molecular structure promotes 1D stacking via synergistic H-bonding and π–π interactions, as it was also observed in compounds **7–14** (Fig. 7). However, it should be highlighted that not all the $C_2$-symmetry monomer designs lead to this type of 1D assembly.[44] For instance, the similar molecular design of **15** but using a benzodithiophene core instead of BODIPY leads to the formation of nanoparticle-like H-bonded assemblies, in which 1D growth is hampered due to distortions in the aromatic backbone upon the polymerization process.[83]

## 4.2. Complex stacked and nanotubular assemblies

Section 4.1 discussed examples of π-conjugated supramolecular polymers formed through the cooperative interplay of two non-covalent interactions along the same dimension. However, in other cases, supramolecular polymers are built by two orthogonal non-covalent interactions that do not act cooperatively or along the same spatial dimension. This often leads to the formation of more complex architectures. In many of such systems, the monomers are carefully designed to first assemble via H-bonding into discrete supramolecular entities, such as dimers or macrocyclic oligomers composed of various units. These discrete entities can be considered a class of supramolecular monomers that subsequently undergo further self-assembly, through π–π stacking interactions or secondary H-bonding motifs, into polymeric structures. Depending on the nature of the initial supramolecular monomers, the resulting polymers can form either fibrillar or tubular structures (Fig. 8).

One of the first examples of this type of assembly was reported by Meijer, Würthner and coworkers.[141,142] They described the self-organization of PBI **16** and melamine scaffolds through the formation of complementary H-bonds between the two units. The PBI was designed with phenoxy groups at the four bay positions, leaving the imidic positions free to enable H-bonding interactions with melamine. Although the exact supramolecular interaction modes were not clearly reported, it was proposed that a rosette-like structure is formed initially, which subsequently stacks into one-dimensional polymers. AFM experiments revealed the formation of fibrillar assemblies (Fig. 8a).

Another important relevant π-conjugated scaffold used to create this type of assembly is the oligo phenylene vinylene (OPV). Meijer and coworkers described an unsymmetrically functionalized OPV with a diamino triazine moiety and a wedge-shaped solubilizing group (**17**).[143] This design enables the self-assembly of the molecules into hexameric rosettes that further organize into supramolecular tubules (Fig. 8b). Later, they designed a similar OPV, but instead of the diamino triazine moiety, they inserted an ureidotriazine unit (**18**).[144,145] This modification led to the molecules to form dimeric H-bonded species that subsequently stack forming a 1D helical stack (Fig. 8c). In a following work, OPV **18** was combined with the PBI **16** to form trimeric discrete supramolecular units that co-assemble forming a chiral 1D

This journal is © The Royal Society of Chemistry 2025

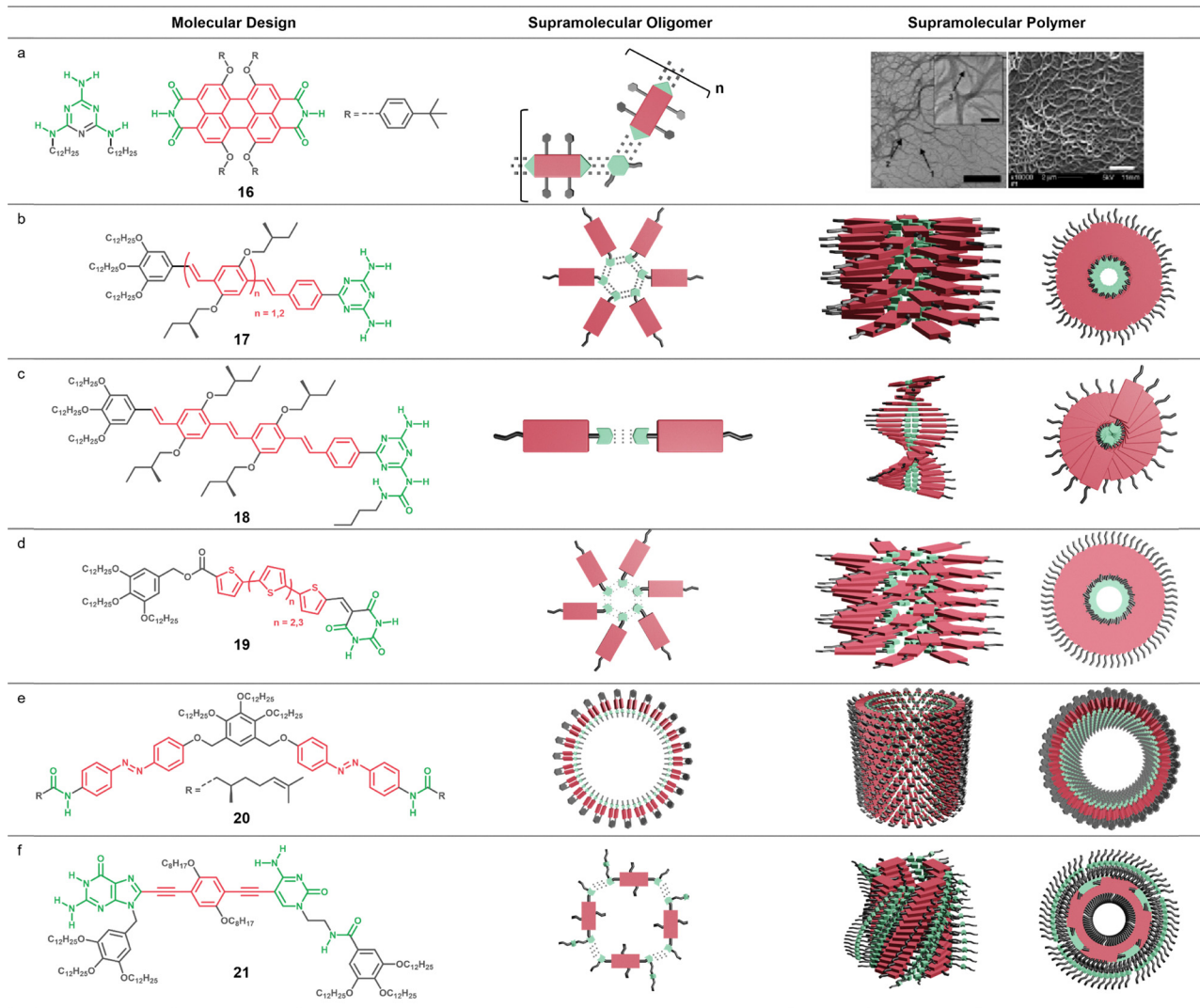*Chem. Soc. Rev.*, 2025, **54**, 11659–11698 | **11669**

Fig. 8 Molecular design, supramolecular oligomer scheme and supramolecular polymer assembly of discrete 1D supramolecular assemblies. (a) PBI **16** assembly with melamine (reproduced from ref. 142 with permission of Wiley-VCH Verlag GmbH & Co. KGaA, Weinheim, copyright 1999). (b) Rosette assembly of OPV **17**. (c) Dimer-based assembly of OPV **18**. (d) Rosettes and nanotube assembly from **19**. (e) Nanotoroidal assembly of bisazobenzene **20**. (f) Nanotubes formed by cytosine and guanine units in **21**.

supramolecular polymer *via* π–π stacking interactions.[146] The three-component supramolecular entity was formed through complementary H-bonding between the imide groups of the PBI and the ureidotriazine units in a 1:2 ratio. This system incorporates both donor and acceptor chromophores and was proposed for photovoltaic applications.

Yagai's group reported a family of barbiturate functionalized π-conjugated systems forming different assembled structures.[147–149] For example, the thienyl[oligo(hexylthiophene)]s **19** utilized the barbiturate unit to form H-bonded supramolecular rosettes composed of six molecular units.[150] These discrete rosettes follow a second assembly process *via* π–π stacking, forming nanorods (Fig. 8d) that were proposed for photovoltaic applications. The same group also reported the formation of tubular assemblies using scissors-shaped molecules.[151–153] This design is based on a bisazobenzene molecule functionalized with two amide groups

and two chiral side chains (**20**). This molecule assembles through a combination of π–π stacking and H-bonding, forming nanotoroidal structures that were clearly observed by AFM. Remarkably, further assembly of these toroidal structures *via* additional π–π stacking interactions led to the formation of nanotubes (Fig. 8e).

A similar strategy was applied by the González group that exploited complementary interactions between nucleobases to develop tubular assemblies.[154] For example, molecule **21** couples a 1,4-diethynylbenzene core with a cytosine and a guanine units, functionalized with benzylic wedges to enhance solubility in organic solvents (Fig. 8f).[155] Importantly, an amide group was introduced into the alkyl chain linking the nucleobase and the dendron **21**. This specific design enables a two-level hierarchical self-assembly process: first, a cyclization in which the monomers interact *via* H-bonding to form a cyclic tetramer; and second, an elongation step where these tetramers stack to

**11670** | *Chem. Soc. Rev.*, 2025, **54**, 11659–11698

This journal is © The Royal Society of Chemistry 2025

form a tubular structure. In this second process, both π–π interactions and H-bonds between the amide groups stabilize the nanotubes along the stacking direction (Fig. 8f).[156,157] These systems were shown to be useful for innovative host–guest functions.[158,159]

### 4.3. Main-chain assemblies

The π-conjugated supramolecular polymers described before are formed via the interplay of two non-covalent interactions, the H-bonds and the π–π stacking, resulting mainly in assemblies based on the stacking of the chromophores. In contrast, main-chain supramolecular polymers feature repeating units connected through end-to-end reversible interactions, such as H-bonds, giving rise to a chain-like supramolecular backbones (Fig. 9a).[160,161] This design generally prevents the excitonic coupling between chromophores but still permit the charge transfer processes between adjacent units.

Earliest examples of H-bond-driven main-chain type supramolecular polymers were reported by Lehn[37] and Meijer (Fig. 2, compounds 2 and 3).[38,162] In the context of π-conjugated systems, one of the earliest examples was again reported by Lehn and co-workers. They designed two different anthracene derivatives 22 and 23,[163,164] functionalised with two uracil and two 2,6-diacylaminopyridine motifs, respectively. The equimolar mixture of the two compounds leads to the formation of polymeric chains by triple H-bonding interactions (Fig. 9b).

Shifting focus to a different central chromophore, Würthner reported a cyanine design inspired by the Hamilton type receptor system described by Lehn in 2002.[165] The cyanine molecule 24 features a cyanine scaffold functionalized with a barbituric acid moiety on one side and two 2,6-diamidopyridine groups on the other side, also known as Hamilton receptor groups (Fig. 9c).[166] This design enables self-assembly through six directional H-bonds, resulting into a supramolecular polymer that forms a fluorescent organogel under the appropriate conditions.[166]

Meijer and co-workers designed a series of dyes bisfunctionalized with UPy moieties to promote the formation of 1D main-chain supramolecular polymers.[167,168] They reported three distinct emissive monomers based on oligofluorene 25, (OPE) 26, and PBI 27 (Fig. 9c). Each of these chromophores self-assembles into linear supramolecular polymers via UPy-UPy quadruple H-bonding (Fig. 2c). Moreover, when mixed under appropriate conditions, the monomers co-assemble into random copolymers. These mixed assemblies exhibit efficient charge transfer along the polymer backbone, making them promising candidates for application in optoelectronic devices.

### 4.4. Stranded assemblies

It is noteworthy that in conventional main-chain π-conjugated supramolecular polymers, additional π–π interactions between different chains are typically absent. However, in some cases, both end-to-end H-bonding and π–π stacking interactions between π-conjugated monomers can occur simultaneously, leading to the formation of 1D stranded structures in which excitonic coupling emerges. In these assemblies, the chromophores first organize into H-bonded chains, which then further associate through π–π interactions into 1D structures composed of a variable number of strands (Fig. 10a). As a result, the π-surfaces of the chromophores align parallel to the fibrillar axis,[169] an arrangement that differs from that observed in more conventional π-conjugated polymers (Fig. 7). The geometry of the interactions between chromophores, as well as the number of strands comprising each fibre, governs the nature and strength of the excitonic coupling, ultimately influencing the properties of the resulting supramolecular structure.

A remarkable example of stranded supramolecular polymers was reported by Frank Würthner and co-workers and consists of a PBI.[170] PBI 28 is functionalized at the four bay positions with wedge-shaped groups to enhance solubility in organic solvents, while presents N–H groups at the imide positions (Fig. 10b). This design promotes the formation, in MCH, of double-stranded cable-like J-aggregates with high fluorescence quantum yields. The assembly is driven by H-bonds between the imide groups, which guide the formation of linear PBI chains that subsequently associate into double-stranded structures through slipped π–π interactions. In subsequent studies, it was demonstrated that the formation of these J-aggregates proceeds via a cooperative mechanism, and that supramolecular chirality can be induced by incorporating chiral side chains into the monomer design.[84] These PBIs were widely studied as supramolecular materials beyond solution-phase behaviour.[64] Notably, they have been reported to form hydrogels that exhibit temperature-dependent polymorphic behaviour, switching between H- and J-type assemblies.[171] In addition, these systems were shown to form liquid-crystalline columnar J-aggregates in
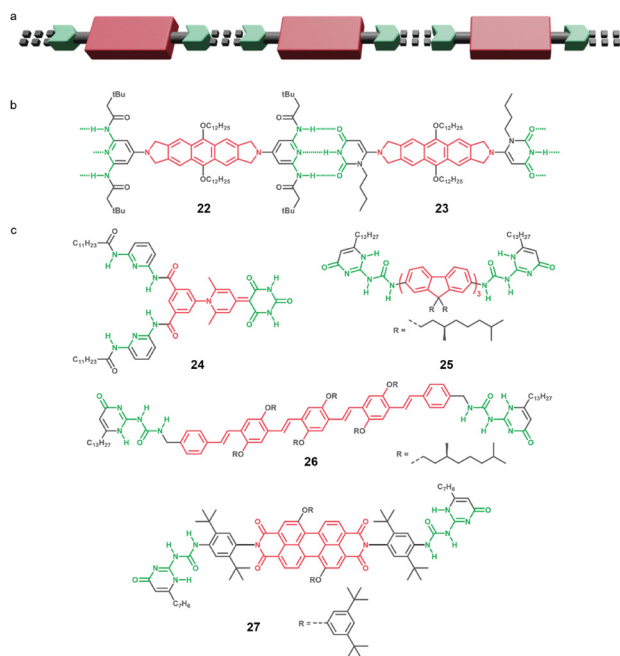


Fig. 9 (a) Schematic representation of a main-chain 1D assembly. (b) Early reported example of main-chain assembly between anthracenes 22 and 23. (c) Molecular structures of compounds 24–27 forming main-chain 1D assemblies.

This journal is © The Royal Society of Chemistry 2025

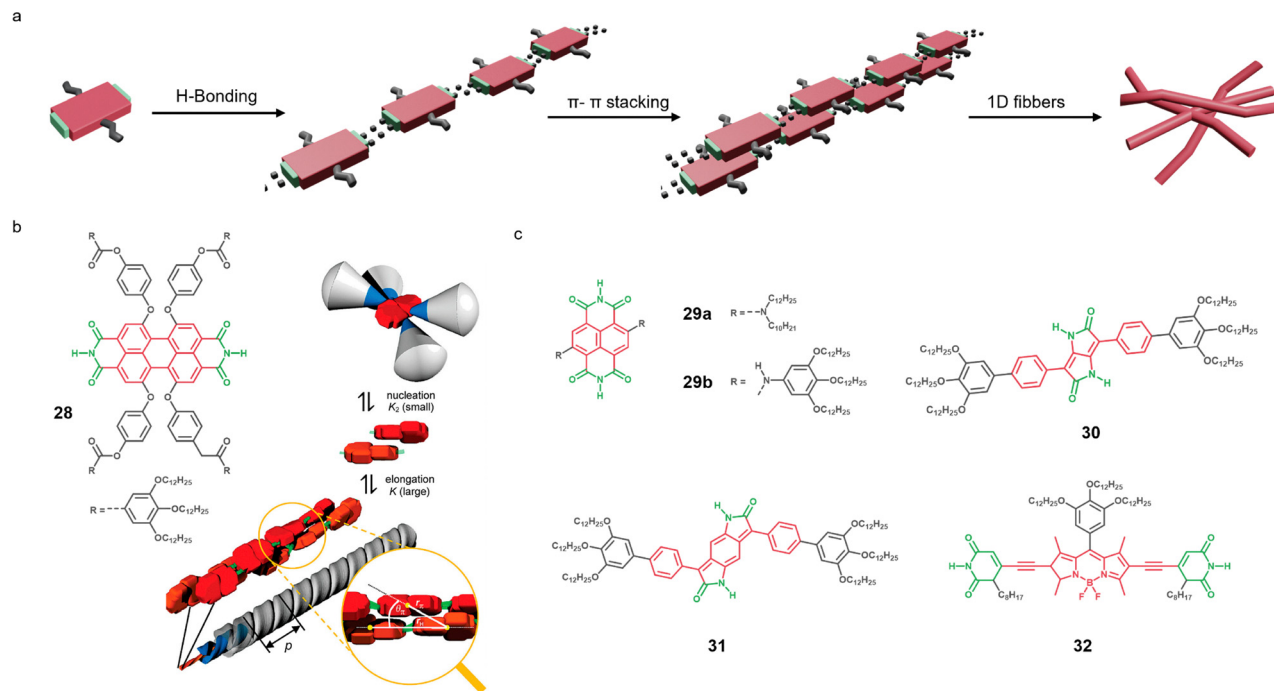Chem. Soc. Rev., 2025, 54, 11659–11698 | 11671

Fig. 10 (a) Schematic representation of the formation of stranded 1D assemblies by H-bonding and $\pi-\pi$ interactions. (b) Earliest example of stranded 1D assembly based on PBI **28** (reproduced from ref. 84 with permission of American Chemical Society, Copyright 2009). (c) Molecular structures of compounds **29–32** self-assembled into stranded 1D supramolecular polymers.

the solid state.[172] Remarkably, solid-state X-ray studies enabled to reveal a correlation between the substitution pattern of the wedge-shaped groups and the number of strands composing the corresponding columnar assemblies.[173]

Similar molecular design was applied to develop NDI stranded supramolecular polymers. Ghosh and coworkers reported NDI **29a** featuring two alkylamino substitutions at the naphthalene positions, while the imidic positions remain unsubstituted (Fig. 10c).[174] This molecular design facilitates self-assembly by H-bonds, into J-type aggregates with a tubular morphology. More recently, it has been described a similar NDI derivative functionalized with wedge-shaped groups (**29b**) (Fig. 10c).[175] This analogue formed fibrillar J-aggregates in MCH and exhibited liquid-crystalline behaviour in the bulk. Interestingly, wide angle X-ray scattering experiments determined the formation of four-stranded columnar liquid-crystalline phase in the solid state.

Such type of stranded assemblies was also achieved with other dyes incorporating lactam units in their core. DPP **30** features two lactam units to enable H-bonding, while the lateral positions are functionalized with wedge-shaped groups (Fig. 10c). The self-assembly process of this compounds follows a nucleation-elongation mechanism.[176] The resulting fibre-like polymers were utilized to prepare anisotropic microfibres by an electrospinning process.[177] The studies in bulk revealed the formation of a columnar liquid-crystalline phase based on a complex assembly mode consisting of the stack of DPP-dimers rotated by 90° forming a quadruple H-bonding motif. More recently, aryldipyrrolidone **31** forming fibrillar stranded assemblies in MCH as well as a liquid-crystalline columnar phase was

reported (Fig. 10c).[178] In all these examples, the realization of solid-state X-ray studies permitted more accurate characterization of the self-assembly mode of the stranded assemblies.

Another molecular design enabling stranded assemblies was reported by Chen and co-workers.[179] They synthesized a BOD-IPY derivative functionalized at the equatorial position with a wedge-shaped group, while the axial positions bear two uracil moieties (**32**) (Fig. 10c). The self-assembly of this compound is driven by H-bonding and slipped $\pi-\pi$ stacking interactions, resulting in J-type aggregates with a fibre/ribbon morphology. Steric effects induced by substituents at the *meso*-position promote the brick-like assembly of the H-bonded strands permitting the J-aggregate formation.

# 5. Chiral supramolecular polymers

Chirality is described as the property of an object that cannot be superimposed on its mirror image, and is ubiquitous in nature, appearing at various scales, from the macroscopic level (*e.g.*, our hands, which are mirror images of each other; Fig. 11a) to the subatomic level (*e.g.*, only left-handed helical neutrinos exist).[180,181] In supramolecular chemistry, chirality is crucial for replicating the stereoselective interactions found in biological systems and for designing functional materials with properties such as CPL, enantioselective recognition, and asymmetric catalysis.[2]

In this line, the self-assembly of monomers endowed with one or more asymmetry (chiral) elements can lead to the formation of homochiral supramolecular polymers, through a
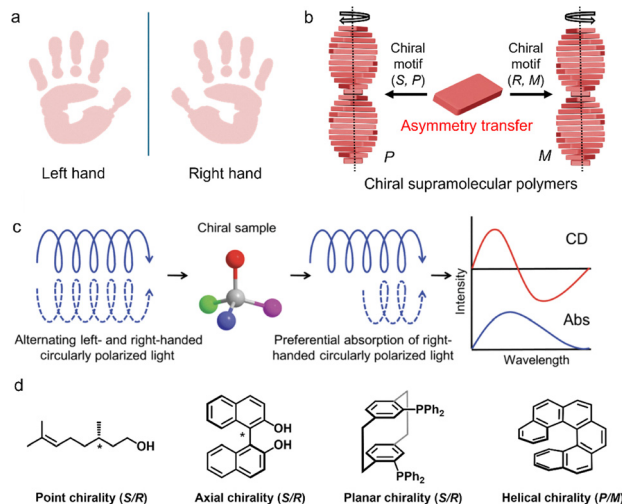
11672 | *Chem. Soc. Rev.*, 2025, **54**, 11659–11698

This journal is © The Royal Society of Chemistry 2025

**Fig. 11** (a) Mirror image of left and right hands as an example of chirality at the macroscopic scale. (b) Schematic representation asymmetry transfer in supramolecular polymers. (c) Schematic representation of circular dichroism (CD) phenomenon (reproduced from ref. 242, with permission of Wiley-VCH Verlag GmbH & Co. KGaA, Weinheim, copyright 2019). (d) Examples of point, axial, planar and helical chirality.

process known as asymmetry transfer (Fig. 11b). In this process, the asymmetry is transmitted from the monomer to the supramolecular structure during the self-assembly. Although it is not necessary, it has been proved that the presence of H-bonding groups in the monomer structure has a positive influence on the transfer of asymmetry.[102] Furthermore, π-conjugated systems are particularly attractive platforms to develop chiral supramolecular polymers due to their inherent electronic properties, which can be enhanced by the introduction of asymmetry.[180] The absorption properties of π-conjugated scaffolds permit the study of supramolecular polymerization by CD, which measures the differential absorption of left- and right-circularly polarized light as a function of wavelength (Fig. 11c). Accordingly, CD spectroscopy emerged as a key tool for the study of chiral supramolecular polymers.

Remarkably, π-conjugated monomers can exhibit various forms of asymmetry (Fig. 11d), which can efficiently render chiral/helical supramolecular polymers. The most common strategy involves introducing point chirality into the monomers, typically by attaching chiral alkyl chains to an otherwise achiral π-conjugated core. Alternatively, monomers based on scaffolds with inherent asymmetry, such as axial or helical chirality, can also be used. Notably, the vast majority of chiral supramolecular polymers are 1D, forming helical fibres (Fig. 11b), although other types of hierarchical chiral assemblies have also been reported.[102] In the following sections, we will examine representative monomer designs that give rise to chiral supramolecular polymers, along with the main approaches used to investigate asymmetry transfer in these systems.

### 5.1. π-Conjugated monomers incorporating point chirality

The incorporation of point chirality into the monomer structure is the most used strategy to assess chiral supramolecular

assemblies. A general monomer design consists of a chromophore functionalized with a H-bonding groups and lateral chains with carbon stereocenters (Fig. 6). Usually one or more chiral centres are introduced in the solubilizing side alkyl chains[137,151,182,183] or in alkyl spacers between the core and the side chains.[118,184] In particular, aliphatic scaffolds of natural origin, like citronellol (3,7-dimethyl-6-octenol) (Fig. 11d) or amino acid derivatives, are utilized. Importantly, the transfer of the asymmetry in the systems is dependent on the number of chiral centres in the monomer, while the spatial distance between the stereocenters and the stacking core has also an influence.[185]

Generally, π-conjugated monomers functionalized with chiral chains form simple 1D stacks with a rotational offset in between molecules, which leads to the induction of helicity (Fig. 11b and 12a, b). Importantly, the helicity of these 1D supramolecular polymers is dictated by the chirality in the alkyl chains (Fig. 11b). One of the first molecules utilized to study chirality in supramolecular polymers was again the BTA analogue (Fig. 2d).[186,187] For example, BTA (*S*)-33 was functionalized with three bipyridine spacers linked to three wedge-shaped solubilizing groups. Importantly, these lateral solubilizing groups incorporated (*S*)-3,7-dimethyloctyl chains, and provided nine chiral centres to the monomer that effectively induced chiral supramolecular polymerization. More recently, L. Sánchez and coworkers studied the asymmetry amplification of other extended BTA analogues as 1,3,5-triphenylbenzenecarboxamides (see Fig. 7, compound 7), OPE-tricarboxamides[188,189] and trisbiphenylamine-tricarboxiamides.[190]

Other $C_3$ N-centered triarylamine trisamides (*S*)-34 and (*S*)-35 functionalized with chiral alkyl chains were also shown to assemble into 1D helical stacks formed by the interplay of triple H-bonds and π–π stacking.[191] In another design, L. Sánchez studied the self-assembly behaviour of chiral N-heterotriangulenes (*S*)-36 and (*R*)-36 in a MCH/toluene mixtures and in CCl$_4$.[192] Remarkably, molecules 34–36 presented pathway complexity (Section 7.1) in their self-assembly processes, forming different helical aggregates with different handedness depending on the experimental conditions. Furthermore, they demonstrated that the branched chiral side chains in (*S*)-36 induce significant kinetic retardation of the polymerization process, compared to the achiral analogue.

In addition to these examples based on $C_3$-symmetric molecules, there are also systems constructed from $C_2$-symmetric monomers. For example, F. Würthner and co-workers designed a PBI (*S*)-37 bearing chiral side chains and two amide groups (Fig. 12b).[193] The authors stated that (*S*)-37 aggregates by π–π stacking and H-bonding forming helical supramolecular polymers. The steric crowding caused by the presence of terminal dimethyl groups in the lateral chains causes the formation of homochiral helical J-type aggregates, while the derivatives bearing simple lineal alkyl chains form achiral H-type aggregates.[193] More recently, L. Sánchez and coworkers designed N-annulated perylene scaffolds bearing four amide groups, and chiral lateral chains, (*S*)- and (*R*)-38 (Fig. 12b).[194]
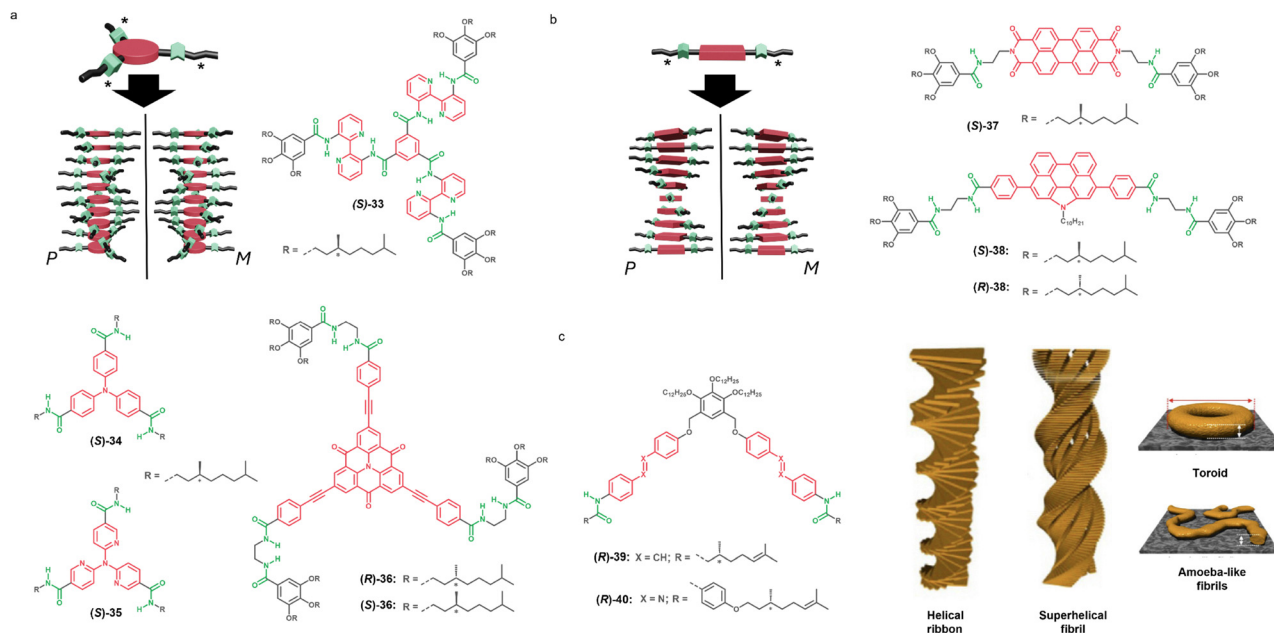
This journal is © The Royal Society of Chemistry 2025

*Chem. Soc. Rev.*, 2025, **54**, 11659–11698 | **11673**

Fig. 12 (a) Schematic representation of the asymmetry transfer in $C_3$-symmetry scaffolds upon aggregation by point chirality and BTA (**S**)-**33**, triarylamines (**S**)-**34** and (**S**)-**35** and N-heterotriangulenes (**S**)-**36** and (**R**)-**36** chemical structures. (b) Schematic representation of $C_2$-symmetry monomer chiral self-assembly and chemical structure for chiral PBI (**S**)-**37** and chiral N-annulated perylenes (**S**)-**38** and (**R**)-**38** (c) Chemical structures of scissor-shaped monomers endowed with point chirality (**R**)-**39** and (**R**)-**40** employed by S. Yagai and coworkers and schematic representation of different supramolecular aggregates than can be observed in the supramolecular polymerization process (**R**)-**39** depending on the molar fraction of the cross-linked specie, namely: helical ribbon, superhelical fibril, toroid and amoeba-like fibrils (reproduced from ref. 196, with permission of Springer Nature, copyright 2015).

Upon self-assembly in organic media, these molecules form P- and M- type helix supramolecular polymers, respectively.

S. Yagai and co-workers have also implemented point chirality to their monomers,[151,153,195–197] but in this case more complex hierarchical chiral supramolecular polymers were obtained instead of the simple stacked assemblies (Fig. 12c). For example, the scissor-schapped stilbene dyad (**R**)-**39**, bearing amide groups and two lateral 3,7-dimethyl-6-octyl chains, self-assembles by π–π stacking and H-bonding forming right-handed superhelical fibrils. Interestingly, upon UV light irradiation the stilbene units suffer a [2+2] photocycloaddition forming a cross-linked dyad which is unable to form well-defined nanoaggregates. However, in the presence of small amounts of these cross-linked species a whole new co-assembly pathway emerges. It is noteworthy to mention that high molar fractions of the cross-linked monomer with respect to **39** deteriorates the aggregation ability. For instance, the presence of only a 0.1 or 0.25 molar fraction of cross-linked monomers triggers the formation of superhelical fibrils with helix inversion, an 0.6 molar ratio produces amorphous amoeba-like fibrils coexisting with annular structures, and the presence of a molar fraction of 0.8 induces the formation of only amoeba-like fibrils.[196] More recently, following a similar molecular design they prepared the scissor-shape dyad (**R**)-**40** bearing two photoresponsive azobenzene units and they studied effects of photoirradiation and secondary nucleation (Section 7.3.3) on the resulting chiral supramolecular arquitectures.[197]

## 5.2. π-Conjugated monomers incorporating axial chirality

Axial chirality is defined as the stereoisomerism that arises from the 3D spatial arrangement of two pairs of substituents around a chiral axis.[198] This type of asymmetry element can be embedded directly within specific π-conjugated scaffolds or introduced into the monomer structure by attaching a chiral axial unit as a pendant group. The synthesis and isolation of these pure chiral compounds is often nontrivial, frequently requiring enantioselective separation of the enantiomers via chiral high-performance liquid chromatography (HPLC).

One of the most relevant examples of supramolecular polymers based on a monomer with axial chirality was reported by S. George and co-workers, combining two NDI units and a binaphthyl core.[199,200] In this design, the main NDI chromophores are achiral, and the pendant binaphthyl unit provides axial chirality to the system (Fig. 13a). The self-assembly behaviour of compounds ((**S**) and (**R**)-**41-42** and (**S**)-**43**) was studied under different conditions including via primary and secondary nucleation events, as well as living supramolecular polymerization (LSP) (Section 7.3). Importantly, despite the strong kinetic effects involved in the system, the pure compounds assemble into 1D stacks whose helicity is dictated by the axial chirality of the pedant binaphtyl group (Fig. 13a). A similar approach to design chiral monomers was applied by utilizing the trans-1,2-bis(amido)cyclohexane moiety linked also to two NDI units.[123,201,202] For example, it has been reported compound (**S,S**)-**44**, with two electron rich NDI units, and compound (**S,S**)-**45** with two electron poor NDI units

**11674** | *Chem. Soc. Rev.*, 2025, **54**, 11659–11698
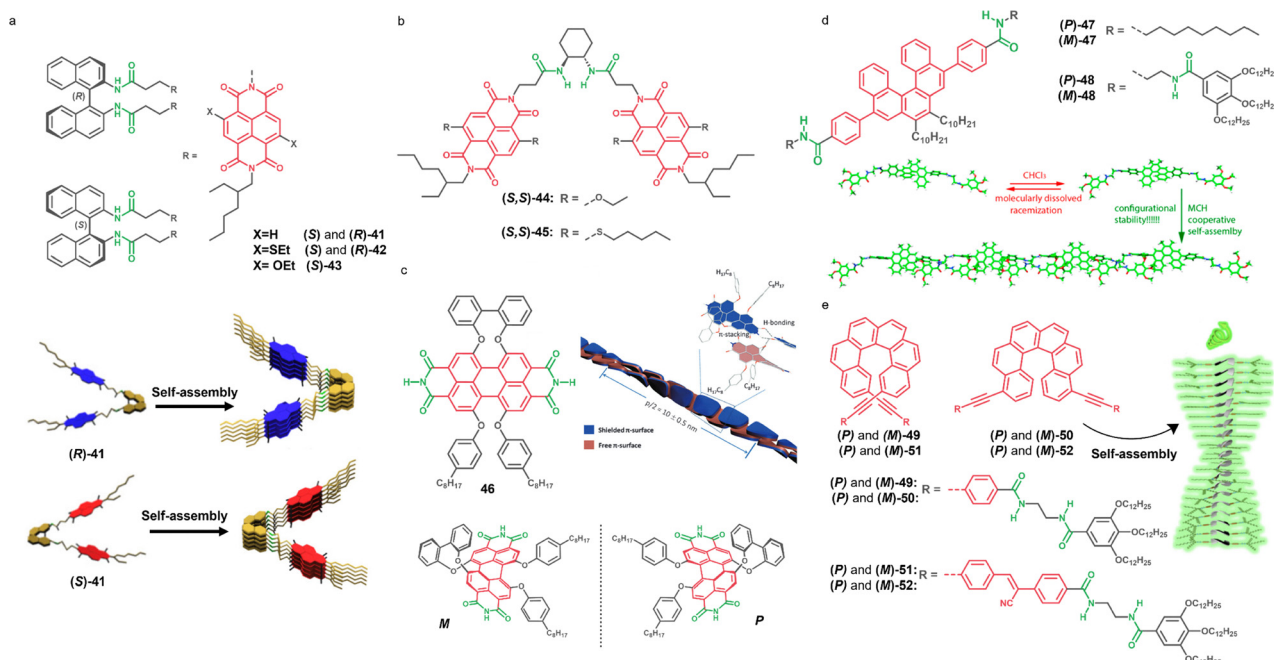
This journal is © The Royal Society of Chemistry 2025

**Fig. 13** (a) Chemical structures of bichromophoric units with axially chiral binaphthyl units **41–43** and schematic representation of the self-assembly for bichromophoric units with binaphtyl axial pendants **(S)-** and **(R)-41** (reproduced from ref. 199 with permission of Wiley-VCH GmbH, copyright 2020). (b) Chemical structure of bichromophoric units with axially chiral *trans*-1,2-bis(amido)cyclohexane moieties **44** and **45**. (c) Chemical structure of core-substituted PBI **46** with a schematic representation of both *M* and *P* atropo-enantiomers *M* and *P* and a schematic representation for the aggregate of the enantiopure M atropo-enantiomer (reproduced from ref. 205 with permission of Wiley-VCH Verlag GmbH & Co. KGaA, Weinheim, copyright 2012). (d) Chemical structure of [5]helicenes **47** and **48** and a schematic representation of the aggregate of the former **(M)-47** in MCH (reproduced from ref. 98 with permission of the American Chemical Society, copyright 2018).(e) Chemical structures of [6]helicenes **49**, **50**, **51**, **52** and schematic representation of the self-assembled structure for **50** and **52** (reproduced from ref. 212 with permission from the Royal Society of Chemistry).

(Fig. 13a). These compounds self-assemble into chiral stacks, and more interestingly the mixtures of the two compounds lead to the formation of block copolymers with controlled stereo-selectivity under thermodynamic conditions.[123]

In other examples, the axial chirality is introduced directly to the main chromophore presenting a permanent chiral axis. With the aim of preventing H-aggregation and favouring J-aggregation, F. Würthner and co-workers developed PBIs with a locked twisted-core by introducing bulky substituents at the bay potions and generating a chiral axis in the π-surface.[203] This initial design was later improved by functionalizing the PBIs with a biphenyl bridge at one of the two bay positions, which facilitated the separation of the two atropoisomers by chiral HPLC.[204] In this line, PBI **46** with N–H groups at the imide positions self-assembles into stranded 1D J-aggregates and its helicity is dictated by the axial chirality of the monomer (Fig. 13c).[205] It is noteworthy that similar helical stranded PBI J-aggregates were also achieved by introducing point chirality in the molecule, specifically through the attachment of wedge-shaped groups bearing chiral alkyl chains at the bay positions (see Fig. 5b, compound **5**).[84]

### 5.3. π-Conjugated monomers incorporating planar and helical chirality

There are various examples of chiral supramolecular polymers based on monomers presenting planar chirality (Fig. 11d),[206–209]

however, these monomers lack either H-bonding groups or chromophoric nature and therefore were not included in this review. In contrast, there are various examples of systems exploiting helical chirality (Fig. 11d). Helicenes are archetypical chiral molecules with strong fluorescence and CPL properties.[210] L. Sánchez and co-workers reported in 2018 two 5,7,8,10-tetrasubstituted [5]helicenes, compounds **(P)-47** and **(M)-47** with two amide groups and compounds **(P)-48** and **(M)-48** with four. The corresponding enantiomers of these compounds could be successfully separated by chiral HPLC of the racemic mixtures, but when left in solution undergo racemization. They stated that **(P)** and **(M)-47** did not form any supramolecular polymer, while **(P)-48** and **(M)-48** could polymerize by a cooperative mechanism due to the presence of the two extra amide groups, demonstrating the relevance of the H-bonding interaction in the supramolecular polymerization process. Interestingly, under the appropriate conditions, the polymerized systems do not suffer racemization. Due to the twisted shape of the helicene moiety, the π–π stacking is not possible, and therefore the resulting assemblies consist of chiral main-chain polymers formed by H-bonding (Fig. 13d).[98]

More recent examples of helicenes in supramolecular polymers are the 2,15- and 4,13- disubstituted [6]-helicenes reported by L. Sánchez and co-workers in collaboration with J. Crassous (Fig. 13e).[211,212] They utilized a 2,15-substituted scaffold to prepare **(P)** and **(M)-49** and **(P)** and **(M)-51**, which assembles with a zig-zag arrangement by H-bonding, since the contorted

This journal is © The Royal Society of Chemistry 2025

*Chem. Soc. Rev.*, 2025, **54**, 11659–11698 | **11675**

shape of the molecule prevents the π–π stacking. In the following work they prepared (*P*) and (*M*)-50 and (*P*) and (*M*)-52.[211,212] In the new compounds, due to the 4,13-disubstitution, the π-surface becomes accessible, resulting in a helical self-assembly by combination of the H-bonding and the π–π stacking interactions (Fig. 13e).

Besides the helical chirality, inherent chirality also has been utilized to prepare chiral supramolecular polymers. Worth to be mentioned, for example, are the corannulene scaffold studied by Aida and co-workers[137] and the subphthalocyanines studied by D. González, T. Torres, E. Ortí and co-workers,[213] among others.

## 5.4. Asymmetry amplification and symmetry breaking

In the previous section, we reviewed various examples of monomeric species capable of forming helical supramolecular polymers as a result of asymmetry transfer from the monomer to the polymer (Fig. 11b). Typical investigations of chiral supramolecular polymers focus on elucidating the mechanism and thermodynamics of the polymerization process, primarily using CD techniques. Additional studies often involve the study of mixtures of a chiral monomer with either an achiral analogue or the corresponding enantiomer. These approaches are valuable for understanding the principles of chirality transfer in supramolecular systems under different conditions. In this context, two of the most representative phenomena are asymmetry amplification and symmetry breaking.

**5.4.1. Asymmetry amplification.** Asymmetry amplification refers to the phenomenon where a small initial chiral bias in the system is enhanced during the assembly process. It was first studied by Green and co-workers in the conventional polymerization of polyisocyanates. During these investigations they discovered two different phenomena: sergeant and soldiers (SaS),[214,215] and Majority rules (MR).[216] These phenomena also occur in supramolecular polymers and were first observed by Meijer and co-workers in extended-core BTAs.[186,217] Briefly, in the SaS experiment, when increasing amounts of a chiral monomer are mixed with an achiral analogue, asymmetry amplification may occur. In such cases, a small number of chiral monomers "sergeants" can direct the helicity of a much larger population of achiral monomers "soldiers".[218,219]

On the other hand, in the Majority rules experiment when monomers bearing opposite chirality (enantiomers) are mixed in varying ratios, asymmetry amplification may lead the predominant monomer to dictate its preferred helicity over the minority enantiomer.[153,220] In both cases, a non-linear increase in the enantiomeric excess (*ee*) is distinctive of the existence of chiral amplification phenomena and can be influenced by different factors, such as the temperature,[221] the number and the positions of stereogenic groups,[189,220] or the shape of the molecule.[222]

A key issue in the asymmetry amplification phenomena is the geometrical complementary of the different monomers and their energetically favoured tendency to co-assemble, if these two factors are not present, self-sorted homopolymers will be obtained and no asymmetry amplification will occur.[102]

The self-assembly mechanism and H-bonding have crucial roles in this process, as scarce examples of asymmetry amplification have been found in isodesmic or slightly cooperative supramolecular polymers.[223,224]

**5.4.2. Symmetry breaking.** Symmetry breaking is a less common way to generate chiral assemblies and refers to the process in which the application of a chiral external stimulus to achiral monomeric units finally yields a chiral aggregate. The application of this external stimulus generates an equimolar mixture of two enantiomers with a slight enantiomeric excess. Many external stimuli can be used, as solvents,[186,225,226] stirring, magnetic field or polarised light.[194,227,228]

## 5.5. Supramolecular polymers exhibiting circularly polarized luminescence (CPL)

As mentioned at the beginning of this chapter, CD has become a fundamental tool to study chiral self-assembly processes of π-conjugated scaffolds. However, more recently, another phenomenon has gained increasing interest in the field due to its potential applications: CPL (Fig. 14a). CPL is the differential emission of left- and right-circularly polarized light from chiral luminophores (single molecule or supramolecular entity) in their excited state. This phenomenon has become one of the cornerstones in the development of functional materials due to its potential applications in several fields such as 3D displaying,[229] encrypted storage and transmission of information,[230,231] chiral sensing,[232–234] or bioimaging.[235,236]

One of the main focuses in this field has been to improve the dissymmetry factor ($g_{lum}$) and consequently the CPL brightness ($B_{CPL}$), both of which are crucial for the performance of any CPL active material.[237–239] The $g_{lum}$ factor can be defined as the parameter that quantifies the difference in luminescence between two enantiomers or as $2(I_L - I_R)/(I_L + I_R)$, where $I_R$ and $I_L$ are the intensity of the right- and left-handed circularly polarized emissions (Fig. 14a), respectively, and its theoretical maximum value is 2. On the other hand, $B_{CPL}$ is expressed as $B_{CPL} = \varepsilon_\lambda \times \Phi_{lum} \times |g_{lum}|/2$, where $\varepsilon_\lambda$ is the molar extinction and $\Phi_{lum}$ is the luminescence quantum yield.

Supramolecular polymerization of π-conjugated systems provides an excellent platform to explore CPL, especially when using chiral monomers with strong photoluminescence and tendency to form ordered chiral aggregates.[240–242] In this context, the formation of low emissive H-aggregates (Section 1.3) is avoided, and instead, the authors have focused on the search of CPL-active J-type aggregates or either aggregation-induced emission (AIE)[243] or aggregation-induced enhanced emission (AIEE).[244]

Luminescent scaffolds utilized to prepare CPL active chiral supramolecular polymers include cyanostilbenes[74,245,246] helicenes,[211,212] and bichromophoric units appended with chiral pendants as the *trans*-1,2-bis(amido)cyclohexane or binaphthyl moieties (see Sections 5.2 and 5.3).[247–251] These systems have shown remarkable $g_{lum}$ and $B_{CPL}$ values through the self-assembly of chiral luminophores.

In addition, S. Ghosh and co-workers designed a chiral sulfur-substituted naphthalene-diimide (*S*)-53 that exhibited

**11676** | *Chem. Soc. Rev.*, 2025, **54**, 11659–11698

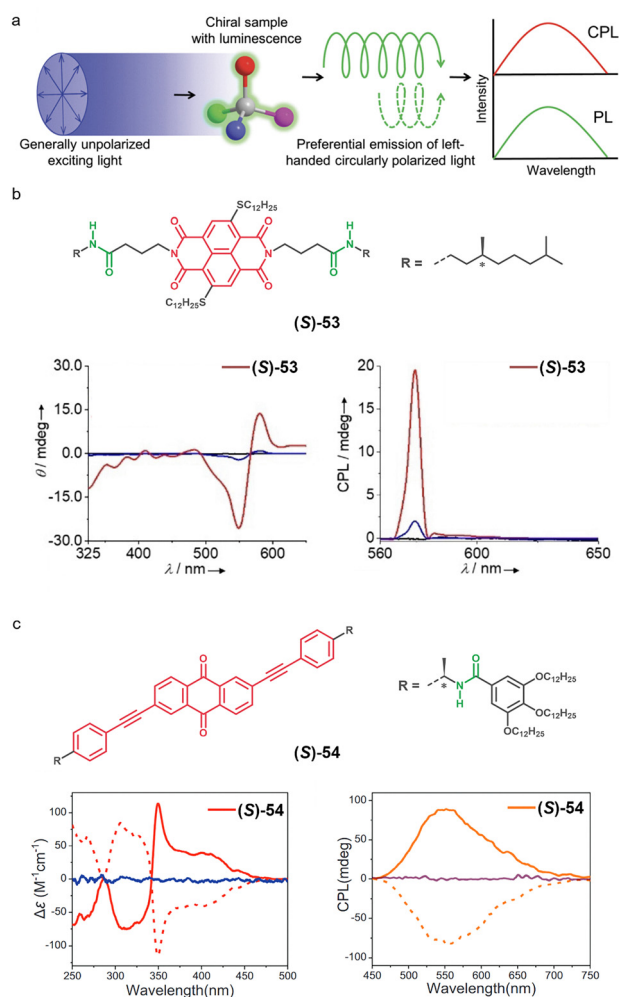This journal is © The Royal Society of Chemistry 2025

**Fig. 14** (a) Schematic representation of the circularly polarized luminescence (CPL) phenomenon (reproduced from ref. 242 with permission of Wiley-VCH Verlag GmbH & Co. KGaA, Weinheim, copyright 2019). (b) Chemical structure of chiral sulfur-substituted naphtalene-diimide **(S)-53** along with its CD and CPL spectra (red lines) in decane/THF (9 : 1) (c = 0.1 mM) (reproduced from ref. 252 with permission of Wiley-VCH Verlag GmbH & Co. KGaA, Weinheim, copyright 2020). (c) Chemical structure of chiral anthraquinone derivative **(S)-54** along with its CD (red line) and CPL ($\lambda_{ex}$ = 365 nm) (orange line) spectra in MCH (c = 20 mM) (reproduced from ref. 239 with permission of Wiley-VCH GmbH, copyright 2025).

Comparative studies with a methylated analogue of **(S)-54** in the amide positions (blocking H-bonding) confirmed the essential role of H-bonds in the aggregation and CPL properties.[239]

Another interesting approach to produce CPL active systems involves the utilization of two components: a helical supramolecular polymer and an achiral emissive chromophore. Liu and co-workers reported the use of 1,3,5-benzenetricarbonyl L-glutamate diethyl ester that gelates forming hexagonal chiral nanotubes which can encapsulate a wide range of guest compounds.[253] In this study, six different achiral luminophores were encapsulated, and in all the cases, the supramolecular polymer matrix was found to be able to transfer the chirality from the gel to the guest molecules, generating CPL-active materials with $g_{lum}$ values ranging from $\pm 0.2 \times 10^{-3}$ and $\pm 1.7 \times 10^{-3}$.

## 6. 2D supramolecular polymers

Most supramolecular polymers based on H-bonded π-conjugated scaffolds have traditionally formed 1D architectures.[7–10] However, probably due to the discovery of the potential of covalent 2D materials, most notably graphene, growing interest has emerged in developing 2D supramolecular polymers.[254] These emerging materials are defined by a self-assembly process of monomers where the polymer is growing in two directions by the interplay of one or more non-covalent interactions. As a result of this growing process, diverse assemblies leading to different 2D morphologies such as nanosheets, spirals, and porous networks have been reported.[255–259]

The earliest approaches to 2D supramolecular polymers were in aqueous environments and relied on amphiphilic monomers composed of hydrophobic π-conjugated cores and hydrophilic side chains.[260–266] M. Lee and co-workers were pioneers in this area, reporting the aqueous self-assembly of an octa-p-phenylene derivative bearing flexible oligoether dendrons. This system formed extended 2D nanosheets in water, establishing a foundational platform that has been expanded with various aromatic cores and solubilizing side chains.[260–266] In general, aqueous assemblies of organic amphiphiles are mainly dependent on the monomer design where the balance of the ratio of the lipophilic and hydrophilic parts defines the morphology of the aggregate. A notable example of hierarchical 2D self-assembly in water includes the work of Montenegro and co-workers, who functionalized a cyclic peptide with apolar residues to guide first the self-assembly into 1D nanotubes via H-bonding and π-stacking and then with directional hydrophobic interactions to form 2D networks.[267]

In organic solvents the obtention of 2D structures is more challenging since it requires a more careful monomer design with the capability to establish directional non-covalent interactions to enable the growth in two dimensions. In this context, hierarchical self-assembly of 1D structures has emerged as a key strategy to achieve 2D polymers. In these systems, monomers first form 1D assemblies, which later associate laterally via secondary non-covalent interactions to generate 2D

H-bonding driven aggregation in decane (Fig. 14b). The cooperative supramolecular polymerization led to J-type aggregates with a fibrillar morphology, confirmed by UV/vis spectroscopy and AFM studies, respectively. Furthermore, CPL spectroscopy studies showed a $g_{lum}$ value of $4.6 \times 10^{-2}$ at the emission maxima, which is among the highest values reported for chiral supramolecular assemblies in solution.[252] More recently, F. Wang and co-workers prepared an anthraquinone derivative with chiral amidic spacers **(S)-54** featuring efficient J-aggregation by π–π stacking and H-bonding. CD spectroscopy corroborated the appearance of a bisignate Cotton signal upon cooling the solution, indicative of the formation of a chiral supramolecular polymer (Fig. 14c). CPL studies revealed a $|g_{lum}|$ value of 0.013 and a $B_{CPL}$ value of 13.8 $M^{-1} cm^{-1}$.

This journal is © The Royal Society of Chemistry 2025

*Chem. Soc. Rev.*, 2025, **54**, 11659–11698 | **11677**

architectures (Fig. 15a). The nature of these secondary interactions is crucial, as their directionality and strength determine the ability of the system to grow in the second dimension. For example, Sugiyasu, Takeuchi, and co-workers reported in a seminal example a family of porphyrins (**55a,b**) self-assembling by H-bonding and π-stacking along one axis and van der Waals interactions between peripheral alkyl chains along the second dimension (Fig. 15b).[268,269] Porphyrins **55a** and **55b** form nanosheets in an organic solvent according to AFM experiments (Fig. 15a, right). Sánchez and co-workers observed a similar behaviour in the N-annulated PBI **56**, achieving J-aggregated 1D stacks that further associate through sidechain van der Waals forces to yield metastable 2D sheets in MCH.[270]

Using more polar organic solvents, Fernández and co-workers utilized amphiphilic bispyridyl Pt(II) complex **57** (Fig. 15b) that also self-assembles into 2D nanostructures in THF/water.[271] In this example, the 2D growth is directed by π–π interactions and orthogonal N–H···Cl H-bonding. In another example, Ghosh and co-workers reported an unsymmetrical NDI derivative **58**, bearing a pendant carboxylic acid group at one of the imide positions, which forms hierarchical 2D assemblies. By modulating the monomer conformation with external additives, they achieved thermodynamically controlled supramolecular polymerization of **58**, driven by synergistic H-bonding and π–π stacking interactions, resulting in the formation of ultra-thin 2D nanosheets.[272] More recently, Tian and co-workers used triphenylamine **59**, with three enaminone-linked pyridine hydrochloride salts at the periphery to obtain H-bonded based 2D assemblies.[273] The resulting assemblies are porous and feature in-plane 1D conduits presenting electron transporting features, which enable a remarkable photocatalytic performance in hydrogen production *via* water splitting.

The hierarchical approximation to develop 2D polymers has also yielded unconventional spiral and toroidal assemblies (Fig. 15c). In non-polar solvents, porphyrin **60**, developed by Sugiyasu and co-workers, self-assembles into a 1D supramolecular polymers that spontaneously coiled into an Archimedean spiral (Fig. 15c). These layered spirals are formed by a nucleation-elongation process and are stabilized by fluorophilic secondary interactions (Fig. 15c).[274] Interestingly, at lower concentrations the same compound produces concentric toroids (Fig. 15c), which can further associate by weaker interactions to yield extended 2D aggregates.[274] The morphology of these exotic spiral assemblies has been well characterized by microscopy experiments (see AFM images in Fig. 15c) when the samples are deposited on surfaces, while their stability in the solution state is not well known. In another example, Sánchez and Yagai reported the on-surface formation of 2D porous networks by the association of nanotoroidal structures based on a scissor-shaped azobenzene dyad.[275]

An alternative and scarcely explored strategy for constructing 2D supramolecular polymers involves the formation of brick-like structures using monomers capable of establishing slipped interactions through one or two non-covalent forces

(Fig. 15d). For example, Shimizu and Soberats designed a bis-urea macrocycle that assembles into brick-like nanosheets *via* directional urea–urea hydrogen bonds.[276] In a similar vein, Würthner and co-workers developed 2D supramolecular polymers from a bis(squaraine) derivative that self-assembles through slipped π–π interactions.[277] This assembly mode has also been reported for a H-bonded π-conjugated system. PBI **61** (Fig. 15d), bearing NH groups at the imide positions, assembles into H-bonded chains in which all molecules adopt the same axial twist (either P or M) due to the flexibility of the molecular structure.[278] The alternating association of P- and M-twisted PBI chains *via* π–π interactions leads to the formation of extended 2D nanosheets (Fig. 15d). Notably, the slipped stacking of the PBI cores in this arrangement results in the emergence of J-type coupling.

# 7. Pathway complexity and controlled supramolecular polymerization

## 7.1. Pathway complexity

Controlling the nanoscale organization of supramolecular polymers based on π-conjugated molecules has proven to be a key challenge for enhancing their optoelectronic properties.[13,17,19] Over the past few decades, significant efforts have been devoted to developing diverse monomeric molecular designs and identifying the structural features that influence the assembly processes.[8,76,279] Other factors such as solvent, temperature, and concentration have also been shown to play a critical role in the thermodynamics of supramolecular polymerization.[8] However, the kinetic aspects of supramolecular polymerization were largely overlooked for many years, despite their crucial importance. Kinetically controlled supramolecular polymerization processes involve more complex scenarios, where intermediate metastable species delaying the progression toward the thermodynamically stable state appear.[280–284] Pathway complexity refers to the coexistence and competition of multiple self-assembly routes that one monomer can follow. Despite this phenomenon was previously observed in various systems,[285–287] the concept gained attention after Meijer and co-workers demonstrated, in 2012, that the self-assembly of the chiral OPV **18** (Fig. 8c) could lead to two competing helical forms: a thermodynamically stable M-type helix and a kinetically favoured P-type helix.[145] Their findings showed that the early-formed P-type helix prevents the direct formation of the more stable M-type helix, which is slowly formed with time (Fig. 16a).

Although the pathway complexity can be simply observed during conventional sample preparation, researchers employ various sample processing methods to access to kinetically trapped states.[280–284] Common strategies to obtain kinetically trapped states include rapid cooling, which prevents equilibration and traps monomers or kinetic aggregates, and solvent-switching protocols, where mixing a good solvent with a poor one modulates the aggregation. Other methods involve adjusting the monomer concentration, using specific co-solvents or

**11678** | *Chem. Soc. Rev.*, 2025, **54**, 11659–11698

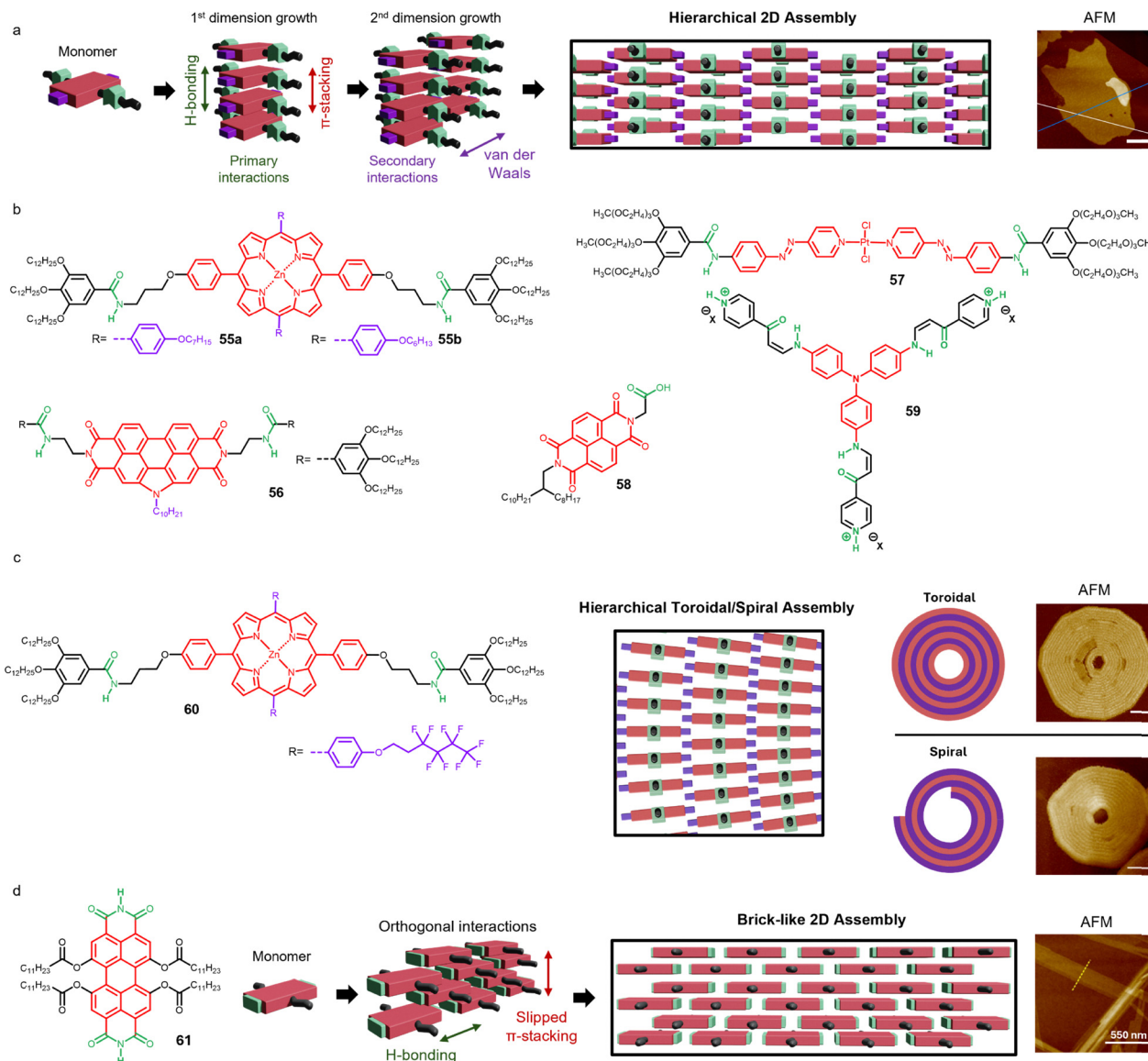This journal is © The Royal Society of Chemistry 2025

Fig. 15 (a) Schematic representation of a hierarchical 2D assembly; from left to right: example of the monomer design, primary interactions, secondary interactions, construction of the 2D sheet and AFM image of the 2D hierarchical system of molecule **55a** (reproduced from ref. 268, with permission of Springer Nature, copyright 2016). (b) Molecular structures of compounds **55–59** yielding 2D hierarchical assemblies. (c) Molecular structure of porphyrin **60** (reproduced from ref. 274, with permission of Springer Nature, copyright 2020) and representation of its self-assembly mode into 2D hierarchical spiral or concentric toroid assemblies. (right) Schematic representation and illustration of the formation of the concentric toroids and spirals and AFM images of the corresponding supramolecular assemblies of compound **60**. (d) From left to right: Molecular structure of PBI **61**, schematic representation of the formation of brick-like 2D assemblies and AFM image of the ribbons formed by PBI **61** (reproduced from ref. 278, with permission of Wiley-VCH Verlag GmbH & Co. KGaA, Weinheim, copyright 2020).

additives, or applying external stimuli such as ultrasonication, stirring, light irradiation, or seed addition.[280–284,288]

Time-dependent interconversion studies are typically used to study pathway complexity. The observation of pathway complexity in different systems has led to the identification of two representative scenarios.[280–284] The consecutive route involves direct transformations between kinetic on-pathway species and thermodynamic species (Fig. 16b), whereas the competitive route involves the formation of an off-pathway intermediate that disassembles into monomers before forming the stable aggregates (Fig. 16c). These kinetically trapped species can be

of monomeric (inactive/dormant) or of aggregated nature. The study of the mechanism in the kinetic transformation of supramolecular polymers is usually studied by time-dependent studies at different concentrations.[280–288]

## 7.2. The role of H-bonding in pathway complexity

Despite the investigations of different processing protocols that can be applied, not all the monomers are able to show pathway complexity and kinetic effects in their polymerization schemes, and some structural features in the monomer are required.[280–284,289] In this regard, the presence of H-bonding

This journal is © The Royal Society of Chemistry 2025

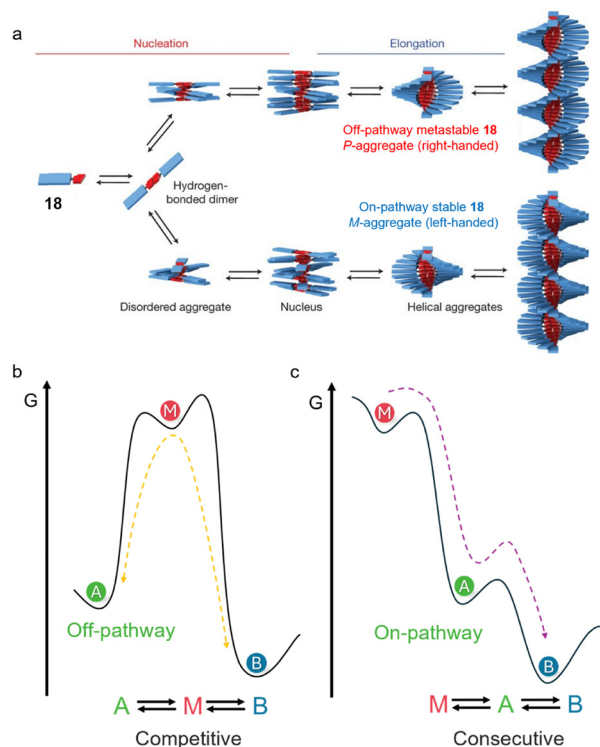*Chem. Soc. Rev.*, 2025, **54**, 11659–11698 | **11679**

**Fig. 16** (a) Schematic illustration of the self-assembly behaviour of chiral compound **18** characterized for two competing pathways (reproduced from ref. 145 with permission of Springer Nature, copyright 2012). Energy landscapes illustrating the pathway complexity for (b) a competitive process and (c) a consecutive process. The competitive process involves an off-pathway kinetically trapped and the consecutive process an on-pathway intermediate. M: monomer; A: kinetically trapped states; and B: thermodynamically stable state.

groups in monomeric π-conjugated species has been shown to be a crucial feature. For example, intramolecular H-bonding can lead to the formation of kinetically trapped monomers under certain conditions.[35,137,290–292] These trapped monomers (inactive or dormant monomers) are unable to undergo supramolecular polymerization, and only the disruption of these intramolecular bonds allows polymerization to proceed, typically through the interplay of H-bonding and π–π interactions. For instance, Würthner and co-workers reported that PBI **12** forms, after rapid cooling of the sample, a kinetically trapped monomeric state (closed form) through intramolecular H-bonds between the amide N–H and the carbonyl groups of the imide part (Fig. 17a).[35] In another example, Aida and co-workers described the $C_5$-symmetric corannulene derivative **10** with five amide-appended side chains, which forms a deeply trapped monomeric state stabilized by fivefold intramolecular H-bonds in nonpolar MCH (Fig. 17a).[137] The concept of H-bond-stabilized inactive monomers has also been achieved though the folding of the monomeric species which has been demonstrated in the pyrene-substituted diamide **62** (Fig. 17a).[290] The evolution of closed state inactive monomers into the extended forms enables the polymerization of the system. The disruption of the intramolecular H-bonds and

the opening of the molecules into their extended form occur over time but can also be triggered by the application of external stimuli.

Alternatively, intramolecular H-bonding in monomeric π-conjugated species can also lead to the formation of kinetically trapped aggregates rather than inactive monomers (Fig. 17b). The tendency of these closed state monomers to form kinetically trapped aggregates is not generally driven by H-bonding interactions and instead arise from the interplay π–π stacking and solvophobic effects, while steric effects may also contribute. Such a case has been observed in various systems based on PBIs,[293,294] N-annulated PBIs,[295,296] N-annulated perylenes,[297] N-heterotriangulenes,[192] diketopyrrolopyrroles,[298] and Pt(II) complexes,[299,300] among others. Functionalizing π-conjugated molecules with various amide groups has been proven to be an effective strategy to promote intramolecular H-bonding patterns enabling the formation of kinetically trapped aggregates.[192,293–300] For example, this behaviour has been observed in the bisdendronized PBI **63** bearing butyl spacers between the core and the wedge-shaped benzeneamide motifs (Fig. 17b).[293] While the derivative **12**, with shorter ethyl spacers, forms a kinetically trapped monomer upon rapid cooling of the solution (Fig. 17a),[35] PBI **63** assembles into an off-pathway nanoparticle-like kinetic aggregate under similar conditions (Fig. 17b). This kinetic aggregate eventually evolves via a competitive process into fibrous aggregates over time. In another example, Sánchez and co-workers reported N-annulated perylene derivative **64** forming kinetically trapped J-aggregates based on intramolecularly H-bonded monomers (Fig. 17b).[296] The kinetic J-aggregates evolved with time to the thermodynamic H-aggregates through a competitive mechanism. Interestingly, the alkyl spacer length between the amide groups and the core was tuned to modulate the kinetics and energy landscape of supramolecular polymerization (Fig. 17b).[296]

The formation of kinetically trapped aggregated species has also been observed in monomers capable of self-assembly via two or more distinct H-bonding patterns.[301–305] This is the case of the pioneering example of the H-bonding porphyrin **65** reported by Sugiyasu, Takeuchi and coworkers (Fig. 17c).[301,302] This type of porphyrins, functionalized with two dendronized amide arms, forms kinetically trapped J-aggregates by tilted H-bonds between amide groups, while this species evolve upon time into more stable H-aggregates characterized by coplanar interactions of the porphyrin cores and more lineal H-bonds (Fig. 17c). This system was utilized to gain control over supramolecular polymerization (see Section 7.3). In a more recent example, BOPHY **66** initially assembles upon cooling into a kinetically favoured H-type supramolecular polymer (**66-AggA**) in MCH, which gradually transforms into a thermodynamically stable structure (**66-AggB**) through a competing pathway (Fig. 17c).[303] Theoretical studies suggest that the $BF_2$ substituents create steric clashes within the antiparallel, face-to-face arrangement of **66-AggA**, prompting the system to reorganize into the more stable polymer **66-AggB**, where the monomer units are laterally offset. This new configuration reduces steric
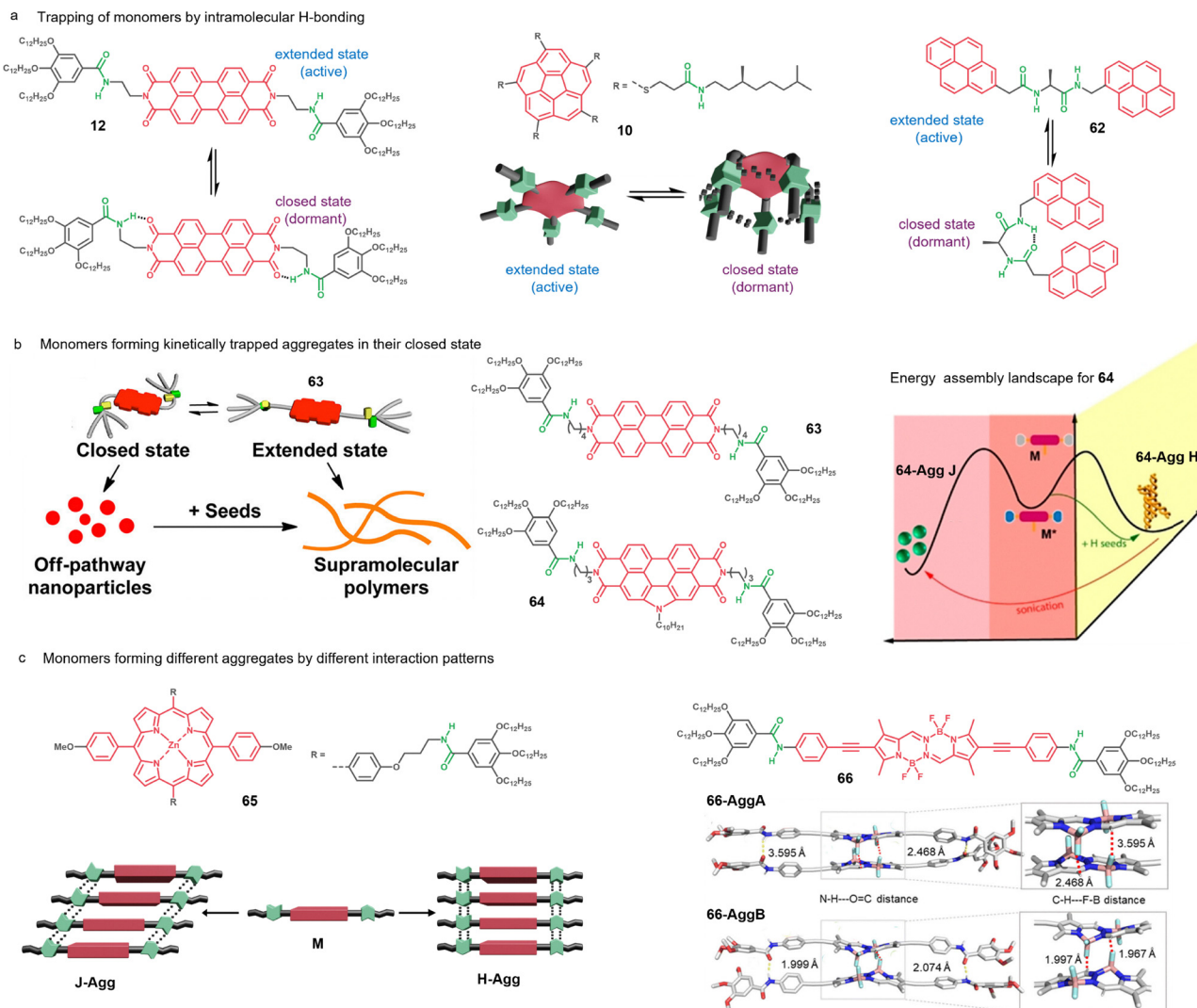
**11680** | *Chem. Soc. Rev.*, 2025, **54**, 11659–11698

This journal is © The Royal Society of Chemistry 2025

**Fig. 17** (a) Molecular structures and the extended and closed forms of the H-bonding monomers **12**, **10** and **62**. (b) (left) Schematic representation of the self-assembly behaviour of compound **63** (reproduced from ref. 293 with permission of American Chemical Society, copyright 2015). (middle) Molecular structures of compounds **63** and **64**. (right) Energy self-assembly landscape for compound **64** (reproduced from ref. 296 with permission of Wiley-VCH GmbH, copyright 2023). (c) Molecular structure of compounds **65** and **66** and the corresponding illustration of the different aggregates they form (reproduced from ref. 303 with permission of the Royal Society of Chemistry, copyright 2024).

strain while preserving the H-bonds between the amide side groups.

### 7.3. Controlled supramolecular polymerization

Controlled supramolecular polymerization represents a significant conceptual advance in supramolecular chemistry, bridging the precision of covalent polymerization with the dynamic nature of non-covalent assembly.[279] Unlike spontaneous supramolecular polymerization, which typically yields polydisperse structures through uncontrolled nucleation and growth, the controlled polymerization relies on suppressing uncontrolled aggregation by creating dormant species. This dormant species can then be activated, by a seed, external stimulus, or initiating species, to trigger a chain-growth mechanism, resulting in some cases in supramolecular polymers with predictable length, low dispersity, and in some cases, living

characteristics.[280–282] Recent advances in the controlled supramolecular polymerization of π-conjugated systems have enabled the formation of well-defined 1D and 2D nanostructures from small-molecule chromophores.

#### 7.3.1. Living supramolecular polymerization.
Advances in the understanding of pathway complexity opened new avenues to control self-assembly processes. In this context, pioneering studies of Manners and co-workers demonstrated the precise synthesis of various higher-order supramolecular assemblies *via* living crystallization-driven self-assembly of polymeric building blocks.[306,307] This approach was extended to small-molecule assemblies, giving rise to the concept of LSP (Fig. 18a).[137,280–284,301] LSP enables controlled polymer growth and can be considered the supramolecular analogue of covalent living polymerization, where polymer chains grow from active ends without undergoing termination.

This journal is © The Royal Society of Chemistry 2025

*Chem. Soc. Rev.*, 2025, **54**, 11659–11698 | **11681**

To achieve LSP, the system may polymerize *via* the cooperative mechanism and present kinetic trapping of either monomers or aggregated species. Those trapped states serve as a reservoir of monomers for the controlled growing of supramolecular polymers from initiator species, which can be designed as single molecules or pre-formed seeds (Fig. 18a). In seeded LSP, pre-formed seeds are prepared *via* ultrasonication and are based on aggregates larger than the critical nucleus. These seeds always consist of the most thermodynamically stable aggregated form of the system. When the seeds (or the initiator) are added to a solution of the kinetically trapped states under specific conditions, the elongation process is directly activated, and the monomers are selectively added at the seed ends in a chain-growth fashion (Fig. 18a). True living behaviour is confirmed only if growth can be repeated in multiple cycles, with kinetic and structural evidence.

Pioneering example of LSP was reported by Sugiyasu and Takeuchi in a H-bonding porphyrin system.[301] Porphyrin **65** (Fig. 17c) initially forms J-type aggregates as nanoparticles that, over time, evolve into thermodynamically stable fibrillar H-type aggregates (Fig. 17c). The kinetic transformation can be significantly accelerated by introducing seeds of the thermodynamically favoured H-type aggregates (Fig. 18a), prepared *via* sonication of preformed fibrillar structures. This process produces fibres with controlled length. Repeating this seeding

process over several cycles yields supramolecular polymers with low polydispersity.[301]

An analogous seeding strategy was followed by the Würthner group in PBI systems.[35,293,294] For example, PBI **67** forms a kinetically trapped H-aggregate based on the closed conformation of the monomer (Fig. 17a). Upon addition of seeds of the thermodynamic J-aggregate, the system undergoes LSP.[294] These studies showed that LSP can be achieved in systems exhibiting off-pathway kinetically trapped aggregates,[293,294] but also in systems presenting trapped monomer species in a closed H-bonded conformation (Fig. 17a).[35] Interestingly, LSP was also applied for the development of PBI based copolymers with precise control over the supramolecular 1D blocky structures.[120]

Another relevant contribution in this area was made by Aida and co-workers in 2015 using a single molecule as the LSP initiator.[137] In this system, the non-methylated corannulene derivative **10** (Fig. 18b) forms intramolecular pentafold H-bonds between amide groups (Fig. 17a), which effectively prevent self-assembly. In contrast, the *N*-methylated analogue **10-Me** are incapable of forming intramolecular H-bonds or self-assemble into polymers. Interestingly, trace amounts of the methylated compound **10-Me** were shown to act as initiators (Fig. 18a) for the LSP triggering the rapid supramolecular polymerization *via* H-bonds in **10** (Fig. 18b).
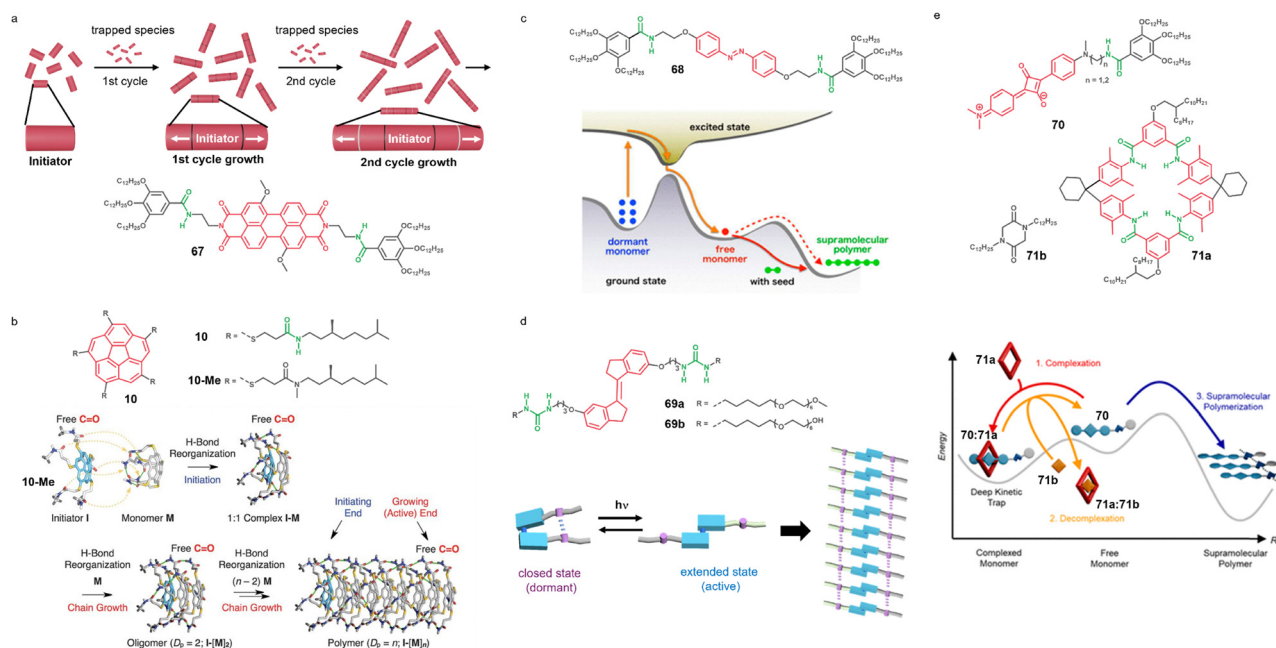


**Fig. 18** (a) Schematic representation of the living supramolecular polymerization process and the molecular structure of PBI **67**. The initiator refers to a seed or a single molecule. The trapped species can consist of kinetically trapped monomeric aggregated species. (b) Molecular structures of compounds **10** and **10-Me**, and a schematic representation of the supramolecular polymerization process triggered by adding small amounts of **10-Me** into a solution of **10** (reproduced from ref. 137 with permission of the American Association for the Advancement of Science, copyright 2015). (c) Molecular structure of compound **68** and the corresponding self-assembly energy landscape of the light controlled self-assembly process (reproduced from ref. 314 with permission of the American Chemical Society, copyright 2016). (d) Molecular structure of compounds **69a,b** and the schematic illustration of the light controlled self-assembly process (reproduced from ref. 315 with permission of the American Chemical Society, copyright 2021). (e) Molecular structures of compounds **70**, **71a** and **71b**, and the corresponding self-assembly energy landscape for the controlled supramolecular polymerization process (reproduced from ref. 317 with permission of the American Chemical Society, copyright 2023).

**11682** | *Chem. Soc. Rev.*, 2025, **54**, 11659–11698

This journal is © The Royal Society of Chemistry 2025

While the majority of examples of supramolecular polymerization target the obtention of 1D structures, the concept has also been extended to 2D polymers.[268,308–310] For example, Sugiyasu and coworkers reported the controlled 2D supramolecular polymerization from a single porphyrin-based monomers **55a,b** (Fig. 15b).[268] Upon cooling the solution, the monomer first assembles into metastable J-aggregate nanoparticles *via* an isodesmic pathway, and then undergo time-dependent autocatalytic transformation into nanosheets through a short-slipping J-aggregation mode. The 2D growth is driven by lateral van der Waals interactions among hexyl side chains and reinforced by H-bonding. This pathway can be selectively activated and precisely controlled using seed fragments, enabling 2D LSP yielding nanosheets with a uniform thickness. More recently a similar approach was applied to grow 2D block copolymers.[311]

**7.3.2. Controlled supramolecular polymerization by external stimuli.** Besides LSP other strategies to gain control over supramolecular polymerization of π-conjugated molecules and involving H-bonding have been developed. This includes the regulation of aggregation by light irradiation.[16,312,313] For example, Sugiyasu and coworkers demonstrated the coupling of photoisomerization in an azobenzene based monomer **68** and supramolecular polymerization (Fig. 18c).[314] The exposure of the sample to UV light generates the inactive monomer in the *cis*-azobenzene conformation. Light activation of the inactive **68** in the presence of a supramolecular polymer seed enabled chain growth at the ends of the seed, allowing the formation of supramolecular polymers with well-defined lengths and low polydispersity.

In another example, Feringa and coworkers reported the stilbene-bis-urea photoswitch **69** showing light-responsive aggregation behaviour (Fig. 18d).[315] While the *cis*-isomer is an inactive monomer stabilized by an intramolecular H-bond, the *trans*-form self-assembles into H-bonded fibrous aggregates. Thus, the light controlled *cis–trans* photoisomerization of this compound enables the rapid, reversible polymerization and gelation. Unlike conventional light irradiation, vibrational strong coupling has recently been applied to direct supramolecular polymerization toward otherwise inaccessible structures. By coupling the C–H stretching vibration in NDI based polymers, vibrational strong coupling redirected the assembly pathway to form toroids instead of thick fibres, formed under conventional conditions.[316]

Other strategies to control supramolecular polymerization involves the use of chemical additives.[317–320] In a pioneering example, Würthner and coworkers achieved an exquisite control over supramolecular polymerization of squaraine **70** by using a molecular chaperone analogue **71a** (Fig. 18e).[317] In this approach, squaraine monomers are temporarily inactivated by complexation with a tetralactam macrocycle **71a** (chaperone analogue), preventing spontaneous polymerization. Upon addition of a high-affinity initiator (diketopiperazine **71b**), the macrocycle is removed, releasing the squaraine monomers to polymerize *via* π–π stacking and H-bonding (Fig. 18e).

Other approaches to control supramolecular polymerization, not analysed here, include liquid–liquid phase separation events,[321] the use of adaptive systems,[322] or crowding agents.[319,323]

**7.3.3. Secondary nucleation.** A more recent strategy to control supramolecular polymerization exploits the phenomenon of secondary nucleation.[48] This is a surface-catalyzed process, extensively studied in the context of protein assemblies,[324] that enables new growth pathways by initiating nucleation on the surface of existing aggregates (or seeds) (Fig. 19a). Unlike primary nucleation, which involves the spontaneous aggregation of free monomers in solution and typically has a high energy barrier, secondary nucleation has a lower energy barrier because the existing aggregates catalyse the formation of new nuclei on their surface. This process provide access to complex morphologies like hierarchical fibres, helical bundles, or even catenated structures.[325] Secondary nucleation in supramolecular polymerization can be achieved in specific monomers and by the careful choice of solvent, and controlling the slow-fast cooling rates during aggregation.[200,274,324,326–333] The introduction of seeds is typically used to direct the assembly process by catalysing secondary nucleation.

While secondary nucleation in supramolecular polymerization was observed by Bert Meijer and co-workers in 2008 in chiral oligothiophenes,[326] the phenomenon was not clearly demonstrated until recently. The most exhaustive studies of secondary nucleation were reported by the Yagai group.[325] For example, the barbituric acid-functionalized π-conjugated compound **72** self-assembles into toroidal nanostructures through hierarchical supramolecular polymerization (Fig. 19b).[327,328] Each toroid originates from H-bonded rosettes formed by approximately 600 molecules. Remarkably, secondary nucleation on the inner surfaces of these toroids drives the formation of complex interlocked topologies known as nano-poly[*n*]catenanes, including [2]- to [22]-catenanes. The AFM image of a nano-poly[5]catenane is shown in Fig. 19b. van der Waals interactions between monomers and toroid surfaces facilitate this hierarchical growth.[327] The utilization of this type of molecules and secondary nucleation provided new tools for the creation of exotic supramolecular topologies.

Sugiyasu and co-workers demonstrated a sophisticated example of secondary nucleation-controlled supramolecular polymerization through the formation of supramolecular concentric toroids using fluoroalkyl-substituted metalloporphyrins **60** (Fig. 15c).[274,329] Upon cooling, primary toroids are formed under dilute conditions through ring closure of curved supramolecular 1D stacks. These toroids acted as seeds for secondary nucleation along their fluorinated inner surfaces, enabling the growth of larger, concentric toroidal structures (Fig. 19c).[329] A solvent-mixing protocol allowed for kinetically controlled toroid synthesis with narrow polydispersity, and monomer addition enabled further size modulation without loss of uniformity.[274] In a second work, site-selective secondary nucleation of different porphyrin monomers led to the construction of 2D block architectures with high sequence control. Notably, selective depolymerization of inner toroids using
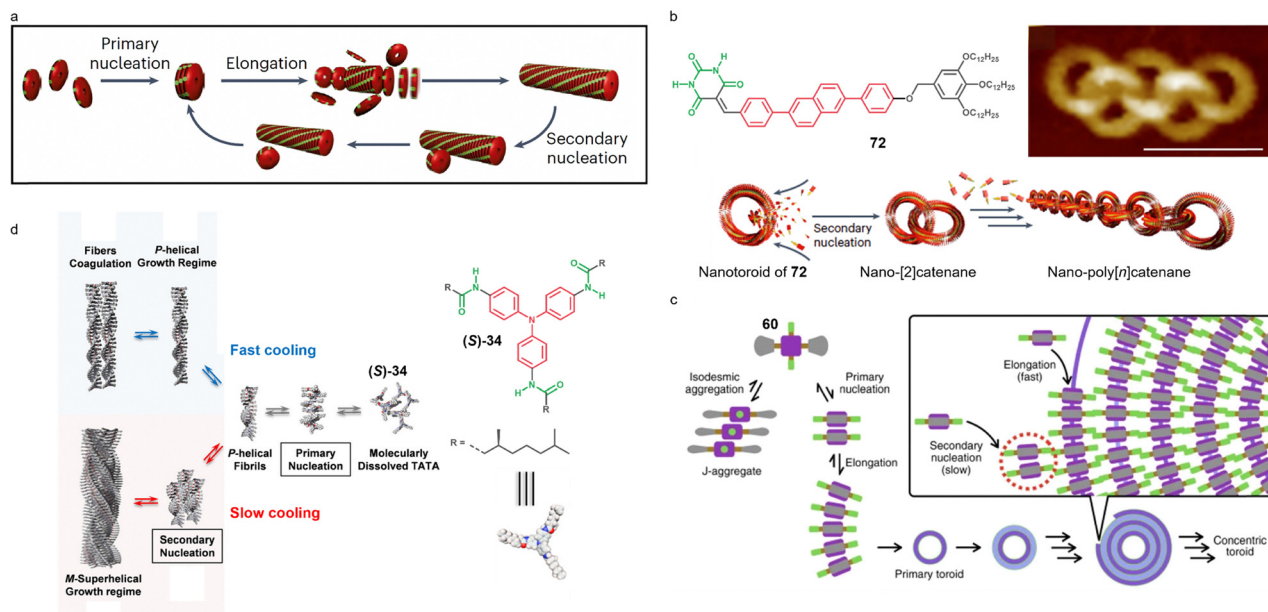
This journal is © The Royal Society of Chemistry 2025

*Chem. Soc. Rev.*, 2025, **54**, 11659–11698 | **11683**

**Fig. 19** (a) Schematic representation of the supramolecular polymerization process composed of a primary nucleation, an elongation and a secondary nucleation step (reproduced from ref. 325 with permission of Springer Nature, copyright 2025). (b) Molecular structure of compound **72** and the corresponding illustration of its the self-assembly behaviour forming nanotoroids and catenane structures *via* secondary nucleation (reproduced from ref. 325 with permission of Springer Nature, copyright 2025). Inset shows the AFM image of a nano-poly[5]catenane (reproduced from ref. 328 with permission of Springer Nature, copyright 2020). (c) Schematic representation of the self-assembly behaviour of porphyrin **60**, leading to the formation of concentric toroidal assemblies *via* secondary nucleation (reproduced from ref. 274, with permission of Springer Nature, copyright 2020). (d) Molecular structure of compound **(S)-34** and the corresponding illustration of its self-assembly behaviour forming chiral helical fibrils by primary nucleation and superhelical assemblies *via* secondary nucleation (reproduced from ref. 330 with permission of Wiley-VCH Verlag GmbH & Co. KGaA, Weinheim, copyright 2019).

4-dimethylaminopyridine revealed reactivity differences between the inner and outer surfaces, attributed to their distinct curvature and side-chain composition.

The secondary nucleation approach has also been employed to construct hierarchical supramolecular polymers from chiral π-conjugated monomers.[200,330–332] Giuseppone and co-workers demonstrated this using a triphenylamine-based monomer **(S)-34**, where the occurrence of secondary nucleation could be finely tuned by varying the concentration and cooling rate.[330] At low concentrations and under fast cooling, P-helical fibrils are formed (Fig. 19d). In contrast, higher concentrations or slower cooling rates promote the secondary nucleation of these fibrils into larger M-helical superstructures, showcasing a clear transition from primary to hierarchical organization (Fig. 19d).

### 7.4. Supramolecular polymorphism

Polymorphism refers to the ability of a molecule or polymer to adopt distinct structural arrangements depending on factors such as solvent, temperature, concentration, or processing conditions.[334] In chemical biology, polymorphism manifest in the tertiary and quaternary structures of amyloid aggregates, with different forms often linked to specific biological functions or pathological effects.[335] In the pharmaceutical industry, crystal polymorphism significantly influences drug solubility, stability, and bioavailability.[336] Likewise, in organic electronics, molecular packing variations directly impact charge transport, optical properties, and overall device performance.[337]

Controlling polymorphism in π-conjugated supramolecular polymers can therefore enable access to diverse supramolecular structures with tailored packing, morphology, and properties.

Systems presenting supramolecular polymorphism are characterized for presenting two or more distinct stable aggregated states.[44,195,278,280,281,338–348] Fig. 20a shows the energy landscape for PBI **73** reported by the Würthner group, which exhibits three distinct one-dimensional supramolecular polymorphs (**73-Agg1–3**) in the same solvent, at the same concentration, and at room temperature.[339] **73-Agg2** and **73-Agg3** were formed from kinetically trapped **73-Agg1** by applying ultrasonication (physical trigger) or seeding (chemical trigger). The three distinct aggregates differ in their π–π stacking arrangements and H-bonding patterns as shown in Fig. 20a. Supramolecular polymorphism was also observed for PBI **61** (Fig. 15d), which features bay-position acyloxy groups and NH at the imide positons.[278] This compound forms either fibrilar or lamellar polymorphs depending on the cooling rate (Fig. 20b). These polymorphic structures arise from homo- or heterochiral self-assembly of atropoenantiomeric PBIs. Fast cooling promotes narcissistic self-sorting into the homochiral form, whereas slower cooling enables a transformation into heterochiral sheet-like assemblies.

Supramolecular polymorphism has also been reported for OPE-based Pt(II) complexes.[340,341] The Fernández group reported the Pt(II) complex **74** that forms two stable polymorphic structures (polymorphs A and B) simultaneously,
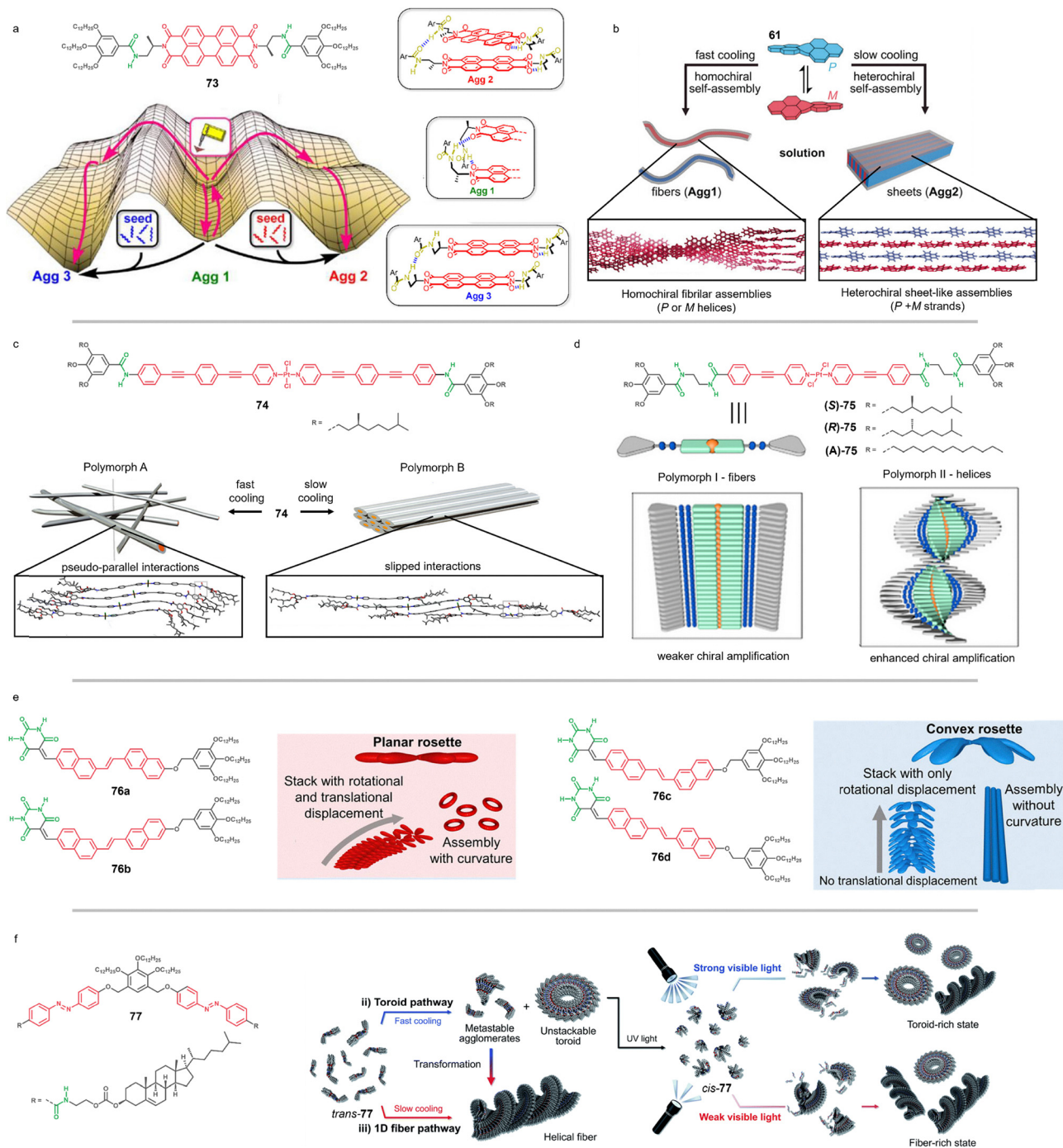
**Fig. 20** (a) Molecular structure of compound **73** and the corresponding self-assembly energy landscape leading to the formation of **Agg1**, **Agg2** and **Agg3**. The assembly mode of the three aggregates is schematically depicted in the inset (reproduced from ref. 339 with permission of the American Chemical Society, copyright 2019). (b) Scheme of the polymorphic behaviour of compound **61** forming fibres or sheet structures depending on the thermal treatment of the sample (reproduced from ref. 278 with permission of Wiley-VCH Verlag GmbH & Co. KGaA, Weinheim, copyright 2020). (c) Molecular structure of compound **74** and the scheme of its self-assembly behaviour forming polymorph A *via* pseudo-parallel interactions or polymorph B *via* slipped interactions depending on the thermal treatment of the sample (reproduced from ref. 340 with permission of American Chemical Society, copyright 2019). (d) Molecular structure of compounds **(S)-75**, **(R)-75** and **(A)-75** and a schematic illustration of the corresponding polymorphs I and II providing distinct chiral amplification behaviour (reproduced from ref. 349 with permission of Wiley-VCH GmbH, copyright 2025). (e) Molecular structure of compounds **76a–d** and a schematic illustration of the corresponding self-assembly behaviour into planar or convex rosettes and the subsequently into toroidal and fibrillar aggregates (reproduced from ref. 342 with permission of the Royal Society of Chemistry, copyright 2023). (f) Molecular structure of compound **77** and a scheme of its self-assembly behaviour including the light modulation of supramolecular polymorphism (reproduced from ref. 195 with permission of the Royal Society of Chemistry, copyright 2022).

This journal is © The Royal Society of Chemistry 2025

*Chem. Soc. Rev.*, 2025, **54**, 11659–11698 | **11685**
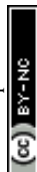
depending on assembly conditions in MCH.[340] Polymorph **74-A** forms under fast cooling conditions (2 K min$^{-1}$) *via* an isodesmic mechanism and features a slipped molecular arrangement stabilized by N–H···Cl–Pt interactions (Fig. 20c). In contrast, polymorph **74-B** emerges through a cooperative mechanism under slow cooling (0.1 K min$^{-1}$), displaying pseudoparallel stacking driven by N–H···O(alkoxy) H-bonds (Fig. 20c). Conversion from polymorphs **74-A** to **74-B** is only possible by thermal annealing, where aggregate **74-A** must fully disassemble into monomers before reassembling into the **74-B** polymorph. In a recent example, the G. Fernández group has demonstrated the relevance of polymorphism in the control of the amplification of asymmetry using chiral Pt(ɪɪ) complexes, (**S**)-**75** and (**R**)-**75**, alongside an achiral model compound (**A**)-**75** (Fig. 20d).[349] The chiral monomers form two stable polymorphs in MCH at room temperature (**AggI** and **AggII**) distinguished by their defined rotational offset during supramolecular polymerization, leading to distinct morphologies and photophysical properties (Fig. 20d). In the asymmetry amplification experiments, both polymorphs showed amplification effects, while **AggII** (with more twisted packing and stronger H-bonding) shows superior performance in SaS experiments with achiral compound (**A**)-**75**. Remarkably, coassembly of (**A**)-**75** and (**S**)-**75** into **AggII** results in CPL, an emergent property absent in the supramolecular polymers of the individual components.[349]

Other examples of supramolecular polymorphism in π-conjugated systems have mainly focused on morphological aspects, even when the molecular packing remains barely altered.[195,319,342,343] Yagai and co-workers reported supramolecular polymorphism in the barbiturate conformers **76a–d** that present different molecular conformations due to the flexible double bond connecting the two naphthalene units (Fig. 20e).[342] These compounds self-assemble into H-bonded cyclic hexamers (rosettes) (Fig. 8d) that subsequently yield toroidal or straight fibrous structures depending on the used conformer. Differences in the rosettes' planarity determine the stacking mode: translationally displaced stacking leads to curved nanorings, while aligned stacking produces straight nanorods (Fig. 20e). The same group also reported the scissor-shaped azobenzene dyad **78** forming nanotoroids as kinetic products and gradually transitions to thermodynamically stable fibres upon cooling (Fig. 20f).[195] Remarkably, the polymorphic behaviour can be controlled by light at constant temperature. Strong visible light irradiation of the *cis*-**77** induces the formation of nanotoroids, while weaker light favours fibre formation (Fig. 20d). This is the first demonstration of light-driven modulation of supramolecular polymorphism, enabling the selective formation of distinct nanostructures without changing temperature.

# 8. Applications of hydrogen bonded π-conjugated supramolecular polymers

As we have seen, depending on their monomer structure and supramolecular organization, π-conjugated supramolecular polymers can exhibit a broad spectrum of properties. Still, the real-world application of supramolecular polymers remains limited, and no truly groundbreaking product has yet reached the market. Nevertheless, their potential is undeniable, and it is likely that supramolecular polymers will play a key role in the development of next-generation materials.[15,350] While applications are not the main focus of this review, this section offers a brief overview of the key characteristics of π-conjugated H-bonded supramolecular polymers that highlight their potential for future applications.

## 8.1. Photonic and optoelectronic applications

Owing to the intrinsic photophysical properties of π-conjugated scaffolds, the supramolecular polymer derivatives are inherently attractive for photonic and optoelectronic applications. In the field of photonics, J-aggregates are of great relevance due to their sharp red-shifted absorption, strong exciton coupling, and efficient light-harvesting properties.[66] For example, J-aggregated cyanines have been used to construct supramolecular structures with light harvesting properties,[59,351,352] or platinum acetylides were found to be good candidates to be used in optical waveguides.[353]

PBI supramolecular polymers often form J-aggregates characterized by strong excitonic coupling and fluorescence properties.[29,64,354] For example, the tetraphenoxy-substituted PBI modified with thiophene side arms (**78**) self-assembles into core–shell columnar structures made of up to seven strands (Fig. 21a).[355,356] The presence of separated electron-accepting and an electron-donating regions allows independent pathways for electrons and holes, enabling efficient charge transport after light excitation. As a result, the material shows strong anisotropic photoconductivity with fast on–off switching under light irradiation (Fig. 21a). PBI J-aggregates have generally been applied in solar cells,[357] thin-film transistors,[358] optical waveguides,[359] and optical microcavities,[360] among others.

H-aggregates have also been exploited for photonic applications, as for example the carbonyl-bridge tryarylamines.[361] Compound **79** self-assembles into fibrillar aggregates with pronounced electronic coupling, enabling coherent exciton transport over distances exceeding 4 μm, limited only by the length of the supramolecular fiber (Fig. 21b). Interestingly, the transport properties of these tryarylamine family can be tuned by changing the peripherical groups.[362–364]

In a prominent example, Aida and coworkers reported amphiphilic hexabenzocoronenes self-assembling into micrometre-scale, graphite-like nanotubes with a uniform wall thickness.[365] Interestingly, these tubular structures supported anisotropic charge transport.[366] In the same context, Giuseppone reported a family of triarylamine scaffolds forming supramolecular 1D structures under different conditions.[134,367] Light-triggered supramolecular polymerization under an electric field enabled the *in situ* growth of **80** nanowires that bridge electrode gaps in a highly ordered fashion (Fig. 21c).[368] These self-assembled organic interconnects exhibit remarkable electronic properties, with an ohmic conductivity of $5 \times 10^3$ S m$^{-1}$, and current densities up to $2 \times 10^6$ A cm$^{-2}$. At cryogenic

**11686** | *Chem. Soc. Rev.*, 2025, **54**, 11659–11698

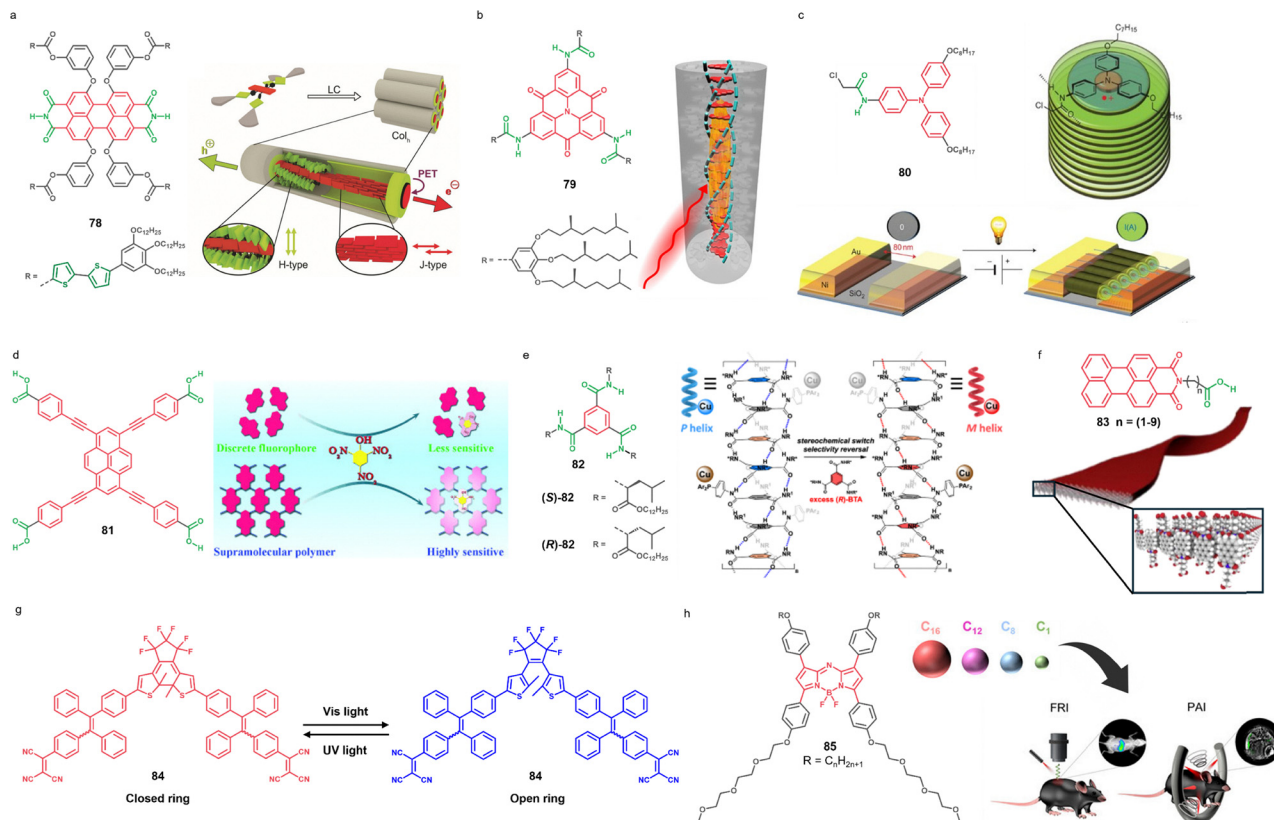This journal is © The Royal Society of Chemistry 2025

**Fig. 21** (a) Molecular structure of **78** and its self-assembled core-shell structure with charge transport properties (reproduced from ref. 356 with permission of Wiley-VCH Verlag GmbH & Co. KGaA, Weinheim, copyright 2019). (b) Molecular structure of **79** and the corresponding representation of its 1D assembly (reproduced from ref. 361 with permission of the American Chemical Society, copyright 2020). (c) Molecular structure of **80**, the self-assembly mode and the representation of the controlled supramolecular polymerization of **80** under the application of an electric field (reproduced from ref. 368 with permission of Springer Nature, copyright 2012). (d) Molecular structure of **81** and scheme of detection of nitrocompounds (reproduced from ref. 377 with permission of Wiley-VCH Verlag GmbH & Co. KGaA, Weinheim, copyright 2014). (e) Representation of the structure of a BTA supramolecular polymer catalyst in which the helicity is induced by adjusting the amount of BTA **(S)-** and **(R)-82** (reproduced from ref. 390 with permission of Springer Nature, copyright 2024). (f) Molecular structure of photocatalyst **83** and its corresponding 2D assembly (reproduced from ref. 394 with permission of Springer Nature, copyright 2014). (g) Closed and open states of the photoswitch **84** (reproduced from ref. 419 with permission of Springer Nature, copyright 2018). (h) Molecular structure of BODIPY **85** and the representation of the formation of spherical aggregates of different sizes depending on the alkyl chain length. Scheme of its function for *in vivo* bioimaging (reproduced from ref. 416 with permission of Wiley-VCH Verlag GmbH & Co. KGaA, Weinheim, copyright 2025).

temperatures, the nanowires show metallic behavior, underscoring their exceptional performance compared to typical organic materials. In another example, urea-functionalized bithiophene derivatives were shown to assemble into nanofibres that support highly mobile charge carriers, as revealed by pulse radiolysis.[369] Similar behaviour was reported for oligothiophene-based chromophores that allows the formation of long-lived photocharges.[370]

These examples underscore the potential of π-conjugated supramolecular polymers in key optoelectronic devices,[29,59,64,351,361,366,369,371,372] including organic field-effect transistors (OFETs),[373] organic light-emitting diodes (OLEDs),[374] and organic photovoltaics.[375]

## 8.2. Sensing and separation

π-Conjugated supramolecular polymers have also emerged as promising platforms for sensing, exploiting their inherent stimuli-responsive properties. For instance, it has been demonstrated that they can be applied to efficiently detect explosive nitroaromatic compounds,[376,377] through fluorescence quenching mechanisms.[17,378] One example of the sensing of explosive nitroaromatic compounds consists of pyrene **81**, forming supramolecular polymers *via* π-stacking and H-bonds (Fig. 21d).[377] The resulting supramolecular structure allows detection due to donor–acceptor interactions and H-bonding between the polymer and the nitrocompound. In the same line, fluorescence quenching mechanisms were used for the detection of metal ions using the bispillar[5]arene-based supramolecular polymer designed by Tai-Bao Wei.[379] This system exhibited AIE, and was successfully applied for the fluorescence detection and removal of mercury(II) through host–guest interactions.

Supramolecular assemblies also have great potential not only for the sensing of chiral compounds, but also for their separation.[380] For example, chiral and achiral hydrazide foldamers were shown to bind selectively to saccharides adopting

This journal is © The Royal Society of Chemistry 2025

*Chem. Soc. Rev.*, 2025, **54**, 11659–11698 | **11687**

well-defined supramolecular helical assemblies or forming host–guest foldamers whose conformation can be monitored by different techniques.[381,382] While still is a growing field, supramolecular assemblies have also been proposed for separation and purification applications, as for example as components in separation membranes.[383–385]

### 8.3. Catalysis

Another emergent application of supramolecular polymers lies in the field of catalysis.[386–388] For instance, a water-soluble BTA derivative functionalized with L-proline co-assembles into homochiral helical supramolecular polymers that exhibit catalytic activity and selectivity in aldol reactions involving *p*-nitrobenzaldehyde and cyclohexanone.[389] More recently, BTA-based supramolecular polymers have been employed to develop a switchable asymmetric copper catalyst that enables selective access to different stereoisomers of an amino alcohol through a hydrosilylation–hydroamination cascade.[390] This was achieved using helical polymers composed of different BTA monomers, where the handedness of the helices was tuned by adding a chiral BTA co-monomer, (**S**) or (**R**)-**82** (Fig. 21e). The helicity of the polymers dictates the outcome of the catalytic transformation of an amino alcohol.

Supramolecular π-conjugated polymers are particularly relevant in photocatalysis, where the chromophore plays a central role in light absorption and energy transfer within the system.[391] Photocatalityc supramolecular polymers are mainly used in aqueous systems, but not always H-bonds are involved. One example of a photocatalytic system consists of a platinum(II) metallacycle with AIE-active TPE units acting as efficient light-harvesting antennas in water.[392] The monomer self-assembles into nanospheres, which enable a highly efficient two-step energy transfer cascade, and the photocatalytic C–H alkylation in water. Other catalytic processes include water splitting and $CO_2$ reduction.[393] Stupp and coworkers reported a hydrogel scaffold formed through the self-assembly of a perylene monoimide amphiphile **83** that acts as both (Fig. 21f) a light-harvesting platform and a host for a nickel-based catalyst.[394,395] This supramolecular material promotes efficient electronic coupling between chromophores and supports photocatalytic hydrogen generation within the three-dimensional hydrogel matrix. Furthermore, it can be easily deployed on surfaces or embedded in porous supports, offering a versatile platform for artificial photosynthesis. In another example, a spherical chromatophore-like nanomicelle system was developed by self-assembly of Zn–porphyrin amphiphiles with a Co catalyst in water.[396] The resulting hierarchical organization generates an antenna effect that promotes $CO_2$-to-$CH_4$ conversion with remarkable performance (TON > 6600, 89% selectivity, 15% solar-to-fuel efficiency).

### 8.4. Biomedical applications

Supramolecular polymers likely exhibit the greatest potential for biomedical applications.[397–400] However, these supramolecular polymers do not always consist of chromophores or involve the participation of H-bonding systems. It should be highlighted the pioneering work of the Stupp group, demonstrating the use of supramolecular polymers in regenerative medicine,[401] muscle actuators,[402] and therapeutics,[403] among others. In addition, numerous studies have shown the potential of supramolecular polymers in drug delivery systems.[404,405]

π-Conjugated supramolecular polymers have been exploited in biomedical applications for their unique electronic and optical properties.[406,407] Various dye-based assemblies have been employed for phototherapy[408–413] and bioimaging,[414–417] enabling both therapeutic and diagnostic functionalities. Chen and Wang reported supramolecular nanoparticles based on a Pt(IV)-modified β-cyclodextrin–ferrocene monomer.[418] In tumors, the nanoparticles dissociate in response to $H_2O_2$, releasing hydroxyl radicals and Pt(IV) prodrugs, which convert to *cis*-platin and amplify $H_2O_2$ generation. This self-augmented cascade enhances chemodynamic therapy while enabling renal clearance for low systemic toxicity. Other systems rely on light stimuli to modulate its function. In this context, Ding, Tang and coworkers developed a smart organic nanoparticle based on the photoswitch **84**, useful for photoacoustic imaging and photodynamic therapy.[419] By light-triggered switching between ring-closed and ring-opened states (Fig. 21g), the nanoparticle directs absorbed energy either to thermal deactivation for photoacoustic imaging or to fluorescence and ROS generation for photodynamic therapy.

More recently, a series of amphiphilic aza-BODIPY dyes (**85**) were shown to self-assemble in water into nanostructures with tunable size and photophysical properties.[416] Smaller assemblies (C1) show weak emission, while longer-chain derivatives (C8–C16) form J-aggregates with strong NIR fluorescence and photoacoustic signals (Fig. 21h). These dye assemblies demonstrate excellent biocompatibility, size-dependent biodistribution, and effective *in vitro* and *in vivo* imaging, highlighting the potential of self-assembled dyes as versatile contrast agents for biomedical applications.

## 9. Conclusions and future outlook

Hydrogen bonding has proven to be one of the most powerful and versatile noncovalent interactions for directing the self-assembly into well-defined supramolecular architectures. The inherent directionality, tunable strength, and reversibility of hydrogen bonds make them ideally suited for programming order from the molecular levels to macroscopic domains. Throughout this review, we have highlighted how hydrogen-bonding motifs can be rationally combined with π-conjugated scaffolds allowing a certain level of control over the self-assembly mechanism, molecular packing, and aggregate morphology, as well as the induction of pathway complexity and tuning of the photophysical properties.

Considering the electronic implications and exciton coupling arising from the interactions between chromophores, the directionality and strength of hydrogen bonds play a pivotal role in guiding the assembly of π-conjugated systems. The general monomer design strategy for developing hydrogen-

**11688** | *Chem. Soc. Rev.*, 2025, **54**, 11659–11698

This journal is © The Royal Society of Chemistry 2025

bonded π-conjugated supramolecular polymers involves the functionalization of the selected chromophoric unit with hydrogen-bonding motifs and the appropriate solubilizing groups. Through careful molecular engineering of these monomeric units, it is possible to achieve a high degree of control over the self-assembly process, guiding the formation of one-dimensional, two-dimensional, and/or chiral supramolecular architectures. The molecular packing within these architectures is critical, as it directly influences exciton coupling and determines whether H-type or J-type aggregates are formed, factors that are essential for tuning the optical, electronic, and functional properties of the resulting materials.

Importantly, the incorporation of hydrogen-bonding motifs and flexible linkers into π-conjugated scaffolds provides an additional versatility and tunability regarding the interaction's possibilities. Hydrogen-bonding units can establish diverse intra- and intermolecular interaction patterns, acting either synergistically or in competition with other noncovalent forces. This interplay gives rise to complex self-assembly landscapes, featuring multiple monomeric or aggregated species that may exist as kinetically trapped intermediates or thermodynamically stable structures. Kinetically trapped species, including dormant monomers or metastable aggregates, have proven particularly valuable for exerting control over the self-assembly process through mechanisms such as living supramolecular polymerization or secondary nucleation.

The integration of hydrogen-bonding units into π-conjugated systems has also enabled the development of adaptive and stimuli-responsive materials. External stimuli such as ultrasonication, light, or chemical additives can modulate the self-assembly processes, in terms of molecular packing, morphology, and optical or electronic behaviour. In this context, supramolecular polymorphism has emerged as a key concept, enabling the formation of two or more stable aggregated states from the same monomeric building blocks.

Despite significant progress, several challenges and opportunities remain in the field of hydrogen-bonded π-conjugated supramolecular assemblies. A more predictive understanding of how subtle variations in hydrogen-bond donor/acceptor patterns, molecular geometry, and solvent environment influence supramolecular outcomes is still lacking. This will be relevant for the development of three-dimensional architectures, but also in relation to pathway complexity, where the critical aspects of monomer design are not yet fully understood. In this context, developing new strategies to control supramolecular polymerization and harness supramolecular polymorphism remains a demanding but promising direction. Moreover, a deeper exploration of stimuli-responsive systems could not only offer new tools to control the kinetics and mechanisms of supramolecular polymerization but also provide a means to modulate in real-time the morphology and properties of the resulting materials.

Looking ahead, the utilization of new tools such as machine learning, molecular simulations, and advanced *in situ* characterization techniques (*e.g.*, cryo-TEM, time-resolved spectroscopy, single-molecule methods, and small-angle X-ray scattering) will be essential to decipher the complex kinetics and thermodynamics of supramolecular assembly processes. These approaches may eventually allow us to design supramolecular systems with predictive control over structure, function, and dynamics, akin to how nature programs molecular machines and complex assemblies *via* hydrogen-bonding in proteins and nucleic acids. Although this review has primarily focused on single-component systems, the rational design of multicomponent supramolecular assemblies with precise sequence and spatial control remains a significant challenge. Gaining control over multicomponent assembly is crucial for progressing toward more complex, multifunctional, and life-like supramolecular systems with advanced levels of structural and functional sophistication.

Owing to their unique electronic properties, π-conjugated supramolecular polymers hold significant potential for applications in optoelectronics, photonics, catalysis, sensing, and biomedicine. However, translating these fundamental properties into practical applications remains a major challenge, largely due to issues related to structural stability, processability, and precise control over molecular organization at larger scales, or in multicomponent environments. Their dynamic, noncovalent nature, while advantageous for self-healing and adaptability, can compromise long-term stability and reproducibility. Bridging the gap between molecular design and application performance will require advances in processing methods, and a deeper understanding of structure–function relationships under operational conditions.

In conclusion, hydrogen-bonding modulation in the self-assembly of π-conjugated systems is not only a powerful strategy to develop functional materials but also a conceptual framework for advancing the field of supramolecular chemistry. As we move toward the development of programmable, adaptive, and responsive supramolecular systems, hydrogen bonding will undoubtedly remain at the heart of molecular design, enabling new frontiers in soft matter, materials science, and nanotechnology.

## Author contributions

D. Martínez and L. Rubert: literature search, data collection and analysis, and writing. P. Ximenis: literature search, data collection and analysis, and writing and editing. B. Soberats: conceiving the topic, literature search, data collection, discussion, writing and editing, and overall supervision.

## Conflicts of interest

There are no conflicts to declare

## Data availability

This review does not include any original research results, software, or code, nor were any new data generated or analyzed.

This journal is © The Royal Society of Chemistry 2025

*Chem. Soc. Rev.*, 2025, **54**, 11659–11698 | **11689**

Additional information about the review is available upon request from the authors.

## Acknowledgements

## Notes and references

1 J.-M. Lehn, *Angew. Chem., Int. Ed. Engl.*, 1988, **27**, 89–112.
2 J. W. Steed and J. L. Atwood, *Supramolecular Chemistry*, John Wiley Sons, Chichester, UK, 2009.
3 C. A. Schalley, *Analytical Methods in Supramolecular Chemistry*, Wiley-VCH Verlag GmbH & Co. KGaA, Weinheim, Germany, 2nd edn, 2012.
4 J. M. Lehn, *Chem. Soc. Rev.*, 2017, **46**, 2378–2379.
5 J. M. Lehn, *Eur. Rev.*, 2009, **17**, 263–280.
6 E. V. Anslyn and D. A. Dougherty, *Modern Physical Organic Chemistry*, University Science Books, California, USA, 2006.
7 L. Brunsveld, B. J. B. Folmer, E. W. Meijer and R. P. Sijbesma, *Chem. Rev.*, 2001, **101**, 4071–4097.
8 T. F. A. De Greef, M. M. J. Smulders, M. Wolffs, A. P. H. J. Schenning, R. P. Sijbesma and E. W. Meijer, *Chem. Rev.*, 2009, **109**, 5687–5754.
9 L. Yang, X. Tan, Z. Wang and X. Zhang, *Chem. Rev.*, 2015, **115**, 7196–7239.
10 E. Krieg, M. M. C. Bastings, P. Besenius and B. Rybtchinski, *Chem. Rev.*, 2016, **116**, 2414–2477.
11 G. Wypych, *Handbook of Polymers*, ChemTec Publishing, Ontario, Canada, 3rd edn, 2022.
12 A. W. Bosman, R. P. Sijbesma and E. W. Meijer, *Mater. Today*, 2004, **7**, 34–39.
13 T. Aida, E. W. Meijer and S. I. Stupp, *Science*, 2012, **335**, 813–817.
14 D. B. Amabilino, D. K. Smith and J. W. Steed, *Chem. Soc. Rev.*, 2017, **46**, 2404–2420.
15 T. D. Clemons and S. I. Stupp, *Prog. Polym. Sci.*, 2020, **111**, 101310.
16 Y. Xue, Y. Jin, Y. Zhang, F. Han and F. Wang, *Chem. Mater.*, 2024, **36**, 6347–6369.
17 H. Wang, X. Ji, Z. Li and F. Huang, *Adv. Mater.*, 2017, **29**, 1606117.
18 S. S. Babu, V. K. Praveen and A. Ajayaghosh, *Chem. Rev.*, 2014, **114**, 1973–2129.
19 D. González-Rodríguez and A. P. H. J. Schenning, *Chem. Mater.*, 2011, **23**, 310–325.
20 A. Khasbaatar, Z. Xu, J. H. Lee, G. Campillo-Alvarado, C. Hwang, B. N. Onusaitis and Y. Diao, *Chem. Rev.*, 2023, **123**, 8395–8487.

21 F. J. M. Hoeben, P. Jonkheijm, E. W. Meijer and A. P. H. J. Schenning, *Chem. Rev.*, 2005, **105**, 1491–1546.
22 Y. Hong, J. W. Y. Lam and B. Z. Tang, *Chem. Soc. Rev.*, 2011, **40**, 5361–5388.
23 F. Würthner, *Angew. Chem., Int. Ed.*, 2020, **59**, 14192–14196.
24 H. Chen and J. F. Stoddart, *Nat. Rev. Mater.*, 2021, **6**, 804–828.
25 A. Jain and S. J. George, *Mater. Today*, 2015, **18**, 206–214.
26 Z.-T. Li and L.-Z. Wu, *Hydrogen bonded supramolecular structures*, Springer, Berlin Heidelberg, Berlin, Germany, 2015.
27 Q. Wan and B. C. Thompson, *Adv. Sci.*, 2024, **11**, 2305356.
28 E. D. Głowacki, M. Irimia-Vladu, S. Bauer and N. S. Sariciftci, *J. Mater. Chem. B*, 2013, **1**, 3742–3753.
29 F. Würthner, C. R. Saha-Möller, B. Fimmel, S. Ogi, P. Leowanawat and D. Schmidt, *Chem. Rev.*, 2016, **116**, 962–1052.
30 A. Das and S. Ghosh, *Chem. Commun.*, 2016, **52**, 6860–6872.
31 B. Matarranz and G. Fernández, *Chem. Phys. Rev.*, 2021, **2**, 041304.
32 A. Ruiz-Carretero, N. R. Á. Rovelo, S. Militzer and P. J. Mésini, *J. Mater. Chem. A*, 2019, **7**, 23451–23475.
33 Z. Chen, B. Fimmel and F. Würthner, *Org. Biomol. Chem.*, 2012, **10**, 5845–5855.
34 X. Q. Li, V. Stepanenko, Z. Chen, P. Prins, L. D. A. Siebbeles and F. Würthner, *Chem. Commun.*, 2006, 3871–3873.
35 S. Ogi, V. Stepanenko, K. Sugiyasu, M. Takeuchi and F. Würthner, *J. Am. Chem. Soc.*, 2015, **137**, 3300–3307.
36 T. Aida, A. Takemura, M. Fuse and S. Inoue, *J. Chem. Soc. Chem. Commun.*, 1988, 391–393.
37 C. Fouquey, J.-M.-M. Lehn and A.-M.-M. Levelut, *Adv. Mater.*, 1990, **2**, 254–257.
38 R. P. Sijbesma, F. H. Beijer, L. Brunsveld, B. J. B. Folmer, J. H. K. K. Hirschberg, R. F. M. Lange, J. K. L. Lowe and E. W. Meijer, *Science*, 1997, **278**, 1601–1604.
39 S. Cantekin, T. F. A. de Greef and A. R. A. Palmans, *Chem. Soc. Rev.*, 2012, **41**, 6125–6137.
40 F. H. Beijer, R. P. Sijbesma, J. A. J. M. Vekemans, E. W. Meijer, H. Kooijman and A. L. Spek, *J. Org. Chem.*, 1996, **61**, 6371–6380.
41 S. Yagai, Y. Kitamoto, S. Datta and B. Adhikari, *Acc. Chem. Res.*, 2019, **52**, 1325–1335.
42 M. Yokoya, S. Kimura and M. Yamanaka, *Chem. Eur. J.*, 2021, **27**, 5601–5614.
43 V. Saez Talens, P. Englebienne, T. T. Trinh, W. E. M. Noteborn, I. K. Voets and R. E. Kieltyka, *Angew. Chem., Int. Ed.*, 2015, **54**, 10502–10506.
44 S. Bujosa, A. Doncel-Giménez, N. Bäumer, G. Fernández, E. Ortí, A. Costa, C. Rotger, J. Aragó and B. Soberats, *Angew. Chem., Int. Ed.*, 2022, **61**, e202213345.
45 S. Bujosa, L. Rubert, C. Rotger and B. Soberats, *Commun. Chem.*, 2024, **7**, 1–11.
46 S. Yadav, K. S. Tiwari, C. Gupta, M. K. Tiwari, A. Khan and S. P. Sonkar, *Results Chem.*, 2023, **5**, 100733.
47 M. Gsänger, D. Bialas, L. Huang, M. Stolte and F. Würthner, *Adv. Mater.*, 2016, **28**, 3615–3645.

**11690** | *Chem. Soc. Rev.*, 2025, **54**, 11659–11698

This journal is © The Royal Society of Chemistry 2025

48 M. Kasha, H. R. Rawls and M. A. El-Bayoumi, *Pure Appl. Chem*, 1965, **11**, 371–392.

49 A. S. Davydov, *Sov. Phys. Uspekhi*, 1964, **7**, 145.

50 *Transition moment in IUPAC Compendium of Chemical Terminology, 5th edition, International Union of Pure and Applied Chemistry*, 2025.

51 F. C. Spano, *Acc. Chem. Res.*, 2010, **43**, 429–439.

52 N. J. Hestand and F. C. Spano, *Chem. Rev.*, 2018, **118**, 7069–7163.

53 J. Franck and E. G. Dymond, *Trans. Faraday Soc.*, 1926, **21**, 536–542.

54 E. Condon, *Phys. Rev.*, 1926, **28**, 1182.

55 K. Huang, A. Rhys and N. F. Mott, *Proc. R. Soc. Lond. Ser. Math. Phys. Sci.*, 1997, **204**, 406–423.

56 F. Würthner, S. Yao, T. Debaerdemaeker and R. Wortmann, *J. Am. Chem. Soc.*, 2002, **124**, 9431–9447.

57 J. Demuth, S. Bednarik, R. Machan, I. Mocak, T. Malinsky, M. A. E. Dahabova, J. Holcak, M. Miletin, J. Labuta, V. Novakova and P. Zimcik, *Inorg. Chem. Front.*, 2025, **12**, 1590–1608.

58 A. Zitzler-Kunkel, E. Kirchner, D. Bialas, C. Simon and F. Würthner, *Chem. Eur. J.*, 2015, **21**, 14851–14861.

59 F. Würthner, *Acc. Chem. Res.*, 2016, **49**, 868–876.

60 J. L. Bricks, Y. L. Slominskii, I. D. Panas and A. P. Demchenko, *Methods Appl. Fluoresc.*, 2017, **6**, 012001.

61 D. Bialas, E. Kirchner, M. I. S. Röhr and F. Würthner, *J. Am. Chem. Soc.*, 2021, **143**, 4500–4518.

62 E. Sebastian and M. Hariharan, *J. Am. Chem. Soc.*, 2021, **143**, 13769–13781.

63 C. Kaufmann, D. Bialas, M. Stolte and F. Würthner, *J. Am. Chem. Soc.*, 2018, **140**, 9986–9995.

64 M. Hecht and F. Würthner, *Acc. Chem. Res.*, 2021, **54**, 2.

65 A. J. Schwalb, C. Naranjo, A. Fernández-Alarcón, F. García, E. Ortí, J. Aragó and L. Sánchez, *J. Am. Chem. Soc.*, 2025, **147**(28), 25024–25034.

66 F. Würthner, T. E. Kaiser and C. R. Saha-Möller, *Angew. Chem., Int. Ed.*, 2011, **50**, 3376–3410.

67 J. Xu, M. Huang, H. Pang, Z. Weng, G. Hu, S. Zhang, Q. Yang and Q. Wu, *Aggregate*, 2024, **5**, e546.

68 P. A. Korevaar, C. Schaefer, T. F. A. D. Greef and E. W. Meijer, *J. Am. Chem. Soc.*, 2012, **134**, 13482–13491.

69 G. Vantomme, G. M. ter Huurne, C. Kulkarni, H. M. M. ten Eikelder, A. J. Markvoort, A. R. A. Palmans and E. W. Meijer, *J. Am. Chem. Soc.*, 2019, **141**, 18278–18285.

70 C. C. Lee, C. Grenier, E. W. Meijer and A. P. H. J. Schenning, *Chem. Soc. Rev.*, 2009, **38**, 671–683.

71 L. Borsdorf, L. Herkert, N. Bäumer, L. Rubert, B. Soberats, P. A. Korevaar, C. Bourque, C. Gatsogiannis and G. Fernández, *J. Am. Chem. Soc.*, 2023, **145**, 8882–8895.

72 D. Basak, D. S. Pal, T. Sakurai, S. Yoneda, S. Seki and S. Ghosh, *Phys. Chem. Chem. Phys.*, 2017, **19**, 31024–31029.

73 Y. Dorca, C. Naranjo, G. Ghosh, B. Soberats, J. Calbo, E. Ortí, G. Fernández and L. Sánchez, *Chem. Sci.*, 2021, **13**, 81–89.

74 L. López-Gandul, C. Naranjo, C. Sánchez, R. Rodríguez, R. Gómez, J. Crassous and L. Sánchez, *Chem. Sci.*, 2022, **13**, 11577–11584.

75 T. Seki, S. Yagai, T. Karatsu and A. Kitamura, *J. Org. Chem.*, 2008, **73**, 3328–3335.

76 M. Hartlieb, E. D. H. Mansfield and S. Perrier, *Polym. Chem.*, 2020, **11**, 1083–1110.

77 C. Kulkarni, S. Balasubramanian and S. J. George, *ChemPhysChem*, 2013, **14**, 661–673.

78 H. Miao, F. Yang, Y. Zhang, H. Li and X. He, *Chem. Eur. J.*, 2025, e202404243.

79 T. Yamaguchi, Y. Naito, C. Kitamura, H. Takeshita, S. Ida, T. Ishi-i, K. Suzuki, T. Matsumoto, Y. Shiota, D. Suzuki, Y. Imai, T. Ikeda and S. Kato, *Chem. Asian J.*, 2024, **19**, e202400829.

80 W. T. Gallonde, M. Shekar, V. Dorcet, S. Rigaut and O. Galangau, *Chem. Eur. J.*, 2025, **31**, e202500443.

81 B. Narayan, C. Kulkarni and S. J. George, *J. Mater. Chem. C*, 2012, **1**, 626–629.

82 J. Gershberg, F. Fennel, T. H. Rehm, S. Lochbrunner and F. Würthner, *Chem. Sci.*, 2016, **7**, 1729–1737.

83 Y. Dorca, C. Naranjo, G. Ghosh, B. Soberats, J. Calbo, E. Ortí, G. Fernández and L. Sánchez, *Chem. Sci.*, 2021, **13**, 81–89.

84 T. E. Kaiser, V. Stepanenko and F. Würthner, *J. Am. Chem. Soc.*, 2009, **131**, 6719–6732.

85 R. R. van der Weegen, P. A. Korevaar, P. Voudouris, I. K. Voets, T. F. A. de Greef, J. A. J. M. Vekemans and E. W. Meijer, *Chem. Commun.*, 2013, **49**, 5532–5534.

86 R. F. Goldstein and L. Stryer, *Biophys. J.*, 1986, **50**, 583–599.

87 I. Helmers, M. S. Hossain, N. Bäumer, P. Wesarg, B. Soberats, L. S. Shimizu and G. Fernández, *Angew. Chem., Int. Ed.*, 2022, **61**, e202200390.

88 A. Rödle, B. Ritschel, C. Mück-Lichtenfeld, V. Stepanenko and G. Fernández, *Chem. Eur. J.*, 2016, **22**, 15772–15777.

89 D. Zhao and J. S. Moore, *Org. Biomol. Chem.*, 2003, **1**, 3471–3491.

90 P. van der Schoot, *Supramolecular Polymers. Theroy of Supramolecular Polymerization*, CRC Press, Netherlands, 2nd edn, 2005.

91 G. Ercolani, *J. Am. Chem. Soc.*, 2003, **125**, 16097–16103.

92 J. F. Douglas, J. Dudowicz and K. F. Freed, *J. Chem. Phys*, 2008, **128**, 35.

93 G. Fernández, M. Stolte, V. Stepanenko and F. Würthner, *Chem. Eur. J.*, 2013, **19**, 206–217.

94 H. M. M. T. Eikelder, B. Adelizzi, A. R. A. Palmans and A. J. Markvoort, *J. Phys. Chem. B*, 2019, **123**, 6627–6642.

95 H. M. M. T. Eikelder, A. J. Markvoort, T. F. A. D. Greef and P. A. J. Hilbers, *J. Phys. Chem. B*, 2012, **116**, 5291–5301.

96 M. M. J. Smulders, M. M. L. Nieuwenhuizen, T. F. A. D. Greef, P. V. D. Schoot, A. P. H. J. Schenning and E. W. Meijer, *Chem. Eur. J.*, 2010, **16**, 362–367.

97 B. Matarranz, S. Díaz-Cabrera, G. Ghosh, I. Carreira-Barral, B. Soberats, M. García-Valverde, R. Quesada and G. Fernández, *Angew. Chem., Int. Ed.*, 2023, **62**, e202218555.

98 J. S. Valera, R. Gómez and L. Sánchez, *Org. Lett.*, 2018, **20**, 2020–2023.

99 Y. Liu, Z. Wang and X. Zhang, *Chem. Soc. Rev.*, 2012, **41**, 5922–5932.

This journal is © The Royal Society of Chemistry 2025

*Chem. Soc. Rev.*, 2025, **54**, 11659–11698 | **11691**

100 R. Vill, J. Gülcher, P. Khalatur, P. Wintergerst, A. Stoll, A. Mourran and U. Ziener, *Nanoscale*, 2019, **11**, 663–674.

101 M. Pons and O. Millet, *Prog. Nucl. Magn. Reson. Spectrosc.*, 2001, **38**, 267–324.

102 F. García, R. Gómez and L. Sánchez, *Chem. Soc. Rev.*, 2023, **52**, 7524–7548.

103 Y. Marechal and A. Witkowski, *J. Chem. Phys*, 1968, **48**, 3697–3705.

104 A. Arnaud and L. Bouteiller, *Langmuir*, 2004, **20**, 6858–6863.

105 S. K. Brar and M. Verma, *TrAC Trends Anal. Chem.*, 2011, **30**, 4–17.

106 C. M. Jeffries, J. Ilavsky, A. Martel, S. Hinrichs, A. Meyer, J. S. Pedersen, A. V. Sokolova and D. I. Svergun, *Nat. Rev. Methods Primer*, 2021, **1**, 70.

107 F. J. Giessibl, *Rev. Mod. Phys.*, 2003, **75**, 949.

108 D. J. Smith, Characterization of Nanomaterials Using Transmission Electron Microscopy, *Nanoscience and Nanotechnology Series*, Royal Society of Chemistry, Cambridge, UK, 2015.

109 D. Bochicchio and G. M. Pavan, *Adv. Phys. X*, 2018, **3**, 1436408.

110 I. A. W. Filot, A. R. A. Palmans, P. A. J. Hilbers, R. A. V. Santen, E. A. Pidko and T. F. A. D. Greef, *J. Phys. Chem. B*, 2010, **114**, 13667–13674.

111 C. Bannwarth, S. Ehlert and S. Grimme, *J. Chem. Theory Comput.*, 2019, **15**, 1652–1671.

112 D. C. Rapaport, J. E. Johnson and J. Skolnick, *Comput. Phys. Commun.*, 1999, **121–122**, 231–235.

113 D. Bochicchio, M. Salvalaglio and G. M. Pavan, *Nat. Commun.*, 2017, **8**, 147.

114 M. Crippa, C. Perego, A. L. de Marco and G. M. Pavan, *Nat. Commun.*, 2022, **13**, 2162.

115 C. M. Atienza and L. Sánchez, *Chem. Eur. J.*, 2024, **30**, e202400379.

116 X. Xiao, H. Chen, X. Dong, J. Zhang, J. Zhang, H. Zhang, D. Wang and W. Tian, *Mater. Chem. Front.*, 2022, **6**, 3261–3270.

117 J. Uchida, B. Soberats, M. Gupta and T. Kato, *Adv. Mater.*, 2022, **34**, 2109063.

118 R. Liao, F. Wang, Y. Guo, Y. Han and F. Wang, *J. Am. Chem. Soc.*, 2022, **144**, 9775–9784.

119 S. H. Jung, D. Bochicchio, G. M. Pavan, M. Takeuchi and K. Sugiyasu, *J. Am. Chem. Soc.*, 2018, **140**, 10570–10577.

120 W. Wagner, M. Wehner, V. Stepanenko and F. Würthner, *J. Am. Chem. Soc.*, 2019, **141**, 12044–12054.

121 S. Sarkar, A. Sarkar, A. Som, S. S. Agasti and S. J. George, *J. Am. Chem. Soc.*, 2021, **143**, 11777–11787.

122 B. Adelizzi, A. Aloi, A. J. Markvoort, H. M. M. Ten Eikelder, I. K. Voets, A. R. A. Palmans and E. W. Meijer, *J. Am. Chem. Soc.*, 2018, **140**, 7168–7175.

123 A. Sarkar, T. Behera, R. Sasmal, R. Capelli, C. Empereur-mot, J. Mahato, S. S. Agasti, G. M. Pavan, A. Chowdhury and S. J. George, *J. Am. Chem. Soc.*, 2020, **142**, 11528–11539.

124 M. M. Safont-Sempere, G. Fernández and F. Würthner, *Chem. Rev.*, 2011, **111**, 5784–5814.

125 A. Das and S. Ghosh, *Angew. Chem., Int. Ed.*, 2014, **53**, 2038–2054.

126 B. Adelizzi, N. J. Van Zee, L. N. J. de Windt, A. R. A. Palmans and E. W. Meijer, *J. Am. Chem. Soc.*, 2019, **141**, 6110–6121.

127 Y. Chen and C. Liu, *ChemPlusChem*, 2024, **89**, e202300623.

128 M. J. Mayoral, C. Rest, J. Schellheimer, V. Stepanenko and G. Fernández, *Chem. Eur. J.*, 2012, **18**, 15607–15611.

129 X. Huang, R. Li, Z. Duan, F. Xu and H. Li, *Soft Matter*, 2022, **18**, 3828–3844.

130 Y. Yasuda, E. Iishi, H. Inada and Y. Shirota, *Chem. Lett*, 1996, **25**, 575–576.

131 K. Hanabusa, C. Koto, M. Kimura, H. Shirai and A. Kakehi, *Chem. Lett*, 1997, **26**, 429–430.

132 F. Aparicio, F. García and L. Sánchez, *Chem. Eur. J.*, 2013, **19**, 3239–3248.

133 J. J. I. Armao, M. Maaloum, T. Ellis, G. Fuks, M. Rawiso, E. Moulin and N. Giuseppone, *J. Am. Chem. Soc.*, 2014, **136**, 11382–11388.

134 E. Moulin, J. J. I. Armao and N. Giuseppone, *Acc. Chem. Res.*, 2019, **52**, 975–983.

135 M. Shirakawa, S. Kawano, N. Fujita, K. Sada and S. Shinkai, *J. Org. Chem.*, 2003, **68**, 5037–5044.

136 J. Kang, D. Miyajima, Y. Itoh, T. Mori, H. Tanaka, M. Yamauchi, Y. Inoue, S. Harada and T. Aida, *J. Am. Chem. Soc.*, 2014, **136**, 10640–10644.

137 J. Kang, D. Miyajima, T. Mori, Y. Inoue, Y. Itoh and T. Aida, *Science*, 2015, **347**, 646–651.

138 X. Dou, W. Pisula, J. Wu, G. J. Bodwell and K. Müllen, *Chem. Eur. J.*, 2008, **14**, 240–249.

139 S. V. Bhosale, M. A. Kobaisi, R. W. Jadhav, P. P. Morajkar, L. A. Jones and S. George, *Chem. Soc. Rev.*, 2021, **50**, 9845–9998.

140 P. Mukhopadhyay, Y. Iwashita, M. Shirakawa, S. Kawano, N. Fujita and S. Shinkai, *Angew. Chem., Int. Ed.*, 2006, **45**, 1592–1595.

141 F. Würthner, C. Thalacker and A. Sautter, *Adv. Mater.*, 1999, **11**, 754–758.

142 F. Würthner, C. Thalacker, A. Sautter, W. Schärtl, W. Ibach and O. Hollricher, *Chem. Eur. J.*, 2000, **6**, 3871–3886.

143 P. Jonkheijm, A. Miura, M. Zdanowska, F. J. M. Hoeben, S. De Feyter, A. P. H. J. Schenning, F. C. De Schryver and E. W. Meijer, *Angew. Chem., Int. Ed.*, 2004, **43**, 74–78.

144 S. J. George, Ž. Tomović, M. M. J. Smulders, T. F. A. de Greef, P. E. L. G. Leclère, E. W. Meijer and A. P. H. J. Schenning, *Angew. Chem., Int. Ed.*, 2007, **46**, 8206–8211.

145 P. A. Korevaar, S. J. George, A. J. Markvoort, M. M. J. Smulders, P. A. J. Hilbers, A. P. H. J. Schenning, T. F. A. De Greef and E. W. Meijer, *Nature*, 2012, **481**, 492–496.

146 A. P. H. J. Schenning, J. v Herrikhuyzen, P. Jonkheijm, Z. Chen, F. Würthner and E. W. Meijer, *J. Am. Chem. Soc.*, 2002, **124**, 10252–10253.

147 B. Adhikari, X. Lin, M. Yamauchi, H. Ouchi, K. Aratsu and S. Yagai, *Chem. Commun.*, 2017, **53**, 9663–9683.

148 H. Ouchi, X. Lin and S. Yagai, *Chem. Lett*, 2019, **48**, 1009–1018.

11692 | *Chem. Soc. Rev.*, 2025, **54**, 11659–11698

This journal is © The Royal Society of Chemistry 2025

149 K. Tashiro, T. Saito, H. Arima, N. Suda, B. Vedhanarayanan and S. Yagai, *Chem. Rec.*, 2022, **22**, e202100252.

150 S. Yagai, M. Suzuki, X. Lin, M. Gushiken, T. Noguchi, T. Karatsu, A. Kitamura, A. Saeki, S. Seki, Y. Kikkawa, Y. Tani and K. Nakayama, *Chem. Eur. J.*, 2014, **20**, 16128–16137.

151 S. Yagai, M. Yamauchi, A. Kobayashi, T. Karatsu, A. Kitamura, T. Ohba and Y. Kikkawa, *J. Am. Chem. Soc.*, 2012, **134**, 18205–18208.

152 T. Saito and S. Yagai, *Eur. J. Org. Chem.*, 2020, 2475–2478.

153 T. Saito, T. Kajitani and S. Yagai, *J. Am. Chem. Soc.*, 2023, **145**, 443–454.

154 A. del Prado, D. González-Rodríguez and Y.-L. Wu, *ChemistryOpen*, 2020, **9**, 409–430.

155 V. Vázquez-González, M. J. Mayoral, R. Chamorro, M. M. R. M. Hendrix, I. K. Voets and D. González-Rodríguez, *J. Am. Chem. Soc.*, 2019, **141**, 16432–16438.

156 V. Vázquez-González, M. J. Mayoral, F. Aparicio, P. Martínez-Arjona and D. González-Rodríguez, *ChemPlusChem*, 2021, **86**, 1087–1096.

157 M. González-Sánchez, J. S. Valera, J. Veiga-Herrero, P. B. Chamorro, F. Aparicio and D. González-Rodríguez, *Chem. Soc. Rev.*, 2025, **54**, 5657–5697.

158 N. Bilbao, I. Destoop, S. De Feyter and D. González-Rodríguez, *Angew. Chem., Int. Ed.*, 2016, **55**, 659–663.

159 I. Sancho-Casado, F. Aparicio, M. González-Sánchez, R. Chamorro, V. Vega-Mayoral, J. Cabanillas-González and D. González-Rodríguez, *Angew. Chem., Int. Ed.*, 2025, e202509156.

160 L. S. Shimizu, *Polym. Int.*, 2007, **56**, 444–452.

161 J. D. Fox and S. J. Rowan, *Macromolecules*, 2009, **42**, 6823–6835.

162 S. H. M. Söntjens, R. P. Sijbesma, M. H. P. van Genderen and E. W. Meijer, *J. Am. Chem. Soc.*, 2000, **122**, 7487–7493.

163 M. Kotera, J.-M. Lehn and J.-P. Vigneron, *Tetrahedron*, 1995, **51**, 1953–1972.

164 M. Kotera, J.-M. Lehn and J.-P. Vigneron, *J. Chem. Soc. Chem. Commun.*, 1994, 197–199.

165 V. Berl, M. Schmutz, M. J. Krische, R. G. Khoury and J.-M. Lehn, *Chem. Eur. J.*, 2002, **8**, 1227–1244.

166 R. Schmidt, M. Stolte, M. Grüne and F. Würthner, *Macromolecules*, 2011, **44**, 3766–3776.

167 S. P. Dudek, M. Pouderoijen, R. Abbel, A. P. H. J. Schenning and E. W. Meijer, *J. Am. Chem. Soc.*, 2005, **127**, 11763–11768.

168 R. Abbel, C. Grenier, M. J. Pouderoijen, J. W. Stouwdam, P. E. L. G. Leclère, R. P. Sijbesma, E. W. Meijer and A. P. H. J. Schenning, *J. Am. Chem. Soc.*, 2009, **131**, 833–843.

169 A. Tsuda, Md. A. Alam, T. Harada, T. Yamaguchi, N. Ishii and T. Aida, *Angew. Chem., Int. Ed.*, 2007, **46**, 8198–8202.

170 T. E. Kaiser, H. Wang, V. Stepanenko and F. Würthner, *Angew. Chem., Int. Ed.*, 2007, **46**, 5541–5544.

171 V. Grande, B. Soberats, S. Herbst, V. Stepanenko and F. Würthner, *Chem. Sci.*, 2018, **9**, 6904–6911.

172 S. Herbst, B. Soberats, P. Leowanawat, M. Lehmann and F. Würthner, *Angew. Chem., Int. Ed.*, 2017, **56**, 2162–2165.

173 S. Herbst, B. Soberats, P. Leowanawat, M. Stolte, M. Lehmann and F. Würthner, *Nat. Commun.*, 2018, **9**, 2646.

174 H. Kar, D. W. Gehrig, N. K. Allampally, G. Fernández, F. Laquai and S. Ghosh, *Chem. Sci.*, 2016, **7**, 1115–1120.

175 E. Castellanos, R. M. Gomila, R. Manha, G. Fernández, A. Frontera and B. Soberats, *J. Mater. Chem. C*, 2023, **11**, 10884–10892.

176 B. Soberats, M. Hecht and F. Würthner, *Angew. Chem., Int. Ed.*, 2017, **56**, 10771–10774.

177 M. Hecht, B. Soberats, J. Zhu, V. Stepanenko, S. Agarwal, A. Greiner and F. Würthner, *Nanoscale Horiz.*, 2018, **4**, 169–174.

178 P. Ximenis, L. Rubert, H. M. A. Ehmann and B. Soberats, *Org. Chem. Front.*, 2025, **12**, 430–436.

179 Y. Zhang, P. Liu, H. Pan, H. Dai, X.-K. Ren and Z. Chen, *Chem. Commun.*, 2020, **56**, 12069–12072.

180 M. Liu, L. Zhang and T. Wang, *Chem. Rev.*, 2015, **115**, 7304–7397.

181 R. A. Hegstrom and D. K. Kondepudi, *Sci. Am.*, 1990, **262**, 108–115.

182 T. Seki, A. Asano, S. Seki, Y. Kikkawa, H. Murayama, T. Karatsu, A. Kitamura and S. Yagai, *Chem. Eur. J.*, 2011, **17**, 3598–3608.

183 F. Helmich, C. C. Lee, A. P. H. J. Schenning and E. W. Meijer, *J. Am. Chem. Soc.*, 2010, **132**, 16753–16755.

184 M. Wehner, M. I. S. Röhr, V. Stepanenko and F. Würthner, *Nat. Commun.*, 2020, **11**, 5460.

185 M. A. Martínez, A. Doncel-Giménez, J. Cerdá, J. Calbo, R. Rodríguez, J. Aragó, J. Crassous, E. Ortí and L. Sánchez, *J. Am. Chem. Soc.*, 2021, **143**, 13281–13291.

186 A. R. A. Palmans, J. A. J. M. Vekemans, E. E. Havinga and E. W. Meijer, *Angew. Chem., Int. Ed. Engl.*, 1997, **36**, 2648–2651.

187 A. J. Wilson, J. V. Gestel, R. P. Sijbesma and E. W. Meijer, *Chem. Commun.*, 2006, 4404–4406.

188 Y. Dorca, R. Sánchez-Naya, J. Cerdá, J. Calbo, J. Aragó, R. Gómez, E. Ortí and L. Sánchez, *Chem. Eur. J.*, 2020, **26**, 14700–14707.

189 E. E. Greciano, J. Calbo, J. Buendía, J. Cerdá, J. Aragó, E. Ortí and L. Sánchez, *J. Am. Chem. Soc.*, 2019, **141**, 7463–7472.

190 Y. Dorca, C. Naranjo, G. Ghosh, R. Gómez, G. Fernández and L. Sánchez, *Org. Mater.*, 2020, **2**, 41–46.

191 B. Adelizzi, I. A. W. Filot, A. R. A. Palmans and E. W. Meijer, *Chem. Eur. J.*, 2017, **23**, 6103–6110.

192 J. S. Valera, R. Gómez and L. Sánchez, *Small*, 2018, **14**, 1702437.

193 S. Ghosh, X.-Q. Li, V. Stepanenko and F. Würthner, *Chem. Eur. J.*, 2008, **14**, 11343–11357.

194 E. E. Greciano, R. Rodríguez, K. Maeda and L. Sánchez, *Chem. Commun.*, 2020, **56**, 2244–2247.

195 N. Suda, T. Saito, H. Arima and S. Yagai, *Chem. Sci.*, 2022, **13**, 3249–3255.

196 M. Yamauchi, T. Ohba, T. Karatsu and S. Yagai, *Nat. Commun.*, 2015, **6**, 8936.

This journal is © The Royal Society of Chemistry 2025

*Chem. Soc. Rev.*, 2025, **54**, 11659–11698 | **11693**

197 T. Saito, D. Inoue, Y. Kitamoto, H. Hanayama, T. Fujita, Y. Watanabe, M. Suda, T. Hirose, T. Kajitani and S. Yagai, *Nat. Nanotechnol.*, 2025, **20**, 825–834.

198 M. Nic, L. Hovorka, J. JIrat, B. Kosata and J. Znamenacek, *IUPAC compendium of chemical terminology-the gold book*, International Union of Pure and Applied Chemistry, 2nd edn, 2005.

199 S. Sarkar, A. Sarkar and S. J. George, *Angew. Chem., Int. Ed.*, 2020, **59**, 19841–19845.

200 S. Sarkar, A. Sarkar, A. Som, S. S. Agasti and S. J. George, *J. Am. Chem. Soc.*, 2021, **143**, 11777–11787.

201 B. Narayan, K. K. Bejagam, S. Balasubramanian and S. J. George, *Angew. Chem., Int. Ed.*, 2015, **54**, 13053–13057.

202 A. Sarkar, S. Dhiman, A. Chalishazar and S. J. George, *Angew. Chem., Int. Ed.*, 2017, **56**, 13767–13771.

203 P. Osswald and F. Würthner, *J. Am. Chem. Soc.*, 2007, **129**, 14319–14326.

204 Z. Xie and F. Würthner, *Org. Lett.*, 2010, **12**, 3204–3207.

205 Z. Xie, V. Stepanenko, K. Radacki and F. Würthner, *Chem. Eur. J.*, 2012, **18**, 7060–7070.

206 T. Ogoshi, T. Furuta and T. A. Yamagishi, *Chem. Commun.*, 2016, **52**, 10775–10778.

207 D. E. Fagnani, M. J. Meese Jr., K. A. Abboud and R. K. Castellano, *Angew. Chem., Int. Ed.*, 2016, **55**, 10726–10731.

208 W. R. Henderson, Y. Zhu, D. E. Fagnani, G. Liu, K. A. Abboud and R. K. Castellano, *J. Org. Chem.*, 2020, **85**, 1158–1167.

209 W. R. Henderson, A. Kumar, K. A. Abboud and R. K. Castellano, *Chem. Eur. J.*, 2020, **26**, 17588–17597.

210 T. Hirose, N. Ito, H. Kubo, T. Sato and K. Matsuda, *J. Mater. Chem. C*, 2016, **4**, 2811–2819.

211 R. Rodríguez, C. Naranjo, A. Kumar, P. Matozzo, T. K. Das, Q. Zhu, N. Vanthuyne, R. Gómez, R. Naaman, L. Sánchez and J. Crassous, *J. Am. Chem. Soc.*, 2022, **144**, 7709–7719.

212 L. López-Gandul, R. Rodríguez, N. Vanthuyne, J. Crassous and L. Sánchez, *Nanoscale*, 2024, **16**, 13041–13049.

213 M. J. Mayoral, J. Guilleme, J. Calbo, J. Aragó, F. Aparicio, E. Ortí, T. Torres and D. González-Rodríguez, *J. Am. Chem. Soc.*, 2020, **142**, 21017–21031.

214 M. M. Green, M. P. Reidy, R. J. Johnson, G. Darling, D. J. O'Leary and G. Willson, *J. Am. Chem. Soc.*, 1989, **111**, 6452–6454.

215 H. Gu, Y. Nakamura, T. Sato, A. Teramoto, M. M. Green, S. K. Jha, C. Andreola and M. P. Reidy, *Macromolecules*, 1998, **31**, 6362–6368.

216 M. M. Green, B. A. Garetz, B. Munoz, H. P. Chang, S. Hoke and R. G. Cooks, *J. Am. Chem. Soc.*, 1995, **117**, 4181–4182.

217 J. V. Gestel, A. R. A. Palmans, B. Titulaer, J. A. J. M. Vekemans and E. W. Meijer, *J. Am. Chem. Soc.*, 2005, **127**, 5490–5494.

218 T. Kim, T. Mori, T. Aida and D. Miyajima, *Chem. Sci.*, 2016, **7**, 6689–6694.

219 A. Das, S. Ghosh and S. J. George, *Angew. Chem., Int. Ed.*, 2023, **62**, e202308281.

220 M. M. J. Smulders, P. J. M. Stals, T. Mes, T. F. E. Paffen, A. P. H. J. Schenning, A. R. A. Palmans and E. W. Meijer, *J. Am. Chem. Soc.*, 2010, **132**, 620–626.

221 M. M. J. Smulders, I. A. W. Filot, J. M. A. Leenders, P. V. D. Schoot, A. R. A. Palmans, A. P. H. J. Schenning and E. W. Meijer, *J. Am. Chem. Soc.*, 2010, **132**, 611–619.

222 Y. Jin, H. Zhao, F. Han, S. Jiang, Y. Xue and F. Wang, *ACS Macro Lett.*, 2025, **14**, 781–787.

223 J. Buendía, J. Calbo, F. García, J. Aragó, P. M. Viruela, E. Ortí and L. Sánchez, *Chem. Commun.*, 2016, **52**, 6907–6910.

224 T. Metzroth, A. Hoffmann, R. Martín-Rapún, M. M. J. Smulders, K. Pieterse, A. R. A. Palmans, J. A. J. M. Vekemans, E. W. Meijer, H. W. Spiess and J. Gauss, *Chem. Sci.*, 2010, **2**, 69–76.

225 B. Isare, M. Linares, L. Zargarian, S. Fermandjian, M. Miura, S. Motohashi, N. Vanthuyne, R. Lazzaroni and L. Bouteiller, *Chem. Eur. J.*, 2010, **16**, 173–177.

226 V. Stepanenko, X. Q. Li, J. Gershberg and F. Würthner, *Chem. Eur. J.*, 2013, **19**, 4176–4183.

227 J. Kim, J. Lee, W. Y. Kim, H. Kim, S. Lee, H. C. Lee, Y. S. Lee, M. Seo and S. Y. Kim, *Nat. Commun.*, 2015, **6**, 6959.

228 J. S. Kang, S. Kang, J. M. Suh, S. M. Park, D. K. Yoon, M. H. Lim, W. Y. Kim and M. Seo, *J. Am. Chem. Soc.*, 2022, **144**, 2657–2666.

229 K. Fu and G. Liu, *ACS Nano*, 2024, **18**, 2279–2289.

230 C. Wagenknecht, C. M. Li, A. Reingruber, X. H. Bao, A. Goebel, Y. A. Chen, Q. Zhang, K. Chen and J. W. Pan, *Nat. Photonics*, 2010, **4**, 549–552.

231 Q. Wang, H. Xu, Z. Qi, J. Mei, H. Tian and D. H. Qu, *Angew. Chem., Int. Ed.*, 2024, **63**, e202407385.

232 T. Zhao, J. Han, P. Duan and M. Liu, *Acc. Chem. Res.*, 2020, **53**, 1279–1292.

233 Y. Yang, R. C. D. Costa, M. J. Fuchter and A. J. Campbell, *Nat. Photonics*, 2013, **7**, 634–638.

234 G. Liu, M. G. Humphrey, C. Zhang and Y. Zhao, *Chem. Soc. Rev.*, 2023, **52**, 4443–4487.

235 G. Muller, *Dalton Trans.*, 2009, 9692–9707.

236 F. Song, G. Wei, X. Jiang, F. Li, C. Zhu and Y. Cheng, *Chem. Commun.*, 2013, **49**, 5772–5774.

237 L. Arrico, L. D. Bari and F. Zinna, *Chem. Eur. J.*, 2021, **27**, 2920–2934.

238 Y. Nagata and T. Mori, *Front. Chem.*, 2020, **8**, 535258.

239 L. Gao, R. Liao, L. Ao, Y. Zhang, J. Jin and F. Wang, *Angew. Chem., Int. Ed.*, 2025, **64**, e202505776.

240 Y. Zhang, W. Yu, H. Li, W. Zheng and Y. Cheng, *Chem. Eur. J.*, 2023, **29**, e202204039.

241 C. Li, X. Jin, J. Han, T. Zhao and P. Duan, *J. Phys. Chem. Lett.*, 2021, **12**, 8566–8574.

242 Y. Sang, J. Han, T. Zhao, P. Duan, M. Liu, Y. Sang, M. Liu, T. Zhao, P. Duan and J. Han, *Adv. Mater.*, 2020, **32**, 1900110.

243 J. Luo, Z. Xie, Z. Xie, J. W. Y. Lam, L. Cheng, H. Chen, C. Qiu, H. S. Kwok, X. Zhan, Y. Liu, D. Zhu and B. Z. Tang, *Chem. Commun.*, 2001, 1740–1741.

244 B. K. An, S. K. Kwon, S. D. Jung and S. Y. Park, *J. Am. Chem. Soc.*, 2002, **124**, 14410–14415.

245 Y. Yin, Z. Chen, Y. Han, R. Liao and F. Wang, *Org. Chem. Front.*, 2021, **8**, 4986.

**11694** | *Chem. Soc. Rev.*, 2025, **54**, 11659–11698

This journal is © The Royal Society of Chemistry 2025

246 L. López-Gandul, C. Naranjo, C. Sánchez, R. Rodríguez, R. Gómez, J. Crassous and L. Sánchez, *Chem. Sci.*, 2022, **13**, 11577–11584.

247 J. Kumar, T. Nakashima, H. Tsumatori, M. Mori, M. Naito and T. Kawai, *Chem. Eur. J.*, 2013, **19**, 14090–14097.

248 J. A. Panis, M. Louis, A. Brosseau, S. Katao, F. de los Reyes, T. Nakashima, R. Métivier, C. Allain and T. Kawai, *Chem. Eur. J.*, 2022, **28**, e202201012.

249 S. Hu, L. Hu, X. Zhu, Y. Wang and M. Liu, *Angew. Chem., Int. Ed.*, 2021, **60**, 19451–19457.

250 M. J. Álvaro-Martins, C. Billiaux, P. Godard, R. Oda, G. Raffy and D. M. Bassani, *Chem. Commun.*, 2023, **59**, 7963–7966.

251 S. Ghorai, S. Show and A. Das, *Angew. Chem., Int. Ed.*, 2025, **64**, e202500879.

252 A. Mukherjee and S. Ghosh, *Chem. Eur. J.*, 2020, **26**, 12874–12881.

253 H. Cao, P. Duan, X. Zhu, J. Jiang and M. Liu, *Chem. Eur. J.*, 2012, **18**, 5546–5550.

254 K. S. Novoselov, A. K. Geim, S. V. Morozov, D. Jiang, Y. Zhang, S. V. Dubonos, I. V. Grigorieva and A. A. Firsov, *Science*, 2004, **306**, 666–669.

255 I. S. Choi, N. Bowden and G. M. Whitesides, *Angew. Chem., Int. Ed.*, 1999, **38**, 3078–3081.

256 C. M. Atienza and L. Sánchez, *Chem. Eur. J.*, 2024, **30**, e202400379.

257 L. Gallego, J. F. Woods and M. Rickhaus, *Org. Mater.*, 2022, **4**, 137–145.

258 I. Insua, J. Bergueiro, A. Méndez-Ardoy, I. Lostalé-Seijo and J. Montenegro, *Chem. Sci.*, 2022, **13**, 3057–3068.

259 X. He, M.-S. Hsiao, C. E. Boott, R. L. Harniman, A. Nazemi, X. Li, M. A. Winnik and I. Manners, *Nat. Mater.*, 2017, **16**, 481–488.

260 Y.-S. Yoo, J.-H. Choi, J.-H. Song, N.-K. Oh, W.-C. Zin, S. Park, T. Chang and M. Lee, *J. Am. Chem. Soc.*, 2004, **126**, 6294–6300.

261 J.-K. Kim, E. Lee, Y.-H. Jeong, J.-K. Lee, W.-C. Zin and M. Lee, *J. Am. Chem. Soc.*, 2007, **129**, 6082–6083.

262 E. Lee, Y.-H. Jeong, J.-K. Kim and M. Lee, *Macromolecules*, 2007, **40**, 8355–8360.

263 S. Shin, S. Lim, Y. Kim, T. Kim, T.-L. Choi and M. Lee, *J. Am. Chem. Soc.*, 2013, **135**, 2156–2159.

264 Y. Kim, S. Shin, T. Kim, D. Lee, C. Seok and M. Lee, *Angew. Chem., Int. Ed.*, 2013, **52**, 6426–6429.

265 B. Sun, B. Shen, A. Urushima, X. Liu, X. Feng, E. Yashima and M. Lee, *Angew. Chem., Int. Ed.*, 2020, **59**, 22690–22696.

266 B. Sun, Y. Kim, Y. Wang, H. Wang, J. Kim, X. Liu and M. Lee, *Nat. Mater.*, 2018, **17**, 599–604.

267 I. Insua and J. Montenegro, *J. Am. Chem. Soc.*, 2020, **142**, 300–307.

268 T. Fukui, S. Kawai, S. Fujinuma, Y. Matsushita, T. Yasuda, T. Sakurai, S. Seki, M. Takeuchi and K. Sugiyasu, *Nat. Chem.*, 2017, **9**, 493–499.

269 N. Sasaki, J. Yuan, T. Fukui, M. Takeuchi and K. Sugiyasu, *Chem. Eur. J.*, 2020, **26**, 7840–7846.

270 E. E. Greciano, J. Calbo, E. Ortí and L. Sánchez, *Angew. Chem., Int. Ed.*, 2020, **59**, 17517–17524.

271 N. Bäumer, K. K. Kartha, J. P. Palakkal and G. Fernández, *Soft Matter*, 2020, **16**, 6834–6840.

272 A. Chakraborty, G. Ghosh, D. S. Pal, S. Varghese and S. Ghosh, *Chem. Sci.*, 2019, **10**, 7345–7351.

273 J.-A. Zhang, X. Xiao, J. Wang, S. Luo, Y. Lu, Y.-Y. Pang and W. Tian, *J. Am. Chem. Soc.*, 2025, **147**, 13447–13460.

274 N. Sasaki, M. F. J. Mabesoone, J. Kikkawa, T. Fukui, N. Shioya, T. Shimoaka, T. Hasegawa, H. Takagi, R. Haruki, N. Shimizu, S. Adachi, E. W. Meijer, M. Takeuchi and K. Sugiyasu, *Nat. Commun.*, 2020, **11**, 3578.

275 J. S. Valera, H. Arima, C. Naranjo, T. Saito, N. Suda, R. Gómez, S. Yagai and L. Sánchez, *Angew. Chem., Int. Ed.*, 2022, **61**, e202114290.

276 L. Rubert, M. F. Islam, A. B. Greytak, R. Prakash, M. D. Smith, R. M. Gomila, A. Frontera, L. S. Shimizu and B. Soberats, *Angew. Chem., Int. Ed.*, 2023, **62**, e202312223.

277 C.-A. Shen, D. Bialas, M. Hecht, V. Stepanenko, K. Sugiyasu and F. Würthner, *Angew. Chem., Int. Ed.*, 2021, **60**, 11949–11958.

278 M. Hecht, P. Leowanawat, T. Gerlach, V. Stepanenko, M. Stolte, M. Lehmann and F. Würthner, *Angew. Chem., Int. Ed.*, 2020, **59**, 17084–17090.

279 G. Ghosh, P. Dey and S. Ghosh, *Chem. Commun.*, 2020, **56**, 6757–6769.

280 J. Matern, Y. Dorca, L. Sánchez and G. Fernández, *Angew. Chem., Int. Ed.*, 2019, **58**, 16730–16740.

281 M. Wehner and F. Würthner, *Nat. Rev. Chem.*, 2020, **4**, 38–53.

282 G. Ghosh, *Giant*, 2023, **14**, 100160.

283 P. A. Korevaar, T. F. A. de Greef and E. W. Meijer, *Chem. Mater.*, 2014, **26**, 576–586.

284 T. Aida and E. w Meijer, *Isr. J. Chem.*, 2020, **60**, 33–47.

285 A. Lohr and F. Würthner, *Angew. Chem., Int. Ed.*, 2008, **47**, 1232–1236.

286 M. M. Bouman and E. W. Meijer, *Adv. Mater.*, 1995, **7**, 385–387.

287 J.-H. Ryu and M. Lee, *J. Am. Chem. Soc.*, 2005, **127**, 14170–14171.

288 S. Dhiman and S. J. George, *Bull. Chem. Soc. Jpn*, 2018, **91**, 687–699.

289 K. Sugiyasu, *Polym. J.*, 2021, **53**, 865–875.

290 S. Ogi, K. Matsumoto and S. Yamaguchi, *Angew. Chem., Int. Ed.*, 2018, **57**, 2339–2343.

291 J. Matern, Z. Fernández, N. Bäumer and G. Fernández, *Angew. Chem., Int. Ed.*, 2022, **61**, e202203783.

292 S. Patra, S. Dhiman and S. J. George, *Chem. Mater.*, 2024, **36**, 9460–9468.

293 S. Ogi, V. Stepanenko, J. Thein and F. Würthner, *J. Am. Chem. Soc.*, 2016, **138**, 670–678.

294 W. Wagner, M. Wehner, V. Stepanenko, S. Ogi and F. Würthner, *Angew. Chem., Int. Ed.*, 2017, **56**, 16008–16012.

295 E. E. Greciano, J. Calbo, E. Ortí and L. Sánchez, *Angew. Chem., Int. Ed.*, 2020, **59**, 17517–17524.

This journal is © The Royal Society of Chemistry 2025

*Chem. Soc. Rev.*, 2025, **54**, 11659–11698 | **11695**

296 C. Naranjo, S. Adalid, R. Gómez and L. Sánchez, *Angew. Chem., Int. Ed.*, 2023, **62**, e202218572.

297 E. E. Greciano, S. Alsina, G. Ghosh, G. Fernández and L. Sánchez, *Small Methods*, 2020, **4**, 1900715.

298 N. Fukaya, S. Ogi, H. Sotome, K. J. Fujimoto, T. Yanai, N. Bäumer, G. Fernández, H. Miyasaka and S. Yamaguchi, *J. Am. Chem. Soc.*, 2022, **144**, 22479–22492.

299 J. Matern, I. Maisuls, C. A. Strassert and G. Fernández, *Angew. Chem., Int. Ed.*, 2022, **61**, e202208436.

300 J. Matern, Z. Fernández and G. Fernández, *Chem. Commun.*, 2022, **58**, 12309–12312.

301 S. Ogi, K. Sugiyasu, S. Manna, S. Samitsu and M. Takeuchi, *Nat. Chem.*, 2014, **6**, 188–195.

302 S. Ogi, T. Fukui, M. L. Jue, M. Takeuchi and K. Sugiyasu, *Angew. Chem., Int. Ed.*, 2014, **53**, 14363–14367.

303 R. M. Veedu, Z. Fernández, N. Bäumer, A. Albers and G. Fernández, *Chem. Sci.*, 2024, **15**, 10745–10752.

304 H. Kar, G. Ghosh and S. Ghosh, *Chem. Eur. J.*, 2017, **23**, 10536–10542.

305 Y. Huang, R. Zhang, C. Shi, C. Wang, R. Liao, C. Zou, F. Wang and N. Huang, *Chem. Eur. J.*, 2025, **31**, e202500120.

306 T. Gädt, N. S. Ieong, G. Cambridge, M. A. Winnik and I. Manners, *Nat. Mater.*, 2009, **8**, 144–150.

307 J. B. Gilroy, T. Gädt, G. R. Whittell, L. Chabanne, J. M. Mitchels, R. M. Richardson, M. A. Winnik and I. Manners, *Nat. Chem.*, 2010, **2**, 566–570.

308 Z. Jin, N. Sasaki, N. Kishida, M. Takeuchi, Y. Wakayama and K. Sugiyasu, *Chem. Eur. J.*, 2023, **29**, e202302181.

309 L. Kleine-Kleffmann, A. Schulz, V. Stepanenko and F. Würthner, *Angew. Chem., Int. Ed.*, 2023, **62**, e202314667.

310 P. Khanra, P. Rajdev and A. Das, *Angew. Chem., Int. Ed.*, 2024, **63**, e202400486.

311 Z. Jin, M. Takeuchi, Y. Wakayama and K. Sugiyasu, *Chem. Eur. J.*, 2023, **29**, e202302181.

312 S. Yagai and A. Kitamura, *Chem. Soc. Rev.*, 2008, **37**, 1520–1529.

313 E. Fuentes, M. Gerth, J. A. Berrocal, C. Matera, P. Gorostiza, I. K. Voets, S. Pujals and L. Albertazzi, *J. Am. Chem. Soc.*, 2020, **142**, 10069–10078.

314 M. Endo, T. Fukui, S. H. Jung, S. Yagai, M. Takeuchi and K. Sugiyasu, *J. Am. Chem. Soc.*, 2016, **138**, 14347–14353.

315 F. Xu, L. Pfeifer, S. Crespi, F. K.-C. Leung, M. C. A. Stuart, S. J. Wezenberg and B. L. Feringa, *J. Am. Chem. Soc.*, 2021, **143**, 5990–5997.

316 S. Imai, T. Hamada, M. Nozaki, T. Fujita, M. Takahashi, Y. Fujita, K. Harano, H. Uji-i, A. Takai and K. Hirai, *J. Am. Chem. Soc.*, 2025, **147**, 23528–23535.

317 L. Kleine-Kleffmann, V. Stepanenko, K. Shoyama, M. Wehner and F. Würthner, *J. Am. Chem. Soc.*, 2023, **145**, 9144–9151.

318 C. Naranjo, Y. Dorca, G. Ghosh, R. Gómez, G. Fernández and L. Sánchez, *Chem. Commun.*, 2021, **57**, 4500–4503.

319 N. Bäumer, E. Castellanos, B. Soberats and G. Fernández, *Nat. Commun.*, 2023, **14**, 1084.

320 T. Fukui, N. Sasaki, M. Takeuchi and K. Sugiyasu, *Chem. Sci.*, 2019, **10**, 6770–6776.

321 H. Fu, J. Huang, J. J. B. van der Tol, L. Su, Y. Wang, S. Dey, P. Zijlstra, G. Fytas, G. Vantomme, P. Y. W. Dankers and E. W. Meijer, *Nature*, 2024, **626**, 1011–1018.

322 T. Dünnebacke, N. Niemeyer, S. Baumert, S. Hochstädt, L. Borsdorf, M. R. Hansen, J. Neugebauer and G. Fernández, *Nat. Commun.*, 2024, **15**, 5695.

323 J. J. B. V. D. Tol, M. M. J. Dekker, Á. Müller, P. Springintveld, E. W. Meijer and G. Vantomme *Angew. Chem., Int. Ed.*, 2025, e202512216.

324 S. I. A. Cohen, S. Linse, L. M. Luheshi, E. Hellstrand, D. A. White, L. Rajah, D. E. Otzen, M. Vendruscolo, C. M. Dobson and T. P. J. Knowles, *Proc. Natl. Acad. Sci. U. S. A.*, 2013, **110**, 9758–9763.

325 S. Datta, H. Itabashi, T. Saito and S. Yagai, *Nat. Chem.*, 2025, **17**, 477–492.

326 M. Wolffs, P. A. Korevaar, P. Jonkheijm, O. Henze, W. James Feast, A. P. H. J. Schenning and E. W. Meijer, *Chem. Commun.*, 2008, 4613–4615.

327 S. Datta, S. Takahashi and S. Yagai, *Acc. Mater. Res.*, 2022, **3**, 259–271.

328 S. Datta, Y. Kato, S. Higashiharaguchi, K. Aratsu, A. Isobe, T. Saito, D. D. Prabhu, Y. Kitamoto, M. J. Hollamby, A. J. Smith, R. Dalgliesh, N. Mahmoudi, L. Pesce, C. Perego, G. M. Pavan and S. Yagai, *Nature*, 2020, **583**, 400–405.

329 N. Sasaki, J. Kikkawa, Y. Ishii, T. Uchihashi, H. Imamura, M. Takeuchi and K. Sugiyasu, *Nat. Chem.*, 2023, **15**, 922–929.

330 A. Osypenko, E. Moulin, O. Gavat, G. Fuks, M. Maaloum, M. A. J. Koenis, W. J. Buma and N. Giuseppone, *Chem. Eur. J.*, 2019, **25**, 13008–13016.

331 R. Laishram, S. Sarkar, I. Seth, N. Khatun, V. K. Aswal, U. Maitra and S. J. George, *J. Am. Chem. Soc.*, 2022, **144**, 11306–11315.

332 S. Sarkar, R. Laishram, D. Deb and S. J. George, *J. Am. Chem. Soc.*, 2023, **145**, 22009–22018.

333 S. R. Pramatha, D. Srideep, U. Pattnaik, R. Sahu, D. I. Suresh, A. C. Yadav, C. Muduli, S. K. Reddy, S. P. Senanayak and K. Venkata Rao, *Nat. Commun.*, 2024, **15**, 10808.

334 J.-P. Brog, C.-L. Chanez, A. Crochet and K. M. Fromm, *RSC Adv*, 2013, **3**, 16905–16931.

335 R. Tycko, *Neuron*, 2015, **86**, 632–645.

336 Q. Shi, H. Chen, Y. Wang, J. Xu, Z. Liu and C. Zhang, *Int. J. Pharm.*, 2022, **611**, 121320.

337 H. Chung and Y. Diao, *J. Mater. Chem. C*, 2016, **4**, 3915–3933.

338 N. M. Matsumoto, R. P. M. Lafleur, X. Lou, K.-C. Shih, S. P. W. Wijnands, C. Guibert, J. W. A. M. van Rosendaal, I. K. Voets, A. R. A. Palmans, Y. Lin and E. W. Meijer, *J. Am. Chem. Soc.*, 2018, **140**, 13308–13316.

339 M. Wehner, M. I. S. Röhr, M. Bühler, V. Stepanenko, W. Wagner and F. Würthner, *J. Am. Chem. Soc.*, 2019, **141**, 6092–6107.

340 A. Langenstroer, K. K. Kartha, Y. Dorca, J. Droste, V. Stepanenko, R. Q. Albuquerque, M. R. Hansen, L. Sánchez and G. Fernández, *J. Am. Chem. Soc.*, 2019, **141**, 5192–5200.

**11696** | *Chem. Soc. Rev.*, 2025, **54**, 11659–11698

This journal is © The Royal Society of Chemistry 2025

341 J. Matern, K. K. Kartha, L. Sánchez and G. Fernández, *Chem. Sci.*, 2020, **11**, 6780–6788.

342 C. Otsuka, S. Imai, T. Ohkubo and S. Yagai, *Chem. Commun.*, 2024, **60**, 1108–1111.

343 C. Otsuka, S. Takahashi, A. Isobe, T. Saito, T. Aizawa, R. Tsuchida, S. Yamashita, K. Harano, H. Hanayama, N. Shimizu, H. Takagi, R. Haruki, L. Liu, M. J. Hollamby, T. Ohkubo and S. Yagai, *J. Am. Chem. Soc.*, 2023, **145**, 22563–22576.

344 L. Rubert, H. M. A. Ehmann and B. Soberats, *Angew. Chem., Int. Ed.*, 2025, **64**, e202415774.

345 I. Debnath, T. Roy, J. Matern, S. A. H. Jansen, G. Fernández and K. Mahata, *Org. Chem. Front.*, 2021, **8**, 5432–5439.

346 S. Datta and D. Chaudhuri, *Angew. Chem., Int. Ed.*, 2022, **61**, e202201956.

347 Y. Hong, Y. Jiang, C. Yuan, D. Wang, Y. Sun and J. Jiang, *Chin. Chem. Lett.*, 2024, **35**, 109909.

348 Y. Kasahara, T. Takeda, S. Dekura, Y. Ishii, H. Anetai, A. Takai, I. Hisaki, M. Takeuchi and T. Akutagawa, *J. Am. Chem. Soc.*, 2025, **147**, 18783–18795.

349 C. Montañez-Moyano, Y. Xue, M. V. Cappellari, A. Martínez-Manjarrés, L. Borsdorf, C. A. Strassert and G. Fernández, *Angew. Chem., Int. Ed.*, 2025, e202509031.

350 J. Li, J. Wang, H. Li, N. Song, D. Wang and B. Z. Tang, *Chem. Soc. Rev.*, 2020, **49**, 1144–1172.

351 D. M. Eisele, J. Knoester, S. Kirstein, J. P. Rabe and D. A. V. Bout, *Nat. Nanotechnol.*, 2009, **4**, 658–663.

352 C. Villegas, E. Krokos, P.-A. Bouit, J. L. Delgado, D. M. Guldi and N. Martín, *Energy Environ. Sci.*, 2011, **4**, 679–684.

353 X. Wang, Y. Han, Y. Liu, G. Zou, Z. Gao and F. Wang, *Angew. Chem., Int. Ed.*, 2017, **56**, 12466–12470.

354 C. Rehhagen, M. Stolte, S. Herbst, M. Hecht, S. Lochbrunner, F. Würthner and F. Fennel, *J. Phys. Chem. Lett.*, 2020, **11**, 6612–6617.

355 M. Hecht, T. Schlossarek, S. Ghosh, Y. Tsutsui, A. Schmiedel, M. Holzapfel, M. Stolte, C. Lambert, S. Seki, M. Lehmann and F. Würthner, *ACS Appl. Nano Mater.*, 2020, **3**, 10234–10245.

356 M. Hecht, T. Schlossarek, M. Stolte, M. Lehmann and F. Würthner, *Angew. Chem., Int. Ed.*, 2019, **58**, 12979–12983.

357 Z. Xie, B. Xiao, Z. He, W. Zhang, X. Wu, H. Wu, F. Würthner, C. Wang, F. Xie, L. Liu, Y. Ma, W.-Y. Wong and Y. Cao, *Mater. Horiz.*, 2015, **2**, 514–518.

358 M. Gsänger, J. H. Oh, M. Könemann, H. W. Höffken, A.-M. Krause, Z. Bao and F. Würthner, *Angew. Chem., Int. Ed.*, 2010, **49**, 740–743.

359 H. Liu, X. Cao, Y. Wu, Q. Liao, Á. J. Jiménez, F. Würthner and H. Fu, *Chem. Commun.*, 2014, **50**, 4620–4623.

360 P. Lova, V. Grande, G. Manfredi, M. Patrini, S. Herbst, F. Würthner and D. Comoretto, *Adv. Opt. Mater.*, 2017, **5**, 1700523.

361 A. T. Haedler, K. Kreger, A. Issac, B. Wittmann, M. Kivala, N. Hammer, J. Köhler, H. W. Schmidt and R. Hildner, *Nature*, 2015, **523**, 196–199.

362 A. T. Haedler, S. R. Beyer, N. Hammer, R. Hildner, M. Kivala, J. Köhler and H.-W. Schmidt, *Chem. Eur. J.*, 2014, **20**, 11708–11718.

363 B. Wittmann, F. A. Wenzel, S. Wiesneth, A. T. Haedler, M. Drechsler, K. Kreger, J. Köhler, E. W. Meijer, H.-W. Schmidt and R. Hildner, *J. Am. Chem. Soc.*, 2020, **142**, 8323–8330.

364 A. V. Gorbunov, A. T. Haedler, T. Putzeys, R. H. Zha, H.-W. Schmidt, M. Kivala, I. Urbanaviciute, M. Wübbenhorst, E. W. Meijer and M. Kemerink, *ACS Appl. Mater. Interfaces*, 2016, **8**, 15535–15542.

365 Y. Yamamoto, T. Fukushima, Y. Suna, N. Ishii, A. Saeki, S. Seki, S. Tagawa, M. Taniguchi, T. Kawai and T. Aida, *Science*, 2006, **314**, 1761–1764.

366 Y. Yamamoto, T. Fukushima, W. Jin, A. Kosaka, T. Hara, T. Nakamura, A. Saeki, S. Seki, S. Tagawa and T. Aida, *Adv. Mater.*, 2006, **18**, 1297–1300.

367 J. J. I. Armao, I. Nyrkova, G. Fuks, A. Osypenko, M. Maaloum, E. Moulin, R. Arenal, O. Gavat, A. Semenov and N. Giuseppone, *J. Am. Chem. Soc.*, 2017, **139**, 2345–2350.

368 V. Faramarzi, F. Niess, E. Moulin, M. Maaloum, J.-F. Dayen, J.-B. Beaufrand, S. Zanettini, B. Doudin and N. Giuseppone, *Nat. Chem.*, 2012, **4**, 485–490.

369 F. S. Schoonbeek, J. H. V. Esch, B. Wegewijs, D. B. A. Rep, M. P. D. Haas, T. M. Klapwijk, R. M. Kellogg and B. L. Feringa, *Angew. Chem., Int. Ed.*, 1999, **38**, 1393–1397.

370 R. J. Hafner, D. Görl, A. Sienkiewicz, S. Balog and H. Frauenrath, *Chem. Eur. J.*, 2020, **26**, 9506–9517.

371 J. P. Hill, W. Jin, A. Kosaka, T. Fukushima, H. Ichihara, T. Shimomura, K. Ito, T. Hashizume, N. Ishii and T. Aida, *Science*, 2004, **304**, 1481–1483.

372 M. Sofos, J. Goldberger, D. A. Stone, J. E. Allen, Q. Ma, D. J. Herman, W. W. Tsai, L. J. Lauhon and S. I. Stupp, *Nat. Mater.*, 2009, **8**, 68–75.

373 Y. Guo, G. Yu and Y. Liu, *Adv. Mater.*, 2010, **22**, 4427–4447.

374 G. Hong, X. Gan, C. Leonhardt, Z. Zhang, J. Seibert, J. M. Busch and S. Bräse, *Adv. Mater.*, 2021, **33**, 2005630.

375 K. A. Mazzio and C. K. Luscombe, *Chem. Soc. Rev.*, 2014, **44**, 78–90.

376 S. Shanmugaraju, H. Jadhav, R. Karthik and P. S. Mukherjee, *RSC Adv.*, 2013, **3**, 4940–4950.

377 B. Gole, W. Song, M. Lackinger and P. S. Mukherjee, *Chem. Eur. J.*, 2014, **20**, 13662–13680.

378 T. L. Mako, J. M. Racicot and M. Levine, *Chem. Rev.*, 2019, **119**, 322–477.

379 Q. Lin, X.-M. Jiang, X.-Q. Ma, J. Liu, H. Yao, Y.-M. Zhang and T.-B. Wei, *Sens. Actuators B Chem.*, 2018, **272**, 139–145.

380 Z. Chen, Q. Wang, X. Wu, Z. Li and Y.-B. Jiang, *Chem. Soc. Rev.*, 2015, **44**, 4249–4263.

381 D.-W. Zhang, X. Zhao and Z.-T. Li, *Acc. Chem. Res.*, 2014, **47**, 1961–1970.

382 C. Li, G.-T. Wang, H.-P. Yi, X.-K. Jiang, Z.-T. Li and R.-X. Wang, *Org. Lett.*, 2007, **9**, 1797–1800.

383 F. Nabeel, T. Rasheed, M. Bilal, C. Li, C. Yu and H. M. N. Iqbal, *Sep. Purif. Rev.*, 2020, **49**, 20–36.

This journal is © The Royal Society of Chemistry 2025

*Chem. Soc. Rev.*, 2025, **54**, 11659–11698 | 11697

384 E. Cohen, H. Weissman, E. Shimoni, I. Kaplan-Ashiri, K. Werle, W. Wohlleben and B. Rybtchinski, *Angew. Chem., Int. Ed.*, 2017, **56**, 2203–2207.

385 E. Krieg, H. Weissman, E. Shirman, E. Shimoni and B. Rybtchinski, *Nat. Nanotechnol.*, 2011, **6**, 141–146.

386 L. Bouteiller and M. Raynal, *Supramol. Catal. New Dir. Dev.*, 2021, 93–106.

387 M. Raynal, P. Ballester, A. Vidal-Ferran and P. W. N. M. V. Leeuwen, *Chem. Soc. Rev.*, 2014, **43**, 1660–1733.

388 M. Raynal, P. Ballester, A. Vidal-Ferran and P. W. N. M. V. Leeuwen, *Chem. Soc. Rev.*, 2014, **43**, 1734–1787.

389 L. N. Neumann, M. B. Baker, C. M. A. Leenders, I. K. Voets, R. P. M. Lafleur, A. R. A. Palmans and E. W. Meijer, *Org. Biomol. Chem.*, 2015, **13**, 7711–7719.

390 R. Chen, A. Hammoud, P. Aoun, M. A. Martínez-Aguirre, N. Vanthuyne, R. Maruchenko, P. Brocorens, L. Bouteiller and M. Raynal, *Nat. Commun.*, 2024, **15**, 4116.

391 X.-G. Tan, P. Jeyakkumar, Y.-X. Zhang, L.-W. Chu, Y.-R. Hao, S.-K. Li, K.-Y. Wang and X.-Y. Hu, *cMat*, 2024, **1**, e31.

392 D. Zhang, W. Yu, S. Li, Y. Xia, X. Li, Y. Li and T. Yi, *J. Am. Chem. Soc.*, 2021, **143**, 1313–1317.

393 J. Tian, J. Yu, Q. Tang, J. Zhang, D. Ma, Y. Lei and Z.-T. Li, *Mater. Futur.*, 2022, **1**, 042104.

394 A. S. Weingarten, R. V. Kazantsev, L. C. Palmer, M. McClendon, A. R. Koltonow, A. P. S. Samuel, D. J. Kiebala, M. R. Wasielewski and S. I. Stupp, *Nat. Chem.*, 2014, **6**, 964–970.

395 A. S. Weingarten, R. V. Kazantsev, L. C. Palmer, D. J. Fairfield, A. R. Koltonow and S. I. Stupp, *J. Am. Chem. Soc.*, 2015, **137**, 15241–15246.

396 J. Yu, L. Huang, Q. Tang, S.-B. Yu, Q.-Y. Qi, J. Zhang, D. Ma, Y. Lei, J. Su, Y. Song, J.-C. Eloi, R. L. Harniman, U. Borucu, L. Zhang, M. Zhu, F. Tian, L. Du, D. L. Phillips, I. Manners, R. Ye and J. Tian, *Nat. Catal.*, 2023, **6**, 464–475.

397 R. Dong, Y. Zhou, X. Huang, X. Zhu, Y. Lu and J. Shen, *Adv. Mater.*, 2015, **27**, 498–526.

398 D. Wang, G. Tong, R. Dong, Y. Zhou, J. Shen and X. Zhu, *Chem. Commun.*, 2014, **50**, 11994–12017.

399 R. Dong, Y. Pang, Y. Su and X. Zhu, *Biomater. Sci.*, 2015, **3**, 937–954.

400 N. R. B. Boase, E. R. Gillies, R. Goh, R. E. Kieltyka, J. B. Matson, F. Meng, A. Sanyal and O. Sedláček, *Biomacromolecules*, 2024, **25**, 5417–5436.

401 J. B. Matson and S. I. Stupp, *Chem. Commun.*, 2011, **48**, 26–33.

402 S. M. Chin, C. V. Synatschke, S. Liu, R. J. Nap, N. A. Sather, Q. Wang, Z. Álvarez, A. N. Edelbrock, T. Fyrner, L. C. Palmer,

I. Szleifer, M. O. D. L. Cruz and S. I. Stupp, *Nat. Commun.*, 2018, **9**, 1–11.

403 K. Sato, M. P. Hendricks, L. C. Palmer and S. I. Stupp, *Chem. Soc. Rev.*, 2018, **47**, 7539–7551.

404 M. J. Webber and R. Langer, *Chem. Soc. Rev.*, 2017, **46**, 6600–6620.

405 A. L. Schmitt, S. H.-J. Yoon, W.-D. Jang and H.-J. Yoon, *J. Mater. Chem.*, 2009, **20**, 211–222.

406 T. Jin, C. Huang, M. Cui, Y. Yang, Z. Wang, W. Zhu and X. Qian, *J. Mater. Chem. B*, 2020, **8**, 10686–10699.

407 Z. Shi, X. Han, W. Hu, H. Bai, B. Peng, L. Ji, Q. Fan, L. Li and W. Huang, *Chem. Soc. Rev.*, 2020, **49**, 7533–7567.

408 Y. Chen Liu, G. Jian Liu, W. Zhou, G. Li Feng, Q. Yu Ma, Y. Zhang and G. Wen Xing, *Angew. Chem., Int. Ed.*, 2023, **62**, e202309786.

409 Y. Liu, H. Wang, S. Li, C. Chen, L. Xu, P. Huang, F. Liu, Y. Su, M. Qi, C. Yu and Y. Zhou, *Nat. Commun.*, 2020, **11**, 1724.

410 Y. Dai, J. Sun, X. Zhang, J. Zhao, W. Yang, J. Zhou, Z. Gao, Q. Wang, F. Yu and B. Wang, *Coord. Chem. Rev.*, 2024, **517**, 216054.

411 Y. Chen, X. H. Zhang, D. B. Cheng, Y. Zhang, Y. Liu, L. Ji, R. Guo, H. Chen, X. K. Ren, Z. Chen, Z. Y. Qiao and H. Wang, *ACS Appl. Mater. Interfaces*, 2020, **14**, 3650.

412 N. Kwon, H. Kim, X. Li and J. Yoon, *Chem. Sci.*, 2021, **12**, 7248–7268.

413 X.-Y. Lou, G. Zhang, N. Song and Y.-W. Yang, *Biomaterials*, 2022, **286**, 121595.

414 N. Mehwish, X. Dou, Y. Zhao and C. L. Feng, *Mater. Horiz.*, 2019, **6**, 14–44.

415 G. Fan, Y. X. Lin, L. Yang, F. P. Gao, Y. X. Zhao, Z. Y. Qiao, Q. Zhao, Y. S. Fan, Z. Chen and H. Wang, *Chem. Commun.*, 2015, **51**, 12447–12450.

416 A. Albers, S. Kuberasivakumaran, Z. Fernández, C. G. Daniliuc, Y. Li, M. Lee, C. Geyer, E. Hoffmann, C. Faber, A. Helfen, C. Grashoff, M. Masthoff and G. Fernández, *Angew. Chem., Int. Ed.*, 2025, **64**, e202500144.

417 V. S. Talens, G. Arias-Alpizar, D. M. M. Makurat, J. Davis, J. Bussmann, A. Kros and R. E. Kieltyka, *Biomacromolecules*, 2020, **21**, 1060–1068.

418 K. Yang, G. Yu, Z. Yang, L. Yue, X. Zhang, C. Sun, J. Wei, L. Rao, X. Chen and R. Wang, *Angew. Chem., Int. Ed.*, 2021, **60**, 17570–17578.

419 J. Qi, C. Chen, X. Zhang, X. Hu, S. Ji, R. T. K. Kwok, J. W. Y. Lam, D. Ding and B. Z. Tang, *Nat. Commun.*, 2018, **9**, 1848.

**11698** | *Chem. Soc. Rev.*, 2025, **54**, 11659–11698

This journal is © The Royal Society of Chemistry 2025